SPINDLE CHECKPOINT AT KINETOCHORES

APPROVED BY SUPERVISORY COMMITTEE

Hongtao Yu, Ph.D. (Mentor)

Paul Sternweis, Ph.D. (Chair)

Melanie Cobb, Ph.D.

Luke Rice, Ph.D.

DEDICATION

I would like to thank many people at UT Southwestern who have helped me during my graduate work. First and most importantly, I would like to thank my mentor Dr. Hongtao Yu, who has taught me how to think critically and be an independent scientist. He has continually supported and motivated me in everything I have decided to pursue. His encouragement always has given me fresh energy to persevere. In addition, I would like to thank the past and present members of the lab. I have been enjoying a lot doing research with them in a productive and fun environment. I would also like acknowledge Dr. Xuelian Luo for all the help and guidance. Lastly, I would like to thank my graduate committee for giving me suggestions and advices.

I would also like to acknowledge several others who were crucial in getting me interested in scientific research. First, my previous mentor Dr. Dae-Sik Lim of the KAIST department of Biological Sciences provided me the opportunity to carry out my first step in research while I was a graduate at KAIST. Second, I would like to thank Min-sup Song and Su-jung Song for their patience while teaching me essential experimental techniques, basic scientific reasoning, and how to read scientific literatures.

Finally, I would like to thank my parents. They have supported me in every moment of my life. Their love and trust have been essential to my success undoubtedly. In addition to my parents, I would like to thank my husband, Chul-Hwan Lee. He has been always there beside me when I have faced many challenges and hard times. I would also like to thank my sisters and brother for their help and comport over the years.

SPINDLE CHECKPOINT AT KINETOCHORES

by

SOONJOUNG KIM

DISSERTATION

Presented to the Faculty of the Graduate School of Biomedical Sciences

The University of Texas Southwestern Medical Center at Dallas

In Partial Fulfillment of the Requirements

For the Degree of

DOCTOR OF PHILOSOPHY

The University of Texas Southwestern Medical Center at Dallas

Dallas, Texas

August, 2014

SPINDLE CHECKPOINT AT KINETOCHORES

SOONJOUNG KIM, Ph.D.

The University of Texas Southwestern Medical Center at Dallas, 2014

HONGTAO YU, Ph.D.

The kinetochore—a large protein assembly on centromeric chromatin—functions as the docking site for spindle microtubules and as a signaling hub for the spindle checkpoint. The Constitutive Centromere-Associated Network (CCAN) at the inner kinetochore nucleates the formation of the mature outer kinetochore during mitosis, including the recruitment of the KMN network that consists of Knl1, the Mis12 complex (Mis12C), and the Ndc80 complex (Ndc80C). The KMN is a critical receptor for microtubules, and provides a landing pad for various spindle checkpoint proteins and regulatory factors. The spindle checkpoint protein Mad2 has multiple conformations, including the inactive open Mad2 (O-Mad2) and the active closed Mad2 (C-Mad2). The kinetochore-bound checkpoint protein complex Mad1–Mad2 promotes the conformational activation of O-Mad2 and serves as a catalytic engine of checkpoint signaling. The activated C-Mad2 binds to and inhibits Cdc20, an activator of APC/C, to prevent precocious anaphase onset. Deficient spindle checkpoint

signaling leads to premature sister-chromatid separation and aneuploidy. Research in this thesis has provided several key insights into spindle checkpoint signaling at kinetochores.

First, we show that the conformational transition of Mad2 is regulated by phosphorylation of S195 in its C-terminal region. The phospho-mimicking Mad2^{S195D} mutant and the phospho-S195 Mad2 protein do not form C-Mad2 on their own. Mad2 phosphorylation inhibits its function through differentially regulating its binding to Mad1 and Cdc20. Our results establish for the first time that the conformational change of Mad2 is regulated by posttranslational mechanisms.

Second, we have studied how Mad1 is targeted to kinetochores. We have determined the crystal structure of the conserved C-terminal domain (CTD) of human Mad1. The structure reveals unexpected fold similarity between Mad1 CTD and known kinetochore-binding modules. Functional studies then validate a role of Mad1 CTD in kinetochore targeting and implicate Bub1 as its receptor. Interestingly, deletion of the CTD does not abolish Mad1 kinetochore localization. Non-overlapping Mad1 fragments retain detectable kinetochore targeting. Our results indicate that the CTD–Bub1 connection is one of several mechanisms of targeting Mad1 to kinetochores.

Finally, we show that the proper assembly of KMN is required for generating the spindle checkpoint signal at kinetochores. We have developed several strategies to inactivate KMN at kinetochores in human cells, and demonstrate its requirement for the spindle checkpoint in the absence of microtubules. We further show that two quasi-independent pathways mediate the mitosis-specific assembly of KMN at kinetochores. In one pathway, the centromeric kinase Aurora B phosphorylates the Mis12C component Dsn1, and

strengthens Mis12C binding to the CCAN component CENP-C. In the second pathway, CENP-T anchors the CENP-H/I/K sub-complex at kinetochores, which in turn recruits Ndc80C. Inactivation of both pathways abolishes KMN at kinetochores and causes gross spindle checkpoint defects.

In conclusion, combining cell biology and structural biology methods, our studies have defined a new posttranslational mechanism of Mad2 regulation, uncovered a critical way for targeting Mad1 to kinetochores, and dissected assembly pathways of the KMN checkpoint sensor at kinetochores.

TABLE OF CONTENTS

PRIOR PUBLICATIONS

Kim S, and Yu H. (2014). Assembly pathways of the spindle checkpoint sensor KMN at kinetochores. *Manuscript in preparation.*

Jia L*, Kim S*, Yu H. (2013). Tracking spindle checkpoint signals from kinetochores to APC/C. Trends Biochem Sci. Trends Biochem Sci. 2013 Jun;38(6):302-11.

Kim S*, Sun H*, Tomchick DR, Yu H, Luo X. (2012). Structure of human Mad1 C-terminal domain reveals its involvement in kinetochore targeting. Proc Natl Acad Sci USA. 2012 Apr 24;109(17):6549-54.

Kim S, and Yu H. (2011). Mutual regulation between the spindle checkpoint and APC/C. Semin Cell Dev Biol. 22(6): 551–558.

Kang J, Chaudhary J, Dong H, Kim S, Brautigam CA, and Yu H. (2011). Mitotic centromeric targeting of HP1 and its binding to Sgo1 are dispensable for sister-chromatid cohesion in human cells. Mol Biol Cell *22*, 1181-1190.

Kim S*, Sun H*, Ball HL, Wassmann K, Luo X, Yu H (2010) Phosphorylation of the spindle checkpoint protein Mad2 regulates its conformational transition. Proc Natl Acad Sci USA.107(46):19772-19777.

Song SJ, Kim S, Song MS, Lim DS (2009) Aurora B-mediated phosphorylation of RASSF1A maintains proper cytokinesis by recruiting Syntaxin16 to the midzone and midbody. Cancer Res. 69(22):8540-4.

Song SJ, Song MS, Kim S, Kim SY, Kwon SH, Kim JG, Calvisi DF, Kang D, Lim DS (2009) Aurora A regulates prometaphase progression by inhibiting the ability of RASSF1A to suppress APC-Cdc20 activity. Cancer Res. 69(6):2314-23.

Song MS, Song SJ, Kim S, Nakayama K, Nakayama K I., and Lim DS (2008) Skp2 regulates the antiproliferative function of the tumor suppressor RASSF1A via ubiquitin-mediated degradation at the G_1-S transition. Oncogene 15;27(22):3176-85.

LIST OF FIGURES

LIST OF TABLES

LIST OF DEFINITIONS

APC/C - anaphase-promoting complex/cyclosome
BUB - budding uninhibited by benomyl
CCAN - constitutive centromere-associated network
CDC20 - cell-division cycle protein 20
CDK - cyclin-dependent kinase
CENP - centromere protein
CPC - chromosomal passenger complex
CREST - calcinosis, Raynaud's phenomenon, esophageal dysmotility, sclerodactyly and telangiectasia
CTD - C terminal domain
DAPI - 4',6-diamidino-2-phenylindole
DOX - doxycycline
DSN - dosage suppressor of NNF1
EM - electron microscopy
FACS - Fluorescence-activated cell sorting
GFP - green fluorescent protein
GLEBS - Gle2-binding-sequence
HSQC - Heteronuclear single quantum correlation
INCENP - Inner centromere protein
IP - immunoprecipitation
kD - kilodaltons
Kd - dissociation constant
KEN - lysine-glutamate-asparagine
KMN - Knl1/Mis12C/Ndc80C
KNL - kinetochore null
MAD - mitotic arrest deficiency
MBP - myelin basic protein
MBP1 - Mad2-binding peptide 1
MCC - mitotic checkpoint complex
MIM - Mad2-interacting motif
MIS12 - minichromosome instability-12
Mis12C - Mis12 complex
MPM - Mitotic Protein Monoclonal
MPS1 - Monopolar spindle 1
MST - Microscale thermophoresis
NDC80 - Nuclear division cycle 80

Ndc80C - Ndc80 complex
NLS - NNF1 synthetic lethal
NMR - nuclear magnetic resonance
NNF1 - necessary for nuclear function 1
NUF2 - Nuclear filament-containing protein 2
RING - really interesting new gene
RLK - arginine/leucine/lysine
RNAi - RNA interference
ROI - region of interest
RWD - RING finger-containing proteins, WD-repeat-containing proteins, and yeast DEAD (DEXD)-like helicases
RZZ - Rod/Zwilch/Zw10

CHAPTER I: INTRODUCTION

ASSEMBLY AND FUNCTION OF THE KINETOCHORE

The kinetochore serves both as the docking site for spindle microtubules and as a signaling hub for the spindle checkpoint (Cleveland, Mao et al. 2003). Electron microscopy (EM) of vertebrate chromosomes has long revealed that kinetochores have a layered morphology, including the electron-dense inner and outer plates, the electron-lucent middle layer, and the outermost fibrous corona (Cleveland, Mao et al. 2003). Proteomic analysis coupled with high-resolution fluorescence microscopy has begun to shed light on the molecular identities of each kinetochore layer.

Constitutive Centromere-Associated Network

The centromere is epigenetically marked by CENP-A, a centromere-specific histone H3 variant (Black and Cleveland 2011). A synthetic CENP-A chromatin reconstituted from recombinant human histones is sufficient to assemble functional kinetochores in cell-free *Xenopus* egg extracts (Guse, Carroll et al. 2011), supporting the key functions of the CENP-A nucleosome in defining the centromere locus. In vertebrate cells, the CENP-A nucleosome interacts throughout the cell cycle with the constitutive centromere-associated network (CCAN) (Foltz, Jansen et al. 2006; Okada, Cheeseman et al. 2006; Takeuchi and Fukagawa 2012), which contains CENP-C, -H, -I, -K, -L, -M, -N, -O, -P, -Q, -U, -R, -T, -W, -S, and -X (Figure 1-1). These CCAN components form several functional sub-complexes, including CENP-T–W–S–X, CENP-H–I–K, CENP-L–M–N, and CENP-O–P–Q–U–R. CENP-C and

CENP-N anchor CCAN to centromeric chromatin through direct interactions with the CENP-A nucleosome (Carroll, Silva et al. 2009; Carroll, Milks et al. 2010). The CENP-T–W–S–X sub-complex has folds related to core histones and can bind DNA to form a nucleosome-like structure (Nishino, Takeuchi et al. 2012). Although this sub-complex does not directly bind to CENP-A, its deposition at the centromeres is nonetheless dependent on CENP-A (Hori, Amano et al. 2008).

As its name suggests, CCAN constitutively localizes to centromeres. The protein levels of several CCAN components, including CENP-N, T, U, and W, however, fluctuate during the cell cycle (Kang, Park et al. 2006; Hellwig, Emmerth et al. 2011; Prendergast, van Vuuren et al. 2011). Surprisingly, CENP-U (also known as PBIP1) is degraded in early mitosis, when the outer kinetochore begins to assemble (Kang, Park et al. 2006). The functional significance and molecular mechanisms of the cell-cycle oscillations in the levels of these CENP proteins are unclear.

Assembly of the Outer Kinetochore

The outer kinetochore is assembled onto CCAN at late prophase, just before nuclear envelope breakdown. With astounding speed and accuracy, more than 100 proteins are recruited and pieced together in a hierarchical fashion to form the mature, functional kinetochore. Although much remains to be learned about this fascinating process, recent progress has delineated the molecular pathways that install the core microtubule receptor, the KMN network, at kinetochores (Figure 1-1). The KMN network consists of Knl1 (also known as Blinkin), the Mis12 complex (Mis12C which contains Mis12, Nsl1, Nnf1, and Dsn1), and the Ndc80 complex (Ndc80C which contains Ndc80, Nuf2, Spc24, and Spc25)

(Cheeseman, Chappie et al. 2006). Both Knl1 and Ndc80C have microtubule-binding activities. Mis12C interacts with both Knl1 and Ndc80C, and nucleates the formation of the intact KMN (Petrovic, Pasqualato et al. 2010), which enables cooperative microtubule binding by Knl1 and Ndc80C.

Artificial targeting of CENP-C and CENP-T to an ectopic chromatin locus is sufficient to recruit KMN and specify a functional kinetochore (Gascoigne, Takeuchi et al. 2011), suggesting that the kinetochore-assembly pathway has two branches (Figure 1-1). In one branch, the conserved N-terminal motif of CENP-C interacts with Mis12C and recruits it to the kinetochore (Screpanti, De Antoni et al. 2011). In another branch, CENP-T functions as a direct kinetochore receptor of Ndc80C (Bock, Pagliuca et al. 2012; Schleiffer, Maier et al. 2012). Thus, CENP-C and CENP-T connect KMN to CCAN.

Unlike CCAN, KMN does not localize constitutively to centromeres, and only assembles onto kinetochores during prophase. The mechanisms by which KMN is targeted to kinetochores specifically in mitosis are not understood. The conserved Ndc80C-binding motif of CENP-T contains functionally important Cdk phosphorylation sites (Gascoigne, Takeuchi et al. 2011; Schleiffer, Maier et al. 2012), suggesting the involvement of Cdk-dependent phosphorylation in this process.

Kinetochore Recruitment and Activation of Spindle Checkpoint Proteins

First identified in the budding yeast, the molecular components of the spindle checkpoint have later been shown to be evolutionarily conserved from yeast to man. The kinases Aurora B and Mps1 lie at or near the top of the checkpoint pathway. The centromere-

and kinetochore-targeting of these two kinases has been linked to the activation of their kinase activities (Kang, Chen et al. 2007; Kelly, Sampath et al. 2007; Jelluma, Dansen et al. 2010). The downstream spindle checkpoint proteins Bub1, BubR1, Bub3, Mad1, and Mad2 form three constitutive binary complexes: Bub1–Bub3, BubR1–Bub3, and Mad1–Mad2. They are recruited to the kinetochores during mitosis in a KMN-dependent manner (Figure 1-1A). At the kinetochores, these proteins undergo enzymatic or conformational activation. The activated checkpoint proteins then collaborate to inhibit APC/C^{Cdc20}. A key APC/C inhibitor is the mitotic checkpoint complex (MCC) consisting of BubR1–Bub3, Cdc20, and Mad2.

The kinetochore localization of many if not all checkpoint proteins is required for proper checkpoint signaling. Dissecting the kinetochore-recruitment mechanisms of these checkpoint proteins thus holds the key for the eventual understanding of the generation and propagation of checkpoint signals. The KMN network not only serves as the kinetochore receptor for microtubules, but also interacts directly or indirectly with most spindle checkpoint proteins (Figure 1-1). KMN thus couples spindle checkpoint signaling to microtubule binding. The apparent, mutually exclusive binding of microtubules and checkpoint proteins to KMN may constitute a simple switch for checkpoint activation and inactivation.

Centromere recruitment and checkpoint functions of Aurora B

Aurora B is a conserved serine/threonine kinase and a component of chromosome passenger complex (CPC) which also contains INCENP, Survivin, and Borealin (Ruchaud, Carmena et al. 2007). Aurora B has important functions in multiple mitotic processes,

including sister-chromatid cohesion, spindle assembly, the spindle checkpoint, chromosome bi-orientation, and cytokinesis. Aurora B localizes to inner centromeres in early mitosis. It centromeric localization is mediated by other CPC components INCENP and Survivin. In mitosis, the checkpoint kinase Bub1 phosphorylates the C-terminal tail of histone H2A (H2A-T120 in humans) at the kinetochores (Kawashima, Yamagishi et al. 2010). Phospho-H2A-T120 then serves as an epigenetic mark to recruit the Shugoshin proteins, which interact with INCENP (Kawashima, Yamagishi et al. 2010; Yamagishi, Honda et al. 2010). Another mitotic kinase Haspin phosphorylates histone H3 Thr3 (H3-T3) at the centromeres (Kelly, Ghenoiu et al. 2010; Wang, Dai et al. 2010; Yamagishi, Honda et al. 2010). Phospho-H3-T3 directly binds to survivin. The combined actions of Shugoshin–INCENP and Survivin–phospho-H3-T3 interactions then drive the centromeric localization of CPC and contribute to the activation of Aurora B. Mps1 and the master mitotic kinase Cdk1 also promote Aurora B activation through phosphorylation of Borealin and Survivin, respectively (Jelluma, Brenkman et al. 2008; Tsukahara, Tanno et al. 2010).

While localizing at the inner centromeres, Aurora B promotes sister-chromatid bi-orientation by phosphorylating multiple KMN components at the outer kinetochores and severing improper kinetochore–microtubule attachments (Cheeseman, Chappie et al. 2006; Welburn, Vleugel et al. 2010). For example, Aurora B-mediated phosphorylation of Ndc80 and Knl1 introduces unfavorable negative charges onto the microtubule-binding surface of KMN and reduces its microtubule-binding affinity. The phosphorylation level of an Aurora B target is inversely correlated with its physical distance from Aurora B (Figure 1-2) (Liu, Vader et al. 2009; Wang, Ballister et al. 2011). When a pair of sister kinetochores is captured

by microtubules from the same spindle pole, this pair of sister kinetochores is not under tension, and the distance between Aurora B and its KMN substrates is small. Aurora B then efficiently phosphorylates KMN and severs this type of improper microtubule attachment. When a pair of kinetochores is captured by microtubules from opposing spindle poles, the microtubule-pulling force generates tension across the kinetochores and physically separates Aurora B at the inner centromeres from KMN at the outer kinetochores. It has been proposed that this spatial separation between Aurora B and its substrates decreases the phosphorylation of Ndc80 and Knl1, preserving the correct mode of kinetochore–microtubule attachment (Lampson and Cheeseman 2011).

Unlike other spindle checkpoint proteins, Aurora B is only required for the checkpoint activation and mitotic arrest induced by the microtubule-stabilizing drug taxol, but not for the mitotic arrest induced by the microtubule-destabilizing drug nocodazole (Ruchaud, Carmena et al. 2007). Because of this unique feature of Aurora B, it has been argued that Aurora B is indirectly involved in the spindle checkpoint through severing unstable kinetochore–microtubule attachment in the presence of taxol and transiently producing unattached kinetochores to facilitate the activation of other checkpoint proteins. While this is indeed true in yeast (Pinsky, Kung et al. 2006), two recent studies have shown that Aurora B is critical for the nocodazole-induced mitotic arrest in human cells depleted of Ndc80 (Santaguida, Vernieri et al. 2011; Saurin, van der Waal et al. 2011). These studies establish a microtubule-independent role of Aurora B in the spindle checkpoint, although how Aurora B accomplishes this function remains elusive.

Kinetochore recruitment of Bub1 and BubR1

The spindle checkpoint proteins are recruited to unattached or tensionless kinetochores, where they undergo enzymatic or conformational activation to produce diffusible APC/C inhibitors. Bub1 and BubR1 share extensive sequence similarity and both contain a kinase domain. Both also form a constitutive complex with Bub3. BubR1 is a component of MCC and directly participates in APC/C^{Cdc20} inhibition. Bub1 phosphorylates histone H2A to recruit shugoshin to kinetochores. Bub1 also phosphorylates Cdc20 and contributes to APC/C^{Cdc20} inhibition (Tang, Shu et al. 2004; Kang, Yang et al. 2008). Finally, independently of its kinase activity, Bub1 acts as a scaffold to recruit downstream checkpoint components, including BubR1 and Mad1, to the kinetochores (see below). Several recent studies have refined our understanding of the kinetochore targeting of Bub1 and BubR1.

Bub1 contains an N-terminal tetratricopeptide repeat (TPR) domain, two KEN boxes that interact with Cdc20, and a GLEBS motif that binds to Bub3. The kinetochore localization of Bub1 is strictly dependent on Knl1 (Kiyomitsu, Obuse et al. 2007). The TPR domain of Bub1 binds to a conserved motif in the N-terminal region of Knl1 (Kiyomitsu, Obuse et al. 2007; Kiyomitsu, Murakami et al. 2011). This interaction, however, has a marginal role in the kinetochore localization of Bub1 (Krenn, Wehenkel et al. 2012). Instead, Bub3 binding is critical for the kinetochore targeting of Bub1, as mutations of the Bub1 GLEBS motif abolish its kinetochore localization. Furthermore, Mps1 phosphorylates Knl1 on multiple conserved MELT motifs and promotes the kinetochore targeting of Bub1 in both yeast and human cells (London, Ceto et al. 2012; Shepperd, Meadows et al. 2012; Yamagishi, Yang et al. 2012). In yeast, a phospho-mimicking mutant of Knl1 supports the

kinetochore targeting of Bub1 even in the absence of the Mps1 activity, whereas the phospho-deficient mutant of Knl1 abrogates Bub1 localization. Deletion of Bub3 abolishes the Bub1 kinetochore targeting even in the presence of the phospho-mimicking Knl1. Thus, a plausible model is that Bub3 is involved in the recognition of the phospho-MELT motifs of Knl1 (Figure 1-1A).

Bub1 and BubR1 are structurally related. It is not surprising that similar mechanisms govern their kinetochore targeting. The N-terminal TPR domain of BubR1 binds to a conserved motif in Knl1 that is adjacent to and shares sequence similarity with the Bub1-binding motif of Knl1 (Bolanos-Garcia, Lischetti et al. 2011). Like Bub1, this interaction is largely dispensable for the kinetochore localization of BubR1 (Krenn, Wehenkel et al. 2012), and the BubR1–Bub3 interaction is instead required for the kinetochore targeting of BubR1 (Elowe, Dulla et al. 2010). Moreover, ectopic targeting of Bub1 to the telomere is sufficient to recruit BubR1 to that location (Rischitor, May et al. 2007). Expression of the phospho-mimicking Knl1 recruits BubR1 to kinetochores in the absence of the Mps1 kinase activity, but this recruitment is dependent on Bub1 (Yamagishi, Yang et al. 2012). Thus, the kinetochore targeting of BubR1 requires both Bub1 and Bub3 (Figure 1-1A).

Kinetochore recruitment of Mad1

Throughout the cell cycle, Mad1 and Mad2 form a constitutive heterotetramer referred to as the Mad1–Mad2 core complex. When the spindle checkpoint is active, the Mad1–Mad2 core complex localizes to kinetochores and recruits another copy of Mad2 from the cytosol to catalyze its conformational activation. The kinetochore targeting of the Mad1–

Mad2 core complex is dependent on Ndc80C, Mps1, and Bub1. A recent study has shed more light on the kinetochore-targeting mechanisms of Mad1 (Kim, Sun et al. 2012).

Mad1 has an unusually extensive kinetochore-binding interface, and non-overlapping Mad1 fragments retain partial kinetochore localization in human cells (Kim, Sun et al. 2012). Crystal structure of the conserved C-terminal domain (CTD) of human Mad1 reveals unexpected structural similarity between Mad1 CTD and the kinetochore-binding domain of Spc25 (an Ndc80C component). Indeed, a conserved RLK motif within Mad1 CTD contributes to the kinetochore targeting of Mad1. In yeast, this RLK motif of Mad1 is required for its mitosis-specific interaction with Bub1 (Brady and Hardwick 2000). In human cells, Bub1 is required for the proper kinetochore localization of Mad1. Thus, these results implicate Bub1 as a kinetochore receptor for Mad1 CTD (Figure 1-1A). The N-terminal coiled-coil region of *Xenopus* or human Mad1 retains partial kinetochore targeting (Chung and Chen 2002; Kim, Sun et al. 2012). The kinetochore receptors of the Mad1 N-terminal region have not been identified, but likely involve Ndc80C and Mps1.

The metazoan-specific RZZ complex consisting of Rod, Zwilch, and Zw10 is also required for the Mad1 kinetochore localization (Karess 2005). In *C. elegans*, the RZZ-binding protein Spindly interacts with Mad1 and regulates Mad1 kinetochore localization (Yamamoto, Watanabe et al. 2008). The Spindly–RZZ complex likely contributes to Mad1 kinetochore targeting in metazoans. On the other hand, the microtubule-based motor, dynein–dynactin, strips spindle checkpoint proteins and Spindly from microtubule-attached kinetochores (Howell, McEwen et al. 2001; Gassmann, Holland et al. 2010). This is an important mechanism for checkpoint silencing (see below). Spindly and RZZ serve as

kinetochore receptors for dynein (Barisic, Sohm et al. 2010; Gassmann, Holland et al. 2010). It is also possible that RZZ and Spindly regulate Mad1 kinetochore localization indirectly, through blocking untimely dynein-mediated stripping of Mad1 from kinetochores.

A recent study has investigated the consequences of forced kinetochore targeting of Mad1 (Maldonado and Kapoor 2011). Covalent tethering of Mad1 to Mis12 prevents the timely removal of this fusion protein from kinetochores and causes a prolonged mitotic arrest. Interestingly, this arrest is dependent on upstream checkpoint components, such as Aurora B and Mps1. Thus, Mad1 kinetochore localization by itself is insufficient to sustain the spindle checkpoint, but it may prolong the activation or prevent the inactivation of upstream checkpoint components through a yet uncharacterized feedback mechanism.

Mps1 as a regulator of Mad1 and Mad2 kinetochore targeting

It is well established that Mps1 has a conserved function in regulating the kientochore localization of Mad1 and Mad2 (Abrieu, Magnaghi-Jaulin et al. 2001). Recent studies using chemical inhibitors of Mps1 have revealed additional intricacies in this regulation (Tighe, Staples et al. 2008; Hewitt, Tighe et al. 2010; Kwiatkowski, Jelluma et al. 2010; Maciejowski, George et al. 2010; Santaguida, Tighe et al. 2010). In particular, Hewitt *et al.* have presented data to suggest that Mps1 regulates O-Mad2 recruitment to the Mad1–Mad2 core complex in mitosis of human cells (Hewitt, Tighe et al. 2010). By using a chemical inhibitor AZ3146 to inhibit Mps1 during different cell cycle stages, they have shown that inhibition of the Mps1 kinase activity before mitotic entry disrupts the kinetochore localization of both Mad1 and Mad2. However, inhibition of Mps1 after mitotic entry

prevents O-Mad2 recruitment to kinetochore, but does not affect the kinetochore localization of the Mad1–Mad2 core complex. Therefore, these findings suggest that the recruitment of cytosolic O-Mad2 to kinetochores and possibly Mad2 conformational activation is regulated by upstream checkpoint signaling and is thus sensitive to checkpoint status. How Mps1 regulates Mad1 and O-Mad2 recruitment to kinetochores is not understood.

How is Mps1 itself targeted to and activated at the kinetochores? The kinetochore targeting of Mps1 requires the Ndc80 complex (Martin-Lluesma, Stucke et al. 2002). Mps1 activation is dependent on autophosphorylation events on its activation loop (Kang, Chen et al. 2007). Chemically induced dimerization of Mps1 is sufficient to activate Mps1 (Kang, Chen et al. 2007). Mps1 indeed forms oligomers in mitotic human cells (Hewitt, Tighe et al. 2010). Therefore, the current evidence suggests that Mps1 undergoes dimerization and trans-autophosphorylation at kinetochores, leading to its activation. Interestingly, inhibition of its kinase activity leads to further accumulation of Mps1 at kinetochores, suggesting the existence of negative feedback regulation of Mps1 (Jelluma, Dansen et al. 2010).

INHIBITION OF APC/C^{CDC20} BY THE SPINDLE CHECKPOINT

The core components of the spindle checkpoint include the mitotic arrest deficiency (Mad) 1-3 and budding uninhibited by benomyl (Bub) 1-3 proteins. They were initially discovered through genetic studies in the budding yeast and were later shown to be conserved from yeast to man (Bharadwaj and Yu 2004; Musacchio and Salmon 2007). Upon checkpoint activation, these proteins use multiple strategies to inhibit APC/C^{Cdc20} upon checkpoint activation, including the stoichiometric binding to and sequestration of Cdc20 by Mad2 and BubR1, and phosphorylation of Cdc20 by Bub1 (Yu 2007) (Figure 1-3).

Mechanism of APC/C-dependent ubiquitination

To review how the spindle checkpoint inhibits APC/C, we briefly summarize how APC/C ubiquitinates its substrates. APC/C is a multisubunit ubiquitin ligase distantly related to the cullin-RING family of ubiquitin ligases. The subcomplex of Apc2 (a cullin-like subunit) and Apc11 (a RING-containing subunit) recruits and activates ubiquitin-conjugating enzymes (UBCs) (Tang, Li et al. 2001). Cdc20 or Cdh1 helps to recruit substrates to APC/C for efficient ubiquitination (Peters 2006; Thornton and Toczyski 2006; Yu 2007). All APC/C substrates contain small peptide motifs that are critical for their recognition by APC/C, often referred to as APC/C degrons. The destruction box (D-box, with a consensus of RXXLXXXXN) and the KEN-box (with a consensus of KEN) are two well-characterized APC/C degrons. Cdc20 and Cdh1 contain a C-terminal WD40 domain, which has been shown to contact D-box directly through chemical crosslinking (Kraft, Vodermaier et al.

2005). In addition to Cdc20 or Cdh1, Apc10 has been implicated in D-box recognition (Carroll and Morgan 2002; Carroll, Enquist-Newman et al. 2005). Recent electron microscopy (EM) studies confirm and extend these previous findings, and show that the D-box binds at the interface formed by Cdh1 and Apc10 (Buschhorn, Petzold et al. 2011; da Fonseca, Kong et al. 2011; Schreiber, Stengel et al. 2011). How the KEN-box is recognized remains unclear. It is also unclear why many APC/C substrates contain both D- and KEN-boxes.

Inhibition of Cdc20 by Mad2 and BubR1

Mad2 and BubR1 (the vertebrate homolog of yeast Mad3) directly bind to Cdc20 and inhibit APC/C^{Cdc20} *in vitro* (Fang, Yu et al. 1998; Tang, Bharadwaj et al. 2001). Mad2 and BubR1 together inhibit APC/C with greater efficiency than either alone does (Fang 2002). Indeed, Mad2 and BubR1 are parts of a larger mitotic checkpoint complex (MCC) that contains Mad2, BubR1, Bub3, and Cdc20, and inhibit APC/C^{Cdc20} synergistically *in vivo* (Sudakin, Chan et al. 2001; Yu 2002). On the other hand, depletion of either Mad2 or BubR1 from human cells by RNA interference (RNAi) accelerates mitotic progression and shortens the mitotic duration between nuclear envelope breakdown and anaphase onset (Meraldi, Draviam et al. 2004). Depletion of both has a greater effect than depletion of either alone, suggesting that Mad2 and BubR1 might have residual APC/C-inhibitory activities in the absence of each other.

Conformational activation of Mad2

Mouse genetic studies have demonstrated the physiological importance of the Mad2–Cdc20 interaction in maintaining chromosomal stability (Li, Fang et al. 2009). Consistently, binding of Mad2 to Cdc20 is tightly regulated by the spindle checkpoint. Efforts to understand this regulation have led to the discovery that Mad2 is an unusual two-state protein (Fang, Yu et al. 1998; Luo, Fang et al. 2000; Luo, Tang et al. 2002; Sironi, Mapelli et al. 2002; Luo, Tang et al. 2004; De Antoni, Pearson et al. 2005; Mapelli, Massimiliano et al. 2007; Yang, Li et al. 2008). Mad2 has two native folds: a latent open conformer (O-Mad2; also known as N1-Mad2) and a closed conformer (C-Mad2; also known as N2-Mad2) that is more active in Cdc20 binding and APC/C inhibition. The current available evidence is consistent with the following model for the conformational activation of Mad2 (Mapelli and Musacchio 2007; Luo and Yu 2008) (Figure 1-3). Mad2 binds to its upstream regulator Mad1 throughout the cell cycle, forming a tight Mad1–C-Mad2 core complex. Upon spindle checkpoint activation, the Mad1–Mad2 core complex is targeted to unattached kinetochores, and further recruits cytosolic O-Mad2 through O–C Mad2 dimerization. The asymmetric O–C Mad2 dimerization induces a conformational change of O-Mad2, which adopts a transient intermediate conformation (I-Mad2). I-Mad2 can complete the O–C conformational activation and dissociate from the Mad1–Mad2 core to become C-Mad2 without a ligand, which then binds Cdc20. Alternatively, I-Mad2 is directly captured by kinetochore-bound Cdc20, forming the Mad2–Cdc20 complex. How Mad2 binding to Cdc20 inhibits APC/C is not understood.

BubR1/Mad3 as a pseudo-substrate inhibitor of APC/C^{Cdc20}

BubR1 inhibits the activity of APC/C^{Cdc20} more effectively than Mad2 does *in vitro* (Tang, Bharadwaj et al. 2001; Fang 2002). BubR1 contains an N-terminal tetratricopeptide repeat (TPR) domain required for kinetochore targeting, a conserved GLEBS motif that mediates Bub3 binding, and a C-terminal kinase domain. The kinase domain of BubR1 is not conserved in yeast and is not required for APC/C inhibition. Many studies have been devoted to dissect the functions of various domains of BubR1 and to understand the mechanism by which BubR1 inhibits APC/C^{Cdc20} (Burton and Solomon 2007; King, van der Sar et al. 2007; Sczaniecka, Feoktistova et al. 2008; Malureanu, Jeganathan et al. 2009; Rahmani, Gagou et al. 2009; D'Arcy, Davies et al. 2010; Elowe, Dulla et al. 2010).

Yeast Mad3 contains KEN boxes, which are required for Mad3 binding to Cdc20 and for the spindle checkpoint function of Mad3 (Burton and Solomon 2007; King, van der Sar et al. 2007; Sczaniecka, Feoktistova et al. 2008). Furthermore, the KEN boxes of Mad3 compete with KEN-box-containing APC/C substrates for binding to Cdc20. The requirement for the KEN box of BubR1 in Cdc20 binding and in the spindle checkpoint is conserved in higher organisms, including human, mouse, and fly (Malureanu, Jeganathan et al. 2009; Rahmani, Gagou et al. 2009; Elowe, Dulla et al. 2010). Interestingly, BubR1/Mad3 itself does not undergo APC/C^{Cdc20}-dependent degradation. Therefore, these results suggest that BubR1/Mad3 acts as a competitive, pseudo-substrate inhibitor of APC/C^{Cdc20}.

These findings raise two unresolved questions. First, why is BubR1 not ubiquitinated by APC/C^{Cdc20} and degraded? Acetylation of BubR1 at K250 by the acetyltransferase PCAF has been suggested to allow BubR1 to escape APC/C^{Cdc20}-dependent ubiquitination (Choi,

Choe et al. 2009). The underlying mechanism of how acetylation prevents BubR1 ubiquitination is not established, however. Second, two major APC/C^{Cdc20} substrates, cyclin B and securin, contain a D-box. If BubR1 uses its KEN-box to compete with substrates for binding to APC/C^{Cdc20}, how does it inhibit D-box-dependent ubiquitination? Along this vein, several studies have shown that human BubR1 contains other Cdc20-binding motifs, in addition to the KEN-boxes (Tang, Bharadwaj et al. 2001; Davenport, Harris et al. 2006; Elowe, Dulla et al. 2010). It will be interesting to test whether these BubR1 motifs block D-box-dependent ubiquitination by APC/C^{Cdc20}.

Inhibition of APC/C by MCC

Although BubR1 and Mad2 can independently inhibit APC/C^{Cdc20} *in vitro*, they most likely collaborate with each other to inhibit APC/C^{Cdc20} in cells by forming MCC. By using purified chromosomes from mitotic arrested HeLa extract, Kulukian *et al.* have investigated the role of unattached kinetochores in MCC generation and APC/C^{Cdc20} inhibition (Kulukian, Han et al. 2009). Unattached kinetochores enhance inhibition of APC/C by purified MCC components (Mad2, BubR1, and Bub3) and binding of BubR1 to APC/C^{Cdc20}. This enhancement depends on kinetochore-bound Mad1–Mad2 core complex and Mad2 dimerization. These results suggest that unattached kinetochores produce active Mad2 (C-Mad2) and assemble an initial Mad2–Cdc20 complex to promote further interaction with BubR1–Bub3. Thus, this study provides further support a role of unattached kinetochores in the formation of MCC (Figure 1-3).

How does MCC inhibit APC/C^{Cdc20}? Recent EM studies of APC/C bound to Cdh1 or bound to MCC have provided key insights into this question (Herzog, Primorac et al. 2009; Buschhorn, Petzold et al. 2011; da Fonseca, Kong et al. 2011; Schreiber, Stengel et al. 2011). It appears that Cdc20 alone and Cdc20 as a component of MCC bind to APC/C in different orientations and at different sites. In other words, binding of BubR1–Bub3 and Mad2 to Cdc20 alters the interaction between Cdc20 and APC/C. In doing so, they may compromise the substrate-recognition site formed between Cdc20 and Apc10. Therefore, MCC inhibits the activity of APC/C^{Cdc20} by blocking productive substrate binding both competitively and non-competitively.

Inhibition of APC/C by Cdc20 phosphorylation

Cdc20 can be phosphorylated by Bub1, MAPK, and Cdk1 (Chung and Chen 2003; D'Angiolella, Mari et al. 2003; Tang, Shu et al. 2004). Phosphorylation of Cdc20 at S153 by Bub1 has been shown to inhibit the activity of APC/C^{Cdc20} (Tang, Shu et al. 2004). Similar to BubR1, Bub1 contains KEN-boxes that interact with Cdc20 (Kang, Yang et al. 2008). KEN-box-dependent binding then recruits Cdc20 to Bub1 and enables efficient phosphorylation of Cdc20 by Bub1. Bub1 is phosphorylated in mitosis, and the chromosome-bound Bub1 is hyperphosphorylated, suggesting that the kinase activity of Bub1 might be enhanced during checkpoint activation (Chen 2004). It is unclear how phosphorylation of Cdc20 inhibits APC/C^{Cdc20}. It is also unknown whether and how Bub1-mediated phosphorylation of Cdc20 regulates MCC formation in cells.

SPINDLE CHECKPOINT SILENCING

After all sister chromatids are properly attached to kinetochores, the spindle checkpoint needs to be inactivated to release its inhibition of APC/C^{Cdc20}, allowing anaphase onset. Several mechanisms have been implicated in spindle checkpoint silencing (Figure 1-4 & 1-5), including dynein-dependent removal of checkpoint proteins from kinetochores, $p31^{comet}$ binding to and inhibition of C-Mad2, Mad2 phosphorylation, and APC/C-dependent ubiquitination and proteolysis.

Dynein-mediated removal of checkpoint proteins from kinetochores

The dynein/dynactin complex, a minus-end-directed microtubule motor, is required for transporting Mad1 and Mad2 from kinetochores to spindle poles following kinetochore-microtubule attachment (Howell, McEwen et al. 2001). Blocking this transport by microinjection of a dynein antibody causes prolonged metaphase arrest, indicating a crucial role of this process in checkpoint silencing. Recently, growing evidence has implicated the RZZ complex and spindly in regulating this process (Figure 1-4).

RZZ is an evolutionarily conserved kinetochore complex consisting of Rod–Zwich–ZW10 (Karess 2005). It is transported from kinetochores to spindle poles during checkpoint silencing. Spindly is another conserved kinetochore protein that regulates the dynein-mediated transport of Rod and Mad2 at metaphase (Griffis, Stuurman et al. 2007; Yamamoto, Watanabe et al. 2008; Chan, Fava et al. 2009; Barisic, Sohm et al. 2010; Gassmann, Holland et al. 2010). It is also transported from kinetochores to spindle poles in a dynein-dependent

manner following kinetochore-microtubule attachment. The kinetochore localization of spindly depends on the RZZ complex. Depletion of Spindly reduces dynein localization at kinetochores. Moreover, a conserved motif in spindly has been shown to be critical for targeting dynein to kinetochores (Barisic, Sohm et al. 2010; Gassmann, Holland et al. 2010). Expression of a spindly mutant with this motif mutated in cells depleted of endogenous spindly prevents the dynein-dependent removal of checkpoint proteins, resulting in defective checkpoint inactivation. Therefore, it appears that spindly bridges the interaction between RZZ and dynein, and is critical for checkpoint inactivation (Figure 1-4).

p31^{comet} binding to C-Mad2

The Mad2-binding protein, p31^{comet} (initially called Cmt2), adopts a tertiary fold similar to that of Mad2 (Habu, Kim et al. 2002; Yang, Li et al. 2007). It selectively binds to the active C-Mad2 conformer and blocks its function in two ways (Xia, Luo et al. 2004; Mapelli, Filipp et al. 2006; Yang, Li et al. 2007). First, it binds to the Mad1–Mad2 core complex and prevents the further recruitment and activation of O-Mad2 (Figure 1-4). Second, it binds to Cdc20-bound C-Mad2 and neutralizes the Mad2-inhibitory effects on APC/C^{Cdc20}. Consistent with its Mad2-inhibitory activity, overexpression of p31^{comet} causes mitotic exit in presence of the spindle poison, nocodazole. Conversely, depletion of p31^{comet} delays mitotic exit during the recovery from nocodazole-induced mitotic arrest. Therefore, p31^{comet} is critical for checkpoint silencing. How p31^{comet} blocks the APC/C^{Cdc20}-inhibitory activity of Mad2 without disrupting the Mad2–Cdc20 interaction is not understood.

Phosphorylation of Mad2

Mad2 is phosphorylated on multiple sites in its C-terminal region (Wassmann, Liberal et al. 2003). Phosphorylation appears to inhibit Mad2 function, as Mad2 mutants with multiple phosphorylatable residues mutated to aspartates cannot bind to Mad1 or Cdc20. In a recent study, we have further characterized the effects of Mad2 phosphorylation (Kim, Sun et al. 2010). We show that phosphorylation of Mad2 at a single site, S195, hinders its O–C conformational change. Consistently, the phospho-mimicking Mad2^{S195D} mutant fails to bind to Cdc20, a low-affinity ligand. Interestingly, Mad2^{S195D} still binds to high-affinity ligands, such as Mad1 and MBP1 (an artificial Mad2-binding peptide), forming ligand-bound C-Mad2. Mad2^{S195D} overexpression causes spindle checkpoint defects in human cells. Mad2^{S195D} appears to bind to the Mad1–Mad2 core complex with higher affinity, forming a stable Mad1–Mad2–Mad2 complex. Thus, we speculate that phosphorylation of Mad2 at S195 may prevent unscheduled activation of Mad2. Alternatively, it may contribute to checkpoint inactivation by capping the Mad1–Mad2 complex and blocking further conformational activation of Mad2, a function that is analogous to that of *p*31^{comet}. The kinase responsible for phosphorylating Mad2 S195 is unknown. Given the function of Mps1 in recruiting O-Mad2 to the Mad1–Mad2 core complex at the kinetochores, it will be interesting to test whether Mps1 phosphorylates this site on Mad2.

In the same study (Kim, Sun et al. 2010), we have discovered a peculiar effect of the monomeric mutant of Mad2, Mad2^{R133E,Q134A}. We have shown previously that overexpression of another monomeric Mad2 mutant, Mad2^{R133A}, in HeLa cells causes mitotic arrest in the absence of spindle damage, indicating Mad2 dimerization per se is not required for

APC/C^{Cdc20} inhibition (Luo, Tang et al. 2004). By contrast, overexpression of $Mad2^{R133E,Q134A}$ in human cells not only does not cause mitotic arrest, but also inhibits the functions of the endogenous Mad2 in a dominant-negative manner (Kim, Sun et al. 2010). Because $Mad2^{R133E,Q134A}$ retains its ability to bind to Cdc20, this result suggests that the Mad2 dimerization helix interacts with a yet unidentified protein in cells, and this interaction is critical for APC/C^{Cdc20} inhibition.

APC/C-dependent Cdc20 ubiquitination

APC/C is the molecular target of the spindle checkpoint. Conversely, APC/C targets several spindle checkpoint proteins for degradation, including Mps1 and Bub1 (Palframan, Meehl et al. 2006; Qi and Yu 2007; Cui, Cheng et al. 2010). A recent study has implicated APC/C-dependent ubiquitination in checkpoint silencing (Zeng, Sigoillot et al. 2010). In this study, Zeng *et al.* discover a small molecule called TAME, which prevents APC/C activation by Cdc20 and Cdh1. TAME causes mitotic arrest in human cells. Paradoxically, this mitotic arrest is dependent on the spindle checkpoint, as Mad2 depletion or Aurora B inhibition alleviates TAME–mediated mitotic arrest. A possible explanation for this finding is that partial inhibition of APC/C prevents checkpoint inactivation, but allows cyclin B degradation and mitotic exit in the absence of checkpoint signaling.

The targets of APC/C in checkpoint inactivation remain elusive. Artificial elevation of Mps1 levels or activity can prevent mitotic exit (Palframan, Meehl et al. 2006), although it remains to be demonstrated whether a non-degradable form of Mps1 delays mitotic exit. A non-degradable mutant of Bub1 with its KEN-boxes mutated does not delay anaphase onset

and mitotic exit (Qi and Yu 2007). A caveat of this study is that the KEN-boxes of Bub1 are also required for efficient Cdc20 phosphorylation (Kang, Yang et al. 2008). The non-degradable Bub1 mutant is also partially defective in its checkpoint function. Finally, Cdc20 itself undergoes autoubiquitination (Pan and Chen 2004) (Figure 1-5). There are conflicting results on the functions of Cdc20 ubiquitination.

In yeast, Cdc20 autoubiquitination and degradation require Mad2 and Mad3 binding, and have been proposed as an APC/C^{Cdc20}-inhibitory checkpoint mechanism (Pan and Chen 2004). As discussed above, EM studies suggest that Cdc20 in complex with checkpoint proteins binds to different sites on APC/C, as compared to Cdc20 alone. It is possible that the repositioning of Cdc20 caused by Mad2 and Mad3 binding blocks ubiquitination of securin and cyclin B, but favors Cdc20 autoubiquitination.

Cdc20 autoubiquitination is a conserved process in mammalian cells, and is stimulated by $p31^{comet}$ and UbcH10 (Reddy, Rape et al. 2007; Stegmeier, Rape et al. 2007). In two related studies, Cdc20 ubiquitination is reported to cause dissociation of Mad2 from Cdc20 (Reddy, Rape et al. 2007; Stegmeier, Rape et al. 2007) (Figure 1-5). Moreover, Usp44, a ubiquitin isopeptidase, has been proposed to prevent the autoubiquitination of Cdc20 and maintain the Mad2–Cdc20 interaction during checkpoint activation. Thus, these two studies implicate Cdc20 autoubiquitination as an important mechanism for checkpoint inactivation.

In a later study, Nilsson *et al.* have constructed a lysine-less Cdc20 mutant that cannot be ubiquitinated (Nilsson, Yekezare et al. 2008). They show that this mutant still dissociates from Mad2 when the checkpoint is inactivated, suggesting that Cdc20 autoubiquitination is

not the sole mechanism to dissociate Mad2 from Cdc20. Interestingly, ectopic expression of the lysine-less Cdc20 mutant, even to low levels, causes checkpoint defects. It then appears that Cdc20 ubiquitination might be required for the establishment of the spindle checkpoint, although the underlying mechanism is unclear. Further studies are needed to resolve these apparent discrepancies with respect to Cdc20 autoubiquitination and to uncover the molecular target(s) of APC/C during checkpoint inactivation.

The spindle checkpoint is in essence an intracellular signal transduction system. Checkpoint signals originate at unattached or tensionless kinetochores and are propagated through the combined actions of kinase activation and a regulated conformational change of Mad2. The end point of this signaling system is the sequestration of Cdc20 and inhibition of APC/C. Recent studies highlight partial functional redundancy among multiple mechanisms in each of the key steps of checkpoint signaling, including the kinetochore recruitment of checkpoint proteins, APC/C inhibition, and checkpoint silencing. Structural analysis of regulated protein–protein interactions among kinetochore and checkpoint proteins in this system is required for designing separation-of-function mutants of key players. These reagents will be critical for dissecting the precise contributions of the seemingly redundant mechanisms in living cells.

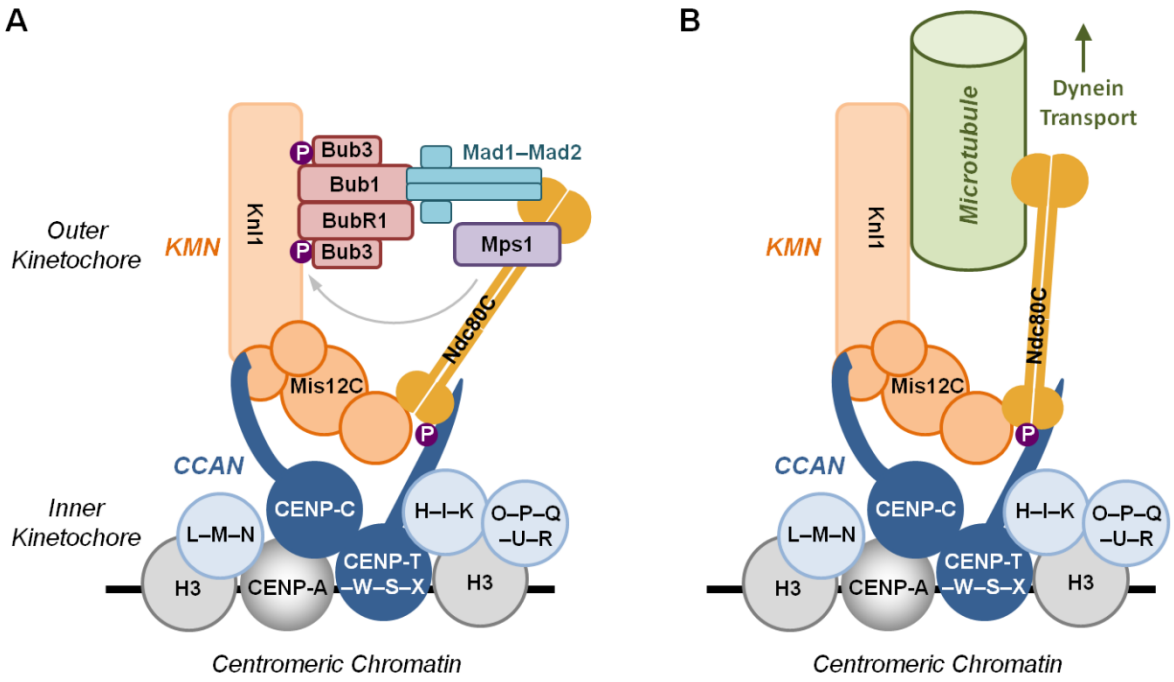

Figure 1-1. Kinetochore targeting of spindle checkpoint proteins and microtubule binding by the KMN network. (A) The CENP-A nucleosome is the key determinant of centromeric chromatin. The constitutive centromere-associated network (CCAN) associates with the CENP-A nucleosome throughout the cell cycle. In mitosis, CENP-C and CENP-T in CCAN recruit the KMN network consisting of Knl1, the Mis12 complex (Mis12C), and the Ndc80 complex (Ndc80C). Mitosis-specific binding of KMN to CCAN is possibly regulated by Cdk1-dependent phosphorylation of CENP-T. KMN serves as an important binding platform for the spindle checkpoint proteins, including Mps1, Bub1–Bub3, BubR1–Bub3, and Mad1–Mad2. Phosphorylation of Knl1 by Mps1 enhances Bub1–Bub3 binding to Knl1. Mad1 has an extensive kinetochore-binding interface, and its C-terminal domain may interact with Bub1. (B) KMN is a key kinetochore receptor of spindle microtubules. It has two microtubule-binding interfaces: the N-terminal region of Knl1 and the head domains of Ndc80 and Nuf2. Microtubule binding to KMN may displace spindle checkpoint proteins. The checkpoint proteins can also be depleted from attached kinetochores through dynein-dependent, poleward transport along microtubules.

Figure 1-2. Models for Aurora B activity gradient. Proper microtubule attachment at kinetochores generates tension across sister kinetochores and physically separate Aurora B and its substrates at the outer kinetochore. Diminished phosphorylation of these substrates enables PP1 binding, which further dephosphorylates key substrates of Aurora B and other substrates and promotes checkpoint silencing.

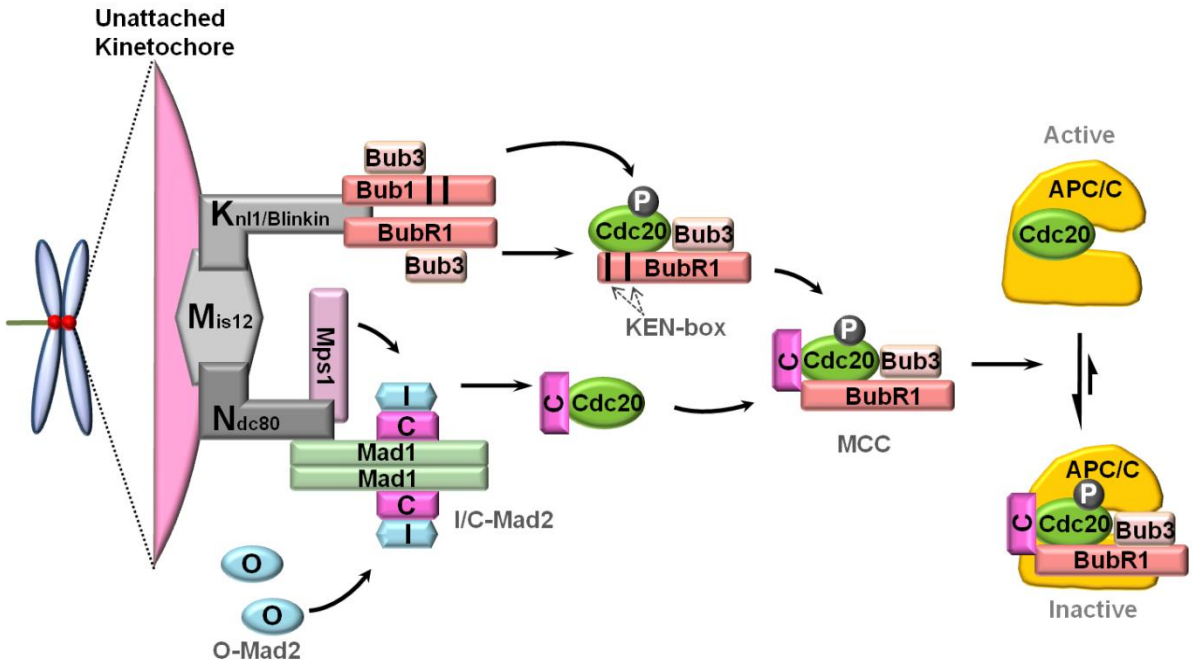

Figure 1-3. Generation of APC/C-inhibitory checkpoint signals by unattached kinetochores. Mad2 and BubR1 directly bind to Cdc20, forming a larger mitotic checkpoint complex (MCC; BubR1–Bub3–Cdc20–Mad2) to inhibit APC/C^{Cdc20}. Unattached kinetochores recruit and activate Mad2 and BubR1 to promote MCC assembly. The KMN (Knl1–Mis12–Ndc80) network of kinetochore proteins provides a major platform for the recruitment of checkpoint proteins, including Bub1 and BubR1. BubR1 and Bub1 bind to Cdc20 through conserved KEN-boxes (indicated as black bars) and other motifs. The kinetochore targeting of the Mad1–Mad2 core complex also depends on Mps1 and Ndc80. Kinetochore-bound Mad1–Mad2 catalyzes O–C conformational activation of Mad2. MCC binds to and inhibits APC/C^{Cdc20} through blocking substrate recognition. Bub1 phosphorylates Cdc20 and contributes APC/C^{Cdc20} inhibition.

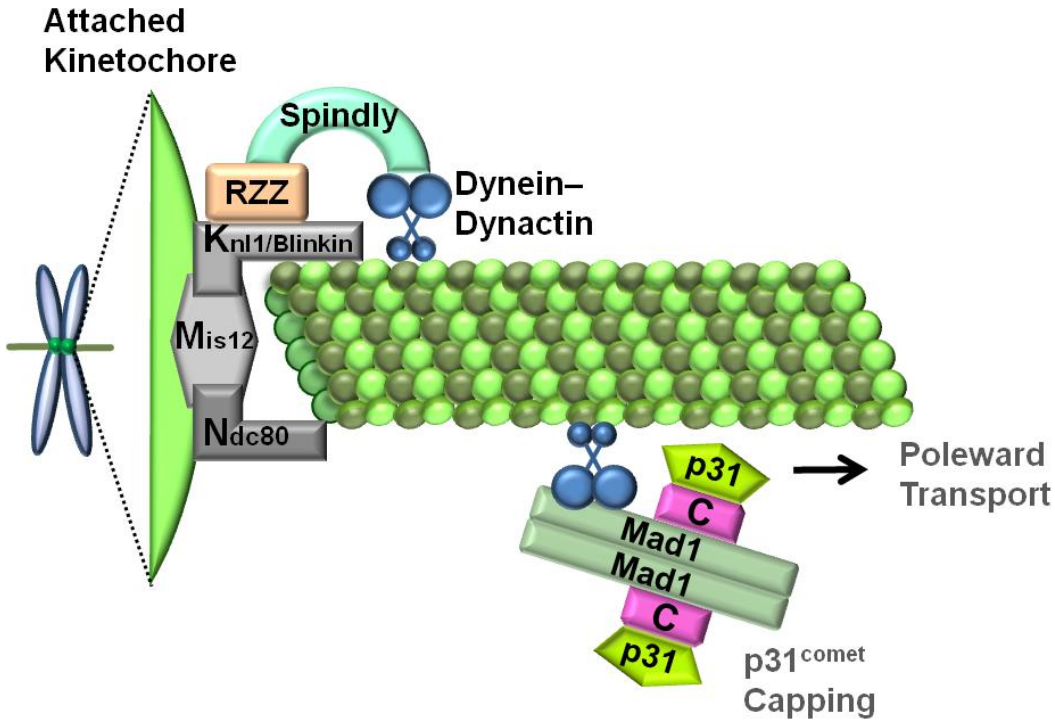

Figure 1-4. Spindle checkpoint inactivation by dynein- and microtubule-dependent removal of Mad1–Mad2 from kinetochores and by p31^{comet} binding to C-Mad2. Dynein–dynactin is recruited to properly attached kinetochores by RZZ and spindly, and mediates the poleward transport of Mad1–Mad2. p31^{comet} binds to C-Mad2 in the Mad1–Mad2 core complex and blocks the recruitment and activation of cytosolic O-Mad2.

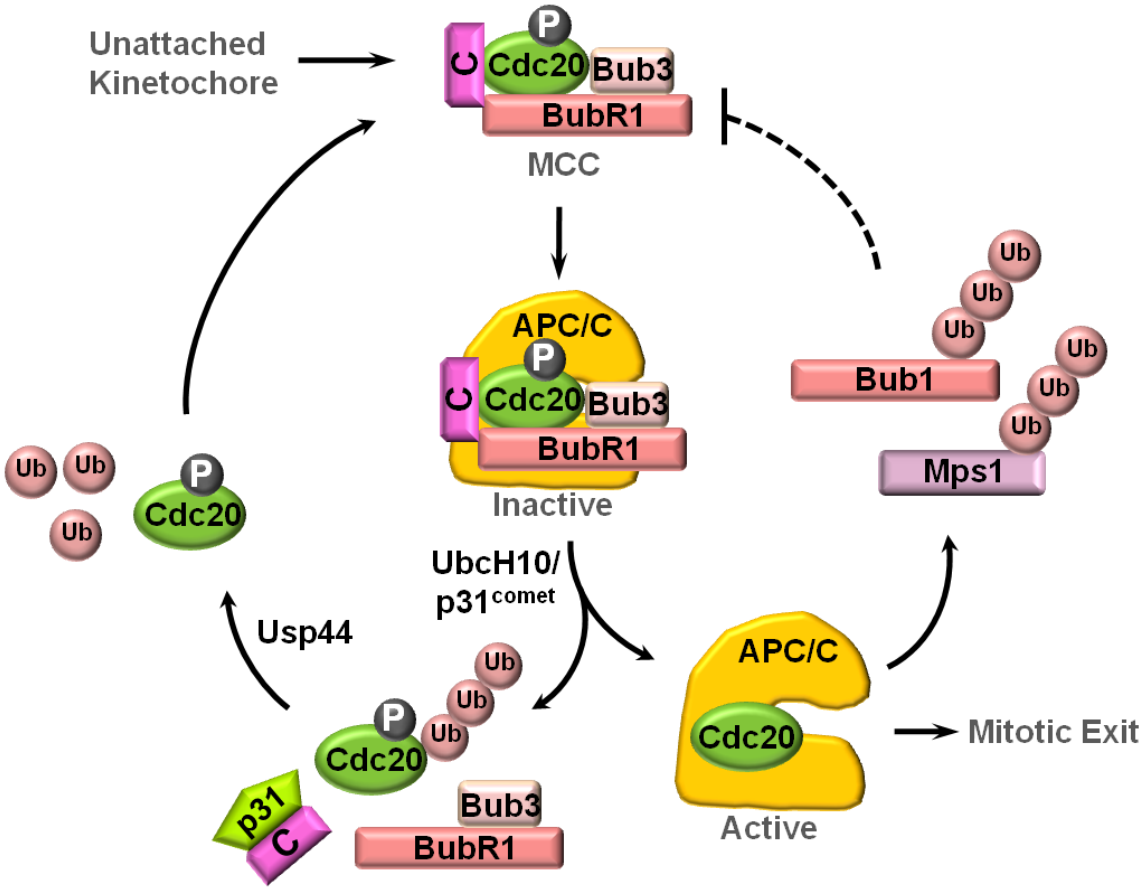

Figure 1-5. Mutual regulation between APC/C^{Cdc20} and the spindle checkpoint. APC/C targets spindle checkpoint proteins, including Bub1 and Mps1, for ubiquitination and degradation, and indirectly regulates the kinetochore-dependent production of MCC. When bound to APC/C, Cdc20 as a subunit of MCC undergoes autoubiquitination, which is stimulated by UbcH10 and p31^{comet} and removed by Usp44. Paradoxically, Cdc20 autoubiquitination has been proposed to regulate both checkpoint activation and inactivation.

CHAPTER II: MAD2 PHOSPHORYLATION REGULATES ITS CONFORMATIONAL TRANSITION

INTRODUCTION

Faithful duplication and segregation of chromosomes are critical tasks during the cell cycle. To ensure accurate chromosome segregation during mitosis, the spindle checkpoint inhibits the anaphase-promoting complex or cyclosome (APC/C) to prevent the degradation of securin and cyclin B, until all sister chromatids are properly attached to spindle microtubules (Bharadwaj and Yu 2004; Musacchio and Salmon 2007). Key components of the spindle checkpoint include the evolutionarily conserved Mad (mitotic arrest deficiency) and Bub (budding uninhibited by benomyl) proteins. In response to unattached or untense kinetochores, these proteins collaborate to inhibit APC/C and block anaphase onset.

Among the APC/C-inhibitory checkpoint mechanisms, Mad2 directly binds to the mitotic APC/C activator Cdc20, as part of a large complex that also contains BubR1 and Bub3, and inhibits its ability to activate APC/C (Yu 2002; Yu 2007). Mad2 is a two-state protein that has two native folds: a latent N1 or open conformer (O-Mad2) and an N2 or closed conformer (C-Mad2) that is more active in Cdc20 binding and APC/C inhibition (Luo, Fang et al. 2000; Luo, Tang et al. 2002; Luo, Tang et al. 2004). A major difference between the two Mad2 conformers lies in the conformation of their C-terminal region. O-Mad2 is a kinetically trapped high-energy conformer and spontaneously converts to C-Mad2 with slow kinetics ($t_{1/2}$ on the order of hours) *in vitro*. In cells, cytosolic O-Mad2 is recruited to the kinetochore-bound Mad1–Mad2 core complex through O-Mad2–C-Mad2 asymmetric

dimerization (Sironi, Mapelli et al. 2002; Luo, Tang et al. 2004; Shah, Botvinick et al. 2004; De Antoni, Pearson et al. 2005; Mapelli, Massimiliano et al. 2007; Mapelli and Musacchio 2007). O-Mad2 bound to the Mad1–Mad2 core converts to an intermediate conformer (I-Mad2), which may directly bind to Cdc20 (see Figure 2-9A below, pathway **a**) (Mapelli, Filipp et al. 2006; Mapelli and Musacchio 2007; Yang, Li et al. 2008). I-Mad2 can also complete the O–C conformational change on its own and dissociates from the Mad1–Mad2 core as unliganded C-Mad2, which then binds to Cdc20 (Figure 2-9A, pathway **b**) (Yu 2006; Luo and Yu 2008; Yang, Li et al. 2008).

After all sister kinetochores attach properly to spindle microtubules, the spindle checkpoint is inactivated to allow APC/C activation and anaphase onset. The Mad2 inhibitor $p31^{comet}$ is critical for checkpoint inactivation (Habu, Kim et al. 2002; Xia, Luo et al. 2004). It binds to the Mad1–Mad2 core complex and prevents further Mad1-assisted conformation activation of Mad2 (Mapelli, Filipp et al. 2006; Yang, Li et al. 2007). It also binds to Cdc20-bound Mad2 and promotes UbcH10-dependent Cdc20 autoubiquitination and the disassembly of the Mad2–Cdc20-containing APC/C-inhibitory complexes (Xia, Luo et al. 2004; Reddy, Rape et al. 2007; Stegmeier, Rape et al. 2007). Consistently, depletion of $p31^{comet}$ by RNA interference (RNAi) from HeLa cells delays mitotic exit following the release from nocodazole-mediated mitotic arrest (Xia, Luo et al. 2004). On the other hand, $p31^{comet}$ depletion does not cause a mitotic arrest in the absence of spindle poisons, suggesting the existence of additional checkpoint inactivation mechanisms.

The $Mad2^{\Delta C}$ mutant with its C-terminal 10 residues deleted only adopts the O-Mad2 conformation and cannot bind to either Mad1 or Cdc20, indicating the importance of the C-

terminal region of Mad2 in its conformational transition (Luo, Tang et al. 2004). Intriguingly, multiple residues in the C-terminal region of Mad2 are phosphorylated, including S170, S178, S185, and S195 (Wassmann, Liberal et al. 2003). Overexpression of phospho-mimicking mutants Mad2-4D (with S170, S178, S185, and S195 mutated to aspartate) and Mad2-3D (with S170, S178, and S195 mutated to aspartate) that do not bind to either Mad1 or Cdc20 in human cells causes checkpoint defects, suggesting that Mad2 phosphorylation inhibits its function and may contribute to checkpoint inactivation (Wassmann, Liberal et al. 2003). The mechanism by which these Mad2 phospho-mimicking mutants abrogate the spindle checkpoint in a dominant-negative manner is not understood.

Here, we investigated the effects of Mad2 phosphorylation on the unusual two-state behavior of Mad2. Using nuclear magnetic resonance (NMR) spectroscopy, we showed that phospho-mimicking mutations blocked the O–C conformational transition of Mad2 and identified S195 as a functionally important phosphorylation site. We synthesized a Mad2 protein specifically phosphorylated on S195 using intein-mediated ligation and confirmed that S195 phosphorylation greatly hindered the conformation change of Mad2. Mad2^{S195D} failed to bind to Cdc20 with appreciable affinity, but retained its binding to Mad1 and MBP1 (an unnatural Mad2-binding peptide identified in phage display). Thus, binding of high-affinity ligands, such as Mad1 and MBP1 to Mad2^{S195D}, compensates for the unfavorable O-C Mad2 conformational change and drives the formation of ligand-bound C-Mad2. Overexpression of the phospho-mimicking Mad2^{S195D} mutant abrogated the spindle checkpoint in cells. Unexpectedly, Mad2^{S195D} exhibited enhanced binding to the Mad1–Mad2 core complex through O–C Mad2 dimerization, suggesting that S195 phosphorylation might

regulate the dimerization between O-Mad2 and C-Mad2. Taken together, our results show that Mad2 phosphorylation regulates its conformational transition and might contribute to checkpoint inactivation through differentially regulating Mad2 binding to Mad1 and Cdc20.

MATERIALS AND METHODS

Cell Culture and Transfection

HeLa Tet-On (Clontech) cells were grown in Dulbecco's modified Eagle's medium (DMEM; Invitrogen) supplemented with 10% fetal bovine serum (FBS). pCS2-Myc Mad2^{S195D}, Mad2^{S195A}, Mad2^{Mono} (Mad2$^{R133A/Q134E}$), and Mad2$^{Mono/S195A}$ vectors were generated using the QuikChange XL site-directed mutagenesis kit (Stratagene). Plasmid transfection was performed with the Effectene reagent (Qiagen) according to manufacturer's instructions. The siRNA oligonucleotides targeting human Mad2 were chemically synthesized and contained sequences corresponding to nucleotides 143-165 of the cording region of Mad2. siRNA transfection was performed with Lipofectamine RNAiMAX (Invitrogen) according to manufacturer's protocols. When indicated, cells were arrested at metaphase with 300 nM nocodazole (Sigma) for 16-18 hrs prior to harvesting.

Flow Cytometry (FACS)

For FACS analysis, cells were collected by trypsinization, washed once with PBS, and fixed with cold 70% ethanol. After overnight fixation at -20˚C, cells were washed with PBS and permeabilized with a 5-min incubation in PBS plus 0.25% (v/v) Triton X-100. Cells were then incubated with α-MPM2 (Millipore) followed by an incubation with fluorescent secondary antibodies (Invitrogen) diluted in PBS plus 1% BSA. After washing with PBS, the cells were stained with propidium iodide (Sigma) at a final concentration of 20 μg/ml; and simultaneously treated with 200 μg/ml RNAase A (Qiagen). The flow cytometry reading was

performed with FacsScan (Becton Dickinson). The results were analyzed with the FlowJo software (Tree Star).

Metabolic ^{32}P Labeling

About 6 X 10^5 HeLa Tet-On cells were transfected with pCS2-Myc Mad2-wt or Mad2^{S195A} for 22 hrs and treated with nocodazole for another 14 hrs. The cells were then released into the labeling medium (phosphate-depleted DMEM plus 5% dialyzed FBS) for 2 hrs followed by another 2 hr-incubation in the labeling medium plus ^{32}P-orthophosphate (0.3-0.5 mCi/60-mm plate; PerkinElmer). The cells were then lysed with the RIPA buffer (1% NP-40, 1% sodium deoxycholate, 0.1% SDS, 10 mM sodium phosphate, pH 7.2, 2 mM EDTA, 50 mM sodium fluoride, 0.2 mM sodium vanadate, and 1X protease inhibitor cocktail). The Myc-Mad2 proteins were immunoprecipitated from the cleared cell lysate with α-Myc antibody (Roche), separated on SDS-PAGE, and transferred to a nitrocellulose membrane. The incorporation of ^{32}P was measured with a phosphorimager (FLA-5100; Fujifilm). The same membrane was blotted with α-Mad2 to compare the total amounts of precipitated proteins.

Protein Expression and Purification

The wild-type and mutant Mad2 proteins were expressed and purified as described (Luo, Tang et al. 2004; Yang, Li et al. 2008).

In Vitro Binding Assay

To assay Mad2 binding to Cdc20 or Mad1, the N-terminal fragment of Cdc20 (residues 1-170; Cdc20N) and full-length Mad1 were translated in reticulocyte lysate in the presence of ^{35}S-methionine. Purified His_6-tagged wt or mutant Mad2 proteins were bound to Ni^{2+}-NTA beads (Qiagen), incubated with ^{35}S-labeled Mad1 or Cdc20N, and washed three times with TBS containing 0.05% Tween. The bound proteins were separated by SDS-PAGE and analyzed with a phosphorimager (Fujifilm).

Intein-mediated Protein Ligation

The cDNA encoding the Mad2N fragment (residues 1-186) was amplified by PCR and cloned into pTXB1 (New England Biolabs) between the NdeI and SapI sites. Expression of pTXB1-Mad2N in BL21(DE3) produced Mad2N-intein-CBD fusion protein, which was bound to chitin beads. Chitin beads were washed with the ligation buffer (50 mM HEPES, pH 7.5, 250 mM NaCl). The ligation peptide containing residues 187-205 of Mad2, except that T187 was replaced with a cysteine and S195 with a phospho-serine, was chemically synthesized. The Mad2N-intein-CBD fusion protein on chitin beads was incubated with 1 mM ligation peptide and 60 mM 2-mercaptoethanesulfonic acid (MESNA) in the ligation buffer at room temperature overnight. The ligation product was eluted from the beads and further purified using anion exchange and size exclusion chromatography. Based on mass spectrometry, the final ligation product contained residues 2-205 of Mad2 with the expected T187C mutation and phospho-S195. The first methionine of Mad2N was presumably removed by bacterial aminopeptidases.

NMR Spectroscopy

NMR experiments were performed at 30˚C on Varian Inova 600 or 800 MHz spectrometers equipped with four channels and pulsed-field gradients. 2D $^{1}H/^{15}N$ HSQC spectra were acquired on samples containing 0.8-1.2 mM ^{15}N-labeled $Mad2^{Mono}$, $Mad2^{Mono/S195D}$, and Mad2-3D in the NMR buffer (50 mM phosphate, pH 6.8, 300 mM KCl, and 1 mM DTT), in the absence or presence of 1:1.2 molar ratio of unlabeled MBP1 or the Mad2-binding fragments of Cdc20 (residues 124-137 of human Cdc20) or Mad1 (residues 495-718 of human Mad1). To monitor the conformational change of Mad2, a series of 1D ^{1}H NMR spectra, each lasting 30 min, was acquired on samples containing 0.1 mM Mad2-wt, Mad2-2D, Mad2-3D, Mad2-4D, $Mad2^{S195D}$, and $Mad2^{pS195}$ initially in the O-Mad2 state in the NMR buffer.

RESULTS AND DISCUSSION

The Phospho-mimicking Mutants of Mad2 Preferentially Adopt the O-Mad2 Conformation

Previous studies showed that multiple residues including S170, S178, S185, and S195 in the C-terminal region of Mad2 were phosphorylated (Wassmann, Liberal et al. 2003). Because the C-terminal region of Mad2 is critical for Mad2 structural conversion, we hypothesized that phosphorylation of this region of Mad2 regulated its conformational change. Two phospho-mimicking mutants of Mad2, Mad2-3D and Mad2-4D, blocked spindle checkpoint signaling in cells in a dominant-negative manner (Wassmann, Liberal et al. 2003). To test the potential effect of phosphorylation on the two-state behavior of Mad2, we first monitored the conformational transition of Mad2-3D and Mad2-4D phospho-mimicking mutants *in vitro* using 1D ^{1}H NMR spectroscopy. The wild-type (wt) Mad2, Mad2-3D, and Mad2-4D were purified in their O-Mad2 state with anion exchange chromatography at 4˚C and immediately analyzed with NMR. The 1D ^{1}H NMR spectra of these proteins were almost identical in the high-field methyl region (Figure 2-1A), indicating that the phospho-mimicking mutations did not grossly alter Mad2 folding and that Mad2-3D and Mad2-4D adopted O-Mad2 conformation. Upon incubation at 30˚C for 24 hrs, Mad2-wt underwent O–C conformational change and formed dimers, as evidenced by line broadening and the appearance of the –0.3 ppm peak that belonged to V197 in C-Mad2 (Luo, Tang et al. 2002; Luo, Tang et al. 2004) (Figure 2-1A; red arrow). By contrast, the spectra of Mad2-3D and Mad2-4D did not change appreciably after the 24-hr incubation at 30˚C, indicating that

these mutants did not undergo the O–C conformational change during this time. Therefore, the phospho-mimicking mutations prevent Mad2 conformational transition.

Mad2-4D contained one additional mutation of S178, as compared to Mad2-3D. The fact that Mad2-3D and Mad2-4D behaved similarly in the cellular assays and in the NMR experiments suggested that phosphorylation of S178 might not be functionally important. Consistently, S178 was not conserved in other species (Figure 2-1B). By contrast, S170, S185, and S195 were conserved in metazoans.

Phosphorylation of S195 Hinders the Conformational Transition of Mad2

We sought to determine which phosphorylation site was critical for regulating the conformational change of Mad2. Inspection of the O- and C-Mad2 structures revealed that S170, S178, and S185 were surface exposed in both Mad2 conformers (Figure 2-1C). By contrast, S195 was located in the C-terminal tail and was surface exposed in O-Mad2, but it became buried in the interior of C-Mad2. Phosphorylation of S195 would introduce negative charges in the hydrophobic core of C-Mad2 and was expected to destabilize C-Mad2 and to favor the O-Mad2 conformation. Furthermore, the S195A mutation further reduced the phosphorylation levels of the Mad2 S170A/S178A double mutant in human cells (Wassmann, Liberal et al. 2003), indicating S195 was phosphorylated *in vivo*.

To verify that phosphorylation of Mad2 S195 occurred *in vivo*, we performed metabolic ^{32}P labeling assays (Figure 2-2A). Briefly, HeLa Tet-On cells were transfected with plasmids encoding Myc-tagged Mad2-wt or Mad2^{S195A}, arrested in mitosis with nocodazole, and released into medium containing ^{32}P-orthophosphate. The cells were lysed

and immunoprecipitated with α-Myc antibodies. The levels of ^{32}P incorporation into Myc-Mad2 were resolved by SDS-PAGE followed by autoradiography (Figure 2-2A). Myc-Mad2^{S195A} had 30% less ^{32}P incorporation, as compared to Myc-Mad2-wt. This result confirmed that Mad2 S195 was indeed phosphorylated *in vivo*, although it was not the only site of phosphorylation.

We next tested whether phosphorylation of the S195 site alone affected the Mad2 conformational change. To do so, we expressed and purified the phospho-mimicking Mad2^{S195D} mutant in the O-Mad2 state. We also generated the phospho-S195 Mad2 protein (Mad2^{pS195}) in the O-Mad2 state using the intein-mediated protein ligation method (Figure 2-2B) (Muralidharan and Muir 2006). Both Mad2^{S195D} and Mad2^{pS195} proteins were incubated at 30˚C for 24 hrs and analyzed with 1D ^{1}H NMR spectroscopy. The spectra of Mad2^{S195D} and Mad2^{pS195} were very similar to that of O-Mad2-wt and remained unchanged after the 24-hr incubation at 30˚C (Figure 2-2C). By contrast, the Mad2-2D mutant with S170 and S185 mutated to aspartate underwent the O–C conformational change after the incubation, similar to Mad2-wt (Figure 2-2C). Therefore, phosphorylation of Mad2 S195 prevents the conformational transition of Mad2. Mad2^{S195D} mimics this effect of S195 phosphorylation. Among the three conserved Mad2 phosphorylation sites, S195 is functionally most critical.

Mad2^{S195D} Binds to Mad1, but Not to Cdc20

Free Mad2^{S195D} cannot form C-Mad2 by itself. We next tested whether Mad2^{S195D} retained binding to Cdc20 or Mad1. We performed *in vitro* binding assays using recombinant purified Mad2-wt, Mad2^{S195D}, and Mad2$^{\Delta C}$ proteins. As the negative control, Mad2$^{\Delta C}$ did not

binding to either Mad1 or Cdc20, as it could not adopt the C-Mad2 conformation (Figure 2-3). Consistent with previous reports (Luo, Tang et al. 2004; Lad, Lichtsteiner et al. 2009; Simonetta, Manzoni et al. 2009), O-Mad2-wt bound less Cdc20 as compared to C-Mad2-wt, because C-Mad2-wt had a faster on-rate in Cdc20 binding (Figure 2-3). O-Mad2-wt bound more Mad1 as compared to C-Mad2-wt, presumably because O-Mad2-wt had a faster on-rate in Mad1 binding. $Mad2^{S195D}$ (which only adopted the O-Mad2 conformation in the absence of ligands) did not bind to Cdc20, but retained Mad1 binding, albeit to a lesser extent than O-Mad2-wt. Because all Mad2 molecules were bound to beads prior to Mad1 addition, this assay measured the formation of the Mad1–Mad2 core complex. As expected from the effect of the S195D mutation in destabilizing the C-Mad2 conformation, $Mad2^{S195D}$ was less efficient than O-Mad2-wt in forming the Mad1–Mad2 core complex *in vitro*.

To confirm the different binding behavior of $Mad2^{S195D}$ towards Mad1 and Cdc20, we monitored the binding between $Mad2^{S195D}$ and the Mad2-binding domains of Cdc20 or Mad1 using NMR. Because C-Mad2 had a tendency to oligomerize, we used ^{15}N-labeled monomeric mutants of Mad2 in these experiments. The 2D $^{1}H/^{15}N$ HSQC spectrum of $Mad2^{S195D}$ after the addition of Cdc20 contained two sets of peaks: one set belonged to free $O\text{-}Mad2^{S195D}$ whereas the other set belonged to the $C\text{-}Mad2^{S195D}$–Cdc20 complex (Figure 2-4). As shown in the inset of Figure 2-4A, the peak intensities of $C\text{-}Mad2^{S195D}$ were about 30% of those of O-Mad2, indicating that less than 50% of $Mad2^{S195D}$ was bound to Cdc20 when both were present at about 100 μM. Therefore, $Mad2^{S195D}$ has minimal affinity towards Cdc20, with K_d of this interaction greater than 100 μM. By contrast, the majority of the peaks in the HSQC spectrum of $Mad2^{S195D}$ disappeared after the addition of Mad1 (Figure 2-4B),

consistent with the formation of the heterotetrameric 100 kD Mad1–Mad2^{S195D} complex whose NMR signals were largely not observable.

To understand the different binding behavior of Mad2^{S195D} towards Mad1 and Cdc20, we need to consider the thermodynamics of the following equilibrium reactions (Figure 2-4C). The conversion of wild-type O-Mad2 to C-Mad2 is thermodynamically favored ($\Delta G1 < 0$). When Mad2 is phosphorylated at S195 or contains the phospho-mimicking S195D mutation, the C-Mad2 conformer is selectively destabilized. The conversion of O-Mad2^{S195D} to C-Mad2^{S195D} is thermodynamically disfavored ($\Delta G2 > 0$). The Gibbs free energy of the ligand-binding reaction of Mad2^{S195D} ($\Delta G4$) is the sum of the free energy of the Mad2^{S195D} conformational change ($\Delta G2$) and the free energy of C-Mad2^{S195D} binding to the ligand ($\Delta G3$). Ligand binding of C-Mad2^{S195D} is a thermodynamically favorable reaction ($\Delta G3 <0$). If $|\Delta G3|$ (the absolute value of $\Delta G3$) is greater than $|\Delta G2|$, $\Delta G4$ is negative, i.e. the formation of the C-Mad2^{S195D}–ligand complex is favorable. Simply put, high-affinity Mad2 ligands can drive the formation the C-Mad2^{S195D}–ligand complex whereas low-affinity Mad2-binding ligands cannot. Because Mad1 binds to Mad2 more tightly than Cdc20, Mad1, but not Cdc20, binds to Mad2^{S195D} with appreciable affinities.

Mad2^{S195D} Forms C-Mad2 when Bound to High-affinity Ligands

Because the NMR signals of the Mad1–Mad2^{S195D} complex were largely not observable, we could not be certain that Mad2^{S195D} indeed formed C-Mad2 when bound to Mad1. To ascertain that Mad2^{S195D} could still form C-Mad2 when bound to high-affinity ligands, we examined by NMR the binding of Mad2^{S195D} to MBP1, a high-affinity (K_d = 87

nM) Mad2-binding peptide (Luo, Tang et al. 2002). Addition of MBP1 caused drastic changes of the HSQC spectrum of O-Mad2, indicating that Mad2 adopted the C-Mad2 conformation when bound to MBP1 (Figure 2-4D). MBP1 addition also greatly altered the spectrum of $Mad2^{S195D}$ (Figure 2-4E). The HSQC spectrum of $Mad2^{S195D}$ bound to MBP1 was highly similar to that of Mad2 bound to MBP1 (Figure 2-4D and 4E). This result confirmed that $Mad2^{S195D}$ could indeed adopt the C-Mad2 conformation in the presence of high-affinity ligands, such as MBP1 and possibly Mad1.

Previous studies have shown that Mad2-3D and Mad2-4D, which contain additional phospho-mimicking mutations, do not bind to Mad1 to form the Mad1–Mad2 core complex (Wassmann, Liberal et al. 2003). Consistently, addition of MBP1 did not alter the HSQC spectrum of Mad2-3D, indicating the lack of binding between Mad2-3D and MBP1 even at high concentrations (Figure 2-4F). This result suggests that, in addition to S195 phosphorylation, other phosphorylation events on Mad2 might introduce more destabilization energy to the C-Mad2 conformation (i.e. $\Delta G2$ of Mad2-3D is greater than that of $Mad2^{S195D}$), which cannot be compensated by the binding energy between Mad2 and its high-affinity ligands, such as Mad1 and MBP1.

$Mad2^{S195D}$ Is Ineffective to Cause Mitotic Arrest

Mad2 S195 phosphorylation hinders the O–C conformational transition and diminishes Cdc20 binding *in vitro*. We tested whether this phosphorylation affected Mad2 function in human cells. HeLa Tet-On cells were transfected with cDNAs encoding Myc-tagged Mad2-wt, $Mad2^{S195D}$, or $Mad2^{S195A}$. The cells were fixed and stained with propidium

iodide (PI) and the mitotic marker α-MPM2 and analyzed by flow cytometry (FACS). Mitotic cells had 4N DNA content and were MPM2-positive. Overexpression of Mad2-wt or Mad2^{S195A} greatly increased the mitotic indices of HeLa cells (Figure 2-5A and 5B), indicating that high levels of Mad2 caused hyperactivation of the spindle checkpoint and blocked mitotic progression in the absence of spindle poisons. By contrast, overexpression of Mad2^{S195D} was much less effective in triggering mitotic arrest. The three Myc-Mad2 proteins were expressed at similar levels (Figure 2-5C). In addition, expression of Mad2-wt or Mad2^{S195A}, but not Mad2^{S195D}, increased the levels of another mitotic marker, phospho-histone H3 at S10 (Figure 2-5C). Therefore, these results indicate that the Mad2^{S195D} mutant is less active than Mad2-wt and Mad2^{S195A}, consistent with S195 phosphorylation playing an inhibitory role.

The inhibitory effect of S195 phosphorylation could be attributed to its expected, selective destabilization of the C-Mad2 conformation. Mad2 adopts the C-Mad2 conformation when bound to Cdc20. In addition, unliganded C-Mad2 binds to Cdc20 with higher affinity than O-Mad2 does, because it binds to Cdc20 with a faster on-rate (Luo, Tang et al. 2004; Lad, Lichtsteiner et al. 2009; Simonetta, Manzoni et al. 2009). Mad2 phosphorylation is thus expected to block the binding of Mad2 to its target Cdc20 and inhibits the function of Mad2. Indeed, as described above, the phospho-mimicking Mad2 mutants failed to bind to Cdc20 and were ineffective in eliciting mitotic arrest when overexpressed in human cells.

Mad2^{S195D} Abrogates the Spindle Checkpoint

We then tested whether Mad2^{S195D} expression affected the ability of HeLa cells to undergo mitotic arrest in the presence of spindle toxins, such as nocodazole. HeLa Tet-On cells were transfected with cDNAs encoding Myc-tagged Mad2-wt, Mad2^{S195D}, or Mad2^{S195A}, treated with 300 nM nocodazole for 16 hrs, stained with α-MPM2 and PI, and subjected to FACS analysis. Overexpression of Mad2^{S195D}, but not Mad2-wt or Mad2^{S195A}, significantly diminished the mitotic index of cells in the presence of nocodazole (Figure 2-6A and 6B). The expression levels of the Myc-tagged Mad2 proteins were similar (Figure 2-6C). Because the endogenous Mad2 protein was not depleted from the cells in this experiment, Mad2^{S195D} abrogated the spindle checkpoint in a dominant-negative manner.

To determine the mechanism by which Mad2^{S195D} blocked the function of endogenous Mad2 and abrogated checkpoint signaling, we examined the binding of Myc-Mad2^{S195D} to the endogenous Mad1 and Cdc20 in HeLa cell lysates. HeLa Tet-On cells were transfected with control vectors or vectors encoding Myc-tagged Mad2-wt, Mad2^{S195D}, or Mad2^{S195A} and arrested in mitosis with nocodazole. The cell lysates were immunoprecipitated with α-Myc and blotted with α-Mad1 and α-Cdc20. Consistent with the effect of S195 phosphorylation in hindering the O–C conformational transition of Mad2, Myc-Mad2^{S195D} failed to bind to Cdc20 whereas Myc-Mad2-wt and Myc-Mad2^{S195A} bound to Cdc20 equally well (Figure 2-7A). By contrast, Myc-Mad2^{S195D} bound more efficiently to Mad1, as compared to Myc-Mad2-wt and Myc-Mad2^{S195A}. The enhanced binding of Mad2^{S195D} to Mad1 was reproducible and was observed in four independent experiments. This observation was completely unexpected. Although Mad1^{S195D} retained binding to Mad1, it still bound with lower affinity to Mad1 as compared to Mad2-wt *in vitro*.

How could Mad2^{S195D} bind more efficiently to Mad1 in human cells then? We reasoned that the enhanced binding seen with Mad2^{S195D} might be owing to its increased binding to the Mad1–Mad2 core complex through O–C Mad2 dimerization in cells. It has been previously shown that the Mad2$^{R133A/Q134E}$ mutant (referred to as Mad2^{Mono} hereafter) could not form O–C Mad2 dimers. We constructed the Mad2$^{Mono/S195D}$ mutant, which lacked the ability to form O–C dimers and was expected to lose its binding to the Mad1–Mad2 core complex. We next examined the binding of Mad2^{Mono} and Mad2$^{Mono/S195D}$ to Mad1 and Cdc20 in HeLa cells. Myc-Mad2^{Mono} bound to similar amounts of Mad1 as Myc-Mad2-wt did (Figure 2-7A), confirming that the observed Mad1 binding to Mad2-wt in this assay was mostly due to the formation of the Mad1–Mad2 core complex. By contrast, Myc-Mad2$^{Mono/S195D}$ bound less Mad1 than Myc-Mad2^{S195D} did, indicating that the enhanced Mad1 binding by Mad2^{S195D} was indeed caused by the binding of a second molecule of Mad2^{S195D} to the Mad1–Mad2 core complex through O–C Mad2 asymmetric dimerization, which eventually adopted the I-Mad2 conformation (Figure 2-7A). Similar results were obtained in Mad2-RNAi cells (Figure 2-8). Therefore, in addition to forming the Mad1–C-Mad2^{S195D} core complex, a second molecule of O-Mad2^{S195D} bound to the Mad1–C-Mad2^{S195D} core complex, forming a Mad1–C-Mad2^{S195D}–I-Mad2^{S195D} complex that was stable during the IP procedure. Our results further suggested that S195 phosphorylation might enhance the binding affinity between C-Mad2 and I-Mad2.

We then tested whether Mad2$^{Mono/S195D}$ overexpression abrogated the spindle checkpoint. HeLa Tet-On cells were transfected with plasmids encoding Myc-tagged Mad2-wt, Mad2^{S195D}, and Mad2$^{Mono/S195D}$, treated with nocodazole, and analyzed with FACS.

Mad2$^{Mono/S195D}$ blocked the spindle checkpoint to a greater extent than Mad2^{S195D} did (Figure 2-7B). Because Mad2$^{Mono/S195D}$ bound to Mad1, but not to Cdc20 or C-Mad2, its dominant-negative effects on the spindle checkpoint is very likely due to the sequestration of Mad1 through the formation of an inactive Mad1–Mad2$^{Mono/S195D}$ core complex.

Mechanisms for the Dominant-negative Effects of Phospho-mimicking Mad2 Mutants

The fact that the phospho-mimicking mutants of Mad2 are inactive is not surprising, but the observation that these phospho-mimicking mutants inhibit the function of endogenous Mad2 and block checkpoint signaling in a dominant-negative fashion is puzzling. In particular, Mad2-3D and Mad2-4D do not bind to either Mad1 or Cdc20. How can they inhibit the functions of the endogenous Mad2? Our findings with Mad2^{S195D} reported herein now provide a solution to this puzzle. Mad2^{S195D} binds more Mad1 than Mad2-wt and Mad2$^{Mono/S195D}$ (a mutant of Mad2 that cannot form O–C Mad2 dimers) do, indicating that the apparently enhanced binding of Mad2^{S195D} to Mad1 is due to a higher affinity of Mad2^{S195D} towards the Mad1–Mad2 core complex. We expect that Mad2-3D and Mad2-4D also bind to the Mad1–Mad2 core complex. Because they do not directly bind to Mad1, their enhanced indirect binding to the Mad1–Mad2 core complex is negated by the loss of the direct binding to Mad1. The fact that Mad2^{S195D} retains Mad1 binding thus allows us to uncover the effect of these phospho-mimicking mutations (and presumably phosphorylation) in enhancing binding affinity of a second Mad2 molecule to the Mad1–Mad2 core complex.

In the framework of the Mad2 conformational activation model (Figure 2-9) (Mapelli and Musacchio 2007; Luo and Yu 2008), these findings provide a straightforward

explanation for the dominant-negative effects of phospho-mimicking mutants in cells. These mutants bind to the Mad1–Mad2 core with higher affinity than the endogenous Mad2, but cannot complete the O–C conformational transition, thereby blocking the conformational activation of the endogenous Mad2. Mad2$^{Mono/S195D}$ binds to Mad1, but not to Cdc20. Because Mad2$^{Mono/S195D}$ cannot form O–C Mad2 dimers, its binding to Mad1 creates a Mad1–Mad2$^{Mono/S195D}$ core complex that cannot further recruit and activate the endogenous O-Mad2 for Cdc20 binding. Therefore, Mad2$^{Mono/S195D}$ also blocks the spindle checkpoint in a dominant-negative manner. It has a stronger dominant-negative effect than Mad2^{S195D} does, because the Mad1–Mad2^{S195D} core complex can still recruit and activate the endogenous O-Mad2, albeit under the competition from free O-Mad2^{S195D}.

Potential Cellular Functions of Mad2 Phosphorylation

What are the physiological functions of Mad2 phosphorylation? Is Mad2 phosphorylation regulated during the cell cycle? What are the kinases responsible for these phosphorylation events? Addressing these questions awaits the development of phospho-specific antibodies that can readily detect the phosphorylated forms of endogenous Mad2 in human cells. Nevertheless, it is clear that phosphorylation of Mad2 negatively regulates its activity. We envision two non-exclusive functions for Mad2 phosphorylation. First, Mad2 phosphorylation may attenuate spontaneous, unregulated conversion of O-Mad2 to C-Mad2 (which is more thermodynamically stable *in vitro*), thereby preventing unscheduled activation of Mad2. Second, Mad2 phosphorylation may contribute to checkpoint inactivation by capping the Mad1–Mad2 complex and blocking further conformational

activation of Mad2, a function that is analogous to that of $p31^{comet}$ (Yang, Li et al. 2007; Luo and Yu 2008).

CONCLUSION

In this study, we have further explored the functions of Mad2 phosphorylation and defined S195 as a critical phosphorylation site for regulating the conformational transition of Mad2. Our studies establish the first posttranslational regulatory mechanism for the conformational change of Mad2. Furthermore, taking advantage of the unique binding properties of the phospho-mimicking $Mad2^{S195D}$ mutant, we have unexpectedly obtained evidence to suggest that S195 phosphorylation regulates O–C Mad2 dimerization. These results provide a straightforward explanation for the dominant-negative effects of Mad2 phospho-mimicking mutants and further support the *in vivo* relevance of conformational activation of Mad2 in the spindle checkpoint.

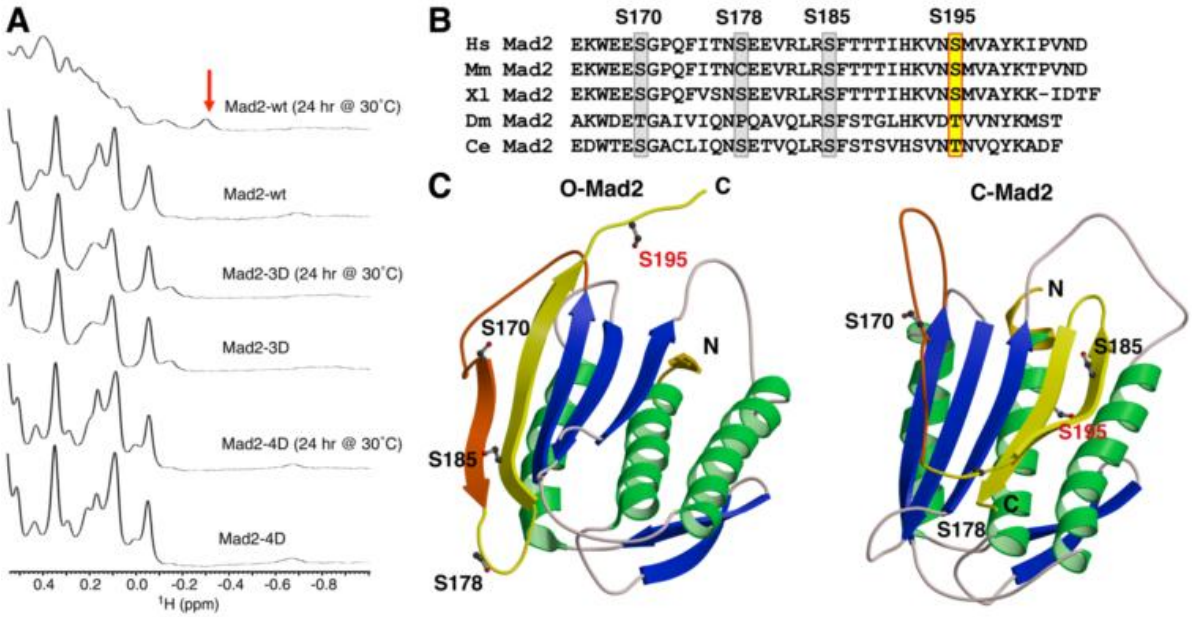

Figure 2-1. The phospho-mimicking mutants of Mad2 fail to undergo the O–C conformational transition. (**A**) The high-field region of the 1D ^{1}H spectra of wild-type Mad2 (Mad2-wt) or its phospho-mimicking mutants, Mad2-3D and Mad2-4D, before and after a 24-hr incubation at 30˚C. Mad2-3D contains S170D, S178D, and S195D mutations. Mad2-4D contains S170D, S178D, S185D, and S195D mutations. The –0.3 ppm peak that is unique to V197 in C-Mad2 is indicated by an arrow. (**B**) Sequence alignment of the C-terminal region of Mad2 proteins from *Homo sapiens* (Hs), *Mus musculus* (Mm), *Xenopus laevis* (Xl), *Drosophila melanogaster* (Dm), and *Caenorhabditis elegans* (Ce). Residues aligning with S170, S178, S185, and S195 of human Mad2 are boxed. (**C**) Ribbon drawing of the structures of O-Mad2 and C-Mad2. The α-helices are colored green, β-strands blue, and loops ivory. The structural elements of Mad2 that undergo major changes between the O and C conformers are in yellow and orange. S170, S178, S185, and S195 are shown as ball-and-stick.

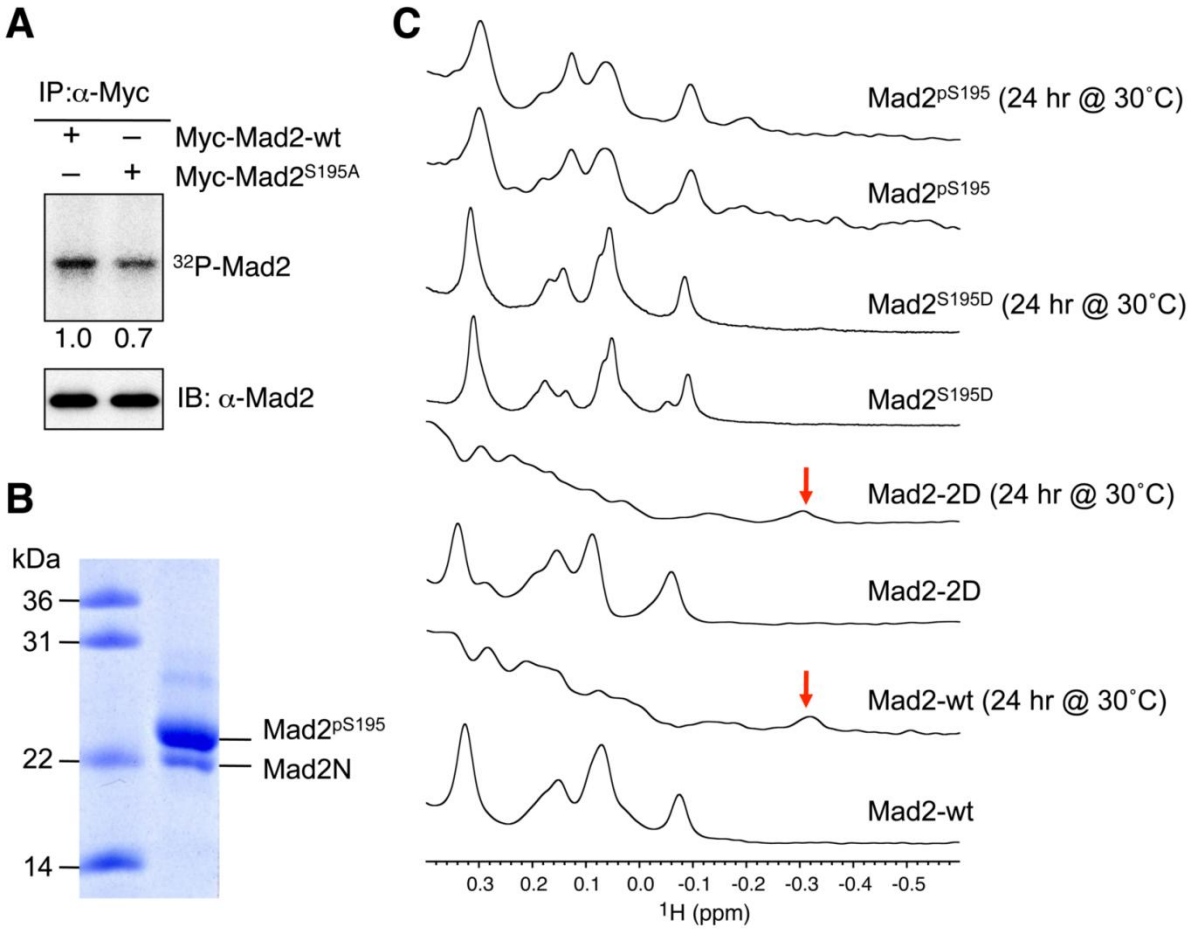

Figure 2-2. Phosphorylation of S195 hinders the conformational transition of Mad2. (**A**) HeLa Tet-On cells were transfected with plasmids encoding Myc-tagged Mad2-wt or Mad2^{S195A}, treated with nocodazole for 14 hrs, released into fresh media for 2 hrs, and labeled with ^{32}P-orthophosphate for another 2 hrs. Myc-Mad2 proteins were immunoprecipitated with α-Myc antibody beads and blotted with α-Myc (lower panel). The levels of ^{32}P incorporation into Myc-Mad2 proteins were analyzed by a phosphoimager (upper panel). The relative intensity of the ^{32}P signal was quantified and normalized by the amounts of Myc-Mad2 proteins. (**B**) Coomassie-stained gel of phospho-S195 Mad2 (Mad2^{pS195}) produced with intein-mediated protein ligation. A small amount of Mad2N not ligated to the C-terminal phospho-peptide was present. (**C**) The high-field region of the 1D ^{1}H spectra of wild-type Mad2 (Mad2-wt), Mad2-2D (contains S170D and S185D mutations), Mad2^{S195D}, and phospho-S195 Mad2 (Mad2^{pS195}) before and after a 24-hr incubation at 30˚C. The –0.3 ppm peak that is unique to V197 in C-Mad2 is indicated by arrows.

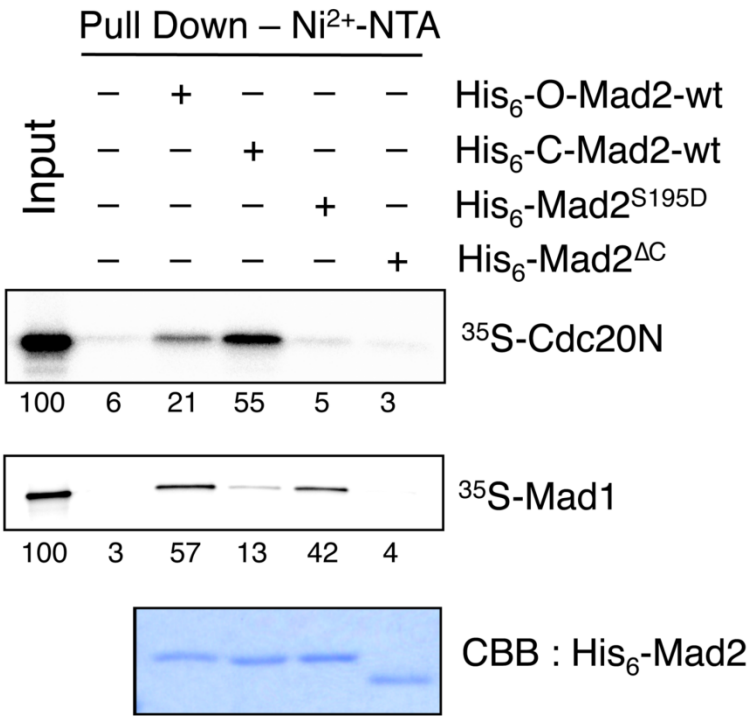

Figure 2-3. Blank Ni^{2+}-NTA beads or beads bound to the indicated His_6-tagged Mad2 proteins were incubated with ^{35}S-labeled Mad1 or Cdc20N. After washing, the proteins retained on the beads were analyzed by SDS-PAGE followed by autoradiography. About 25% of the ^{35}S-labeled proteins used in the binding assays were loaded as input. Mad2 proteins bound to beads were also stained with Coomassie. The relative amounts of Mad1 or Cdc20N bound to beads were quantified.

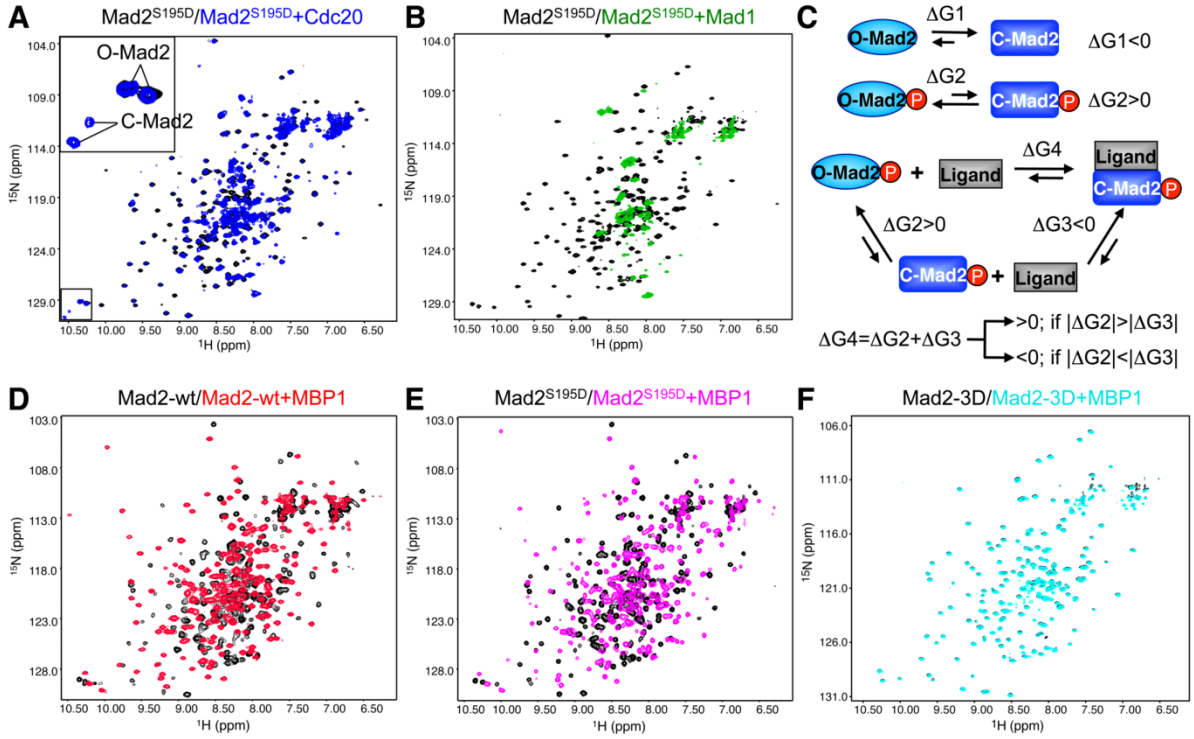

Figure 2-4. Mad2^{S195D} forms C-Mad2 when bound to high-affinity ligands. (*A*) Overlay of the 2D ^{1}H/^{15}N HSQC spectra of ^{15}N-labeled Mad2^{S195D} before (black contours) and after (blue contours) the addition of Cdc20. A region of the spectrum was magnified and shown in the inset, with the peaks belonging to O-Mad2 and C-Mad2 labeled. (*B*) Overlay of the 2D ^{1}H/^{15}N HSQC spectra of ^{15}N-labeled Mad2^{S195D} before (black contours) and after (green contours) the addition of Mad1. (*C*) Reactions equilibria for the conformational change and ligand binding of unmodified or phosphorylated Mad2. (*D*) Overlay of the 2D ^{1}H/^{15}N HSQC spectra of ^{15}N-labeled Mad2-wt before (black contours) and after (red contours) the addition of MBP1. (*E*) Overlay of the 2D ^{1}H/^{15}N HSQC spectra of ^{15}N-labeled Mad2^{S195D} before (black contours) and after (magenta contours) the addition of MBP1. (*F*) Overlay of the 2D ^{1}H/^{15}N HSQC spectra of ^{15}N-labeled Mad2-3D before (black contours) and after (cyan contours) the addition of MBP1.

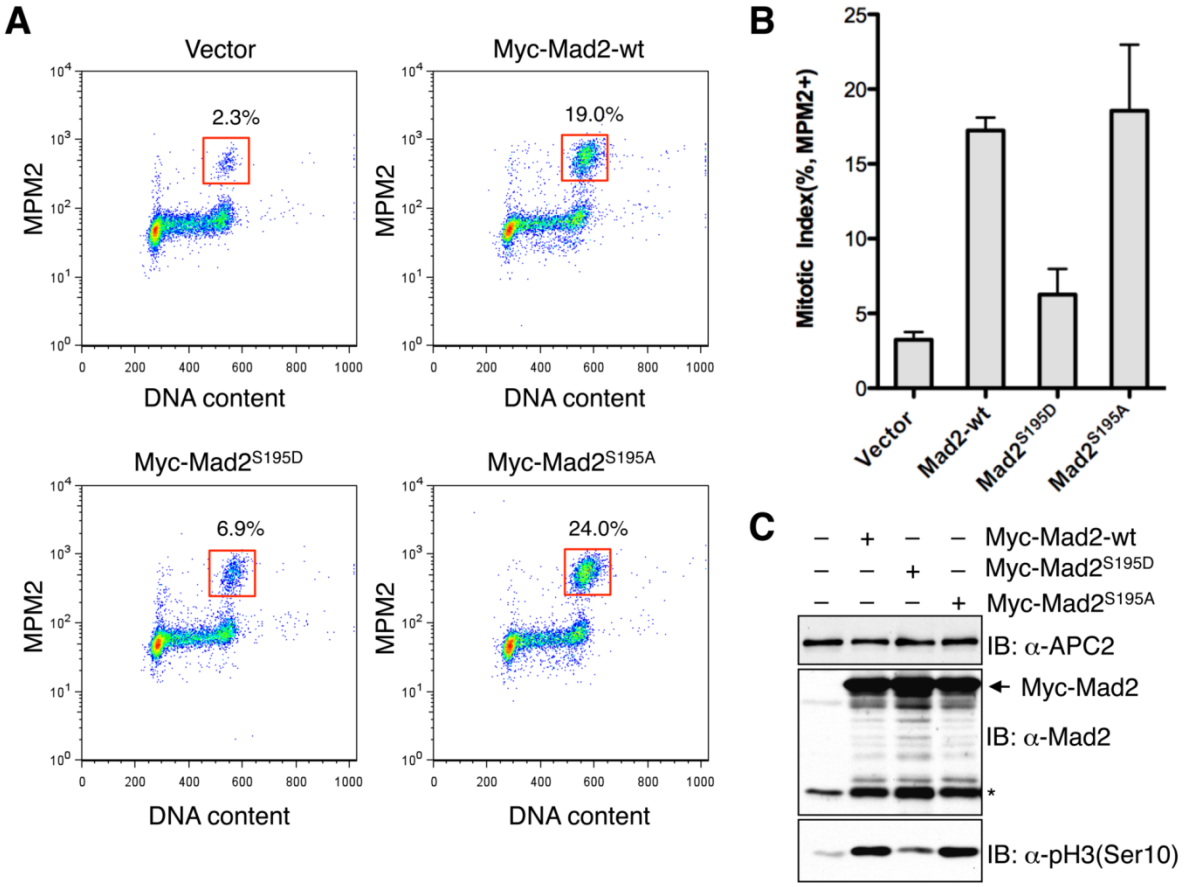

Figure 2-5. Mad2^{S195D} is ineffective in eliciting mitotic arrest of human cells. (**A**) The FACS analysis of HeLa Tet-On cells transfected with the indicated plasmids. The populations of mitotic cells (with 4N DNA content and MPM2+) are boxed with the mitotic indices indicated. (**B**) Quantification of mitotic indices of cells described in (**A**). The means and standard deviations of results from seven experiments are shown. (**C**) Lysates of cells described in (**A**) were blotted with the indicated antibodies. APC2 is used as the loading control. The asterisk indicates the position of the endogenous Mad2. Cells transfected with Myc-Mad2 proteins contained more Mad2 that co-migrated with endogenous Mad2. The origins of these Mad2 species were unknown, but might be due to internal translation start of Myc-Mad2 transgenes or the proteolysis of Myc-Mad2 proteins or both.

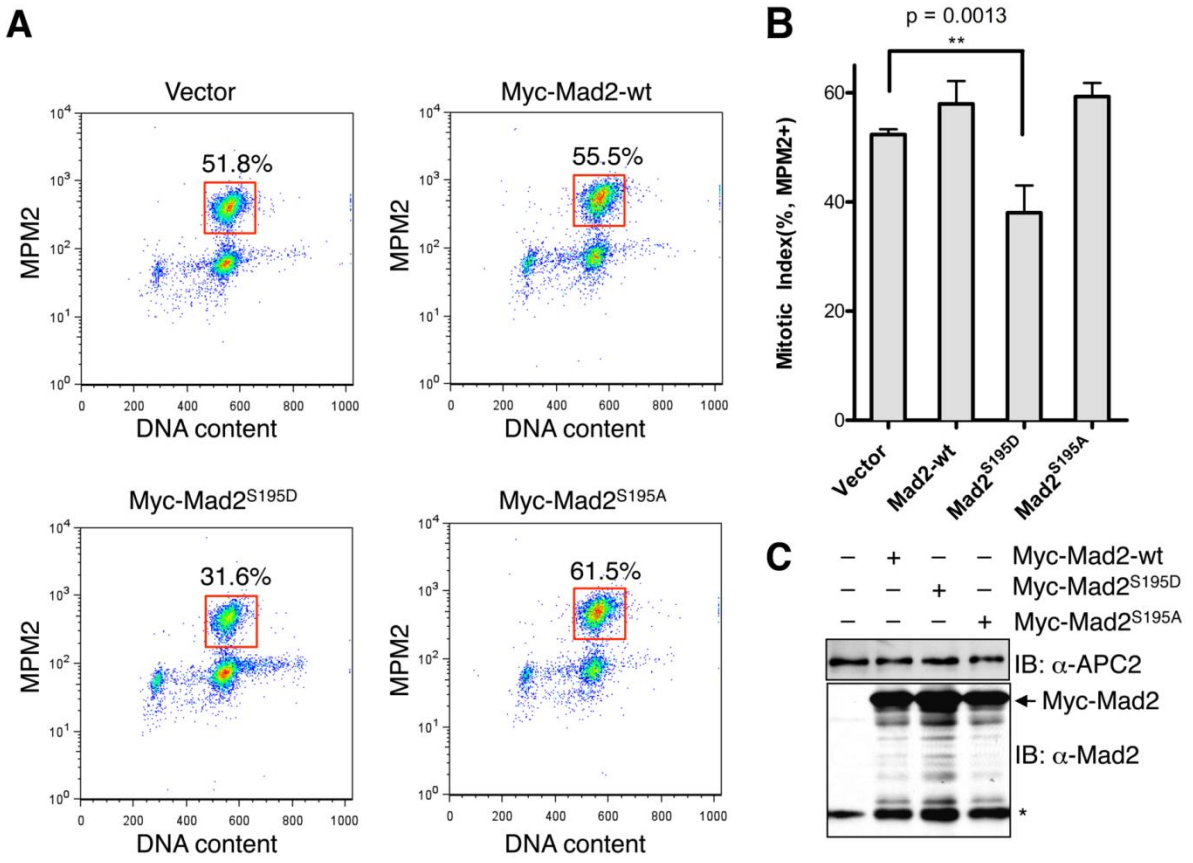

Figure 2-6. Overexpression of Mad2^{S195D} abrogates the spindle checkpoint. (**A**) The FACS analysis of HeLa Tet-On cells transfected with the indicated plasmids and treated with nocodazole. The populations of mitotic cells (with 4N DNA content and MPM2+) are boxed with the mitotic indices indicated. (**B**) Quantification of mitotic indices of cells described in (**A**). The means and standard deviations of results from four experiments are shown. The p-value was calculated between Mad2^{S195D}- and vector-transfected samples. (**C**) Lysates of cells described in (**A**) were blotted with the indicated antibodies. APC2 is used as the loading control. The asterisk indicates the position of the endogenous Mad2.

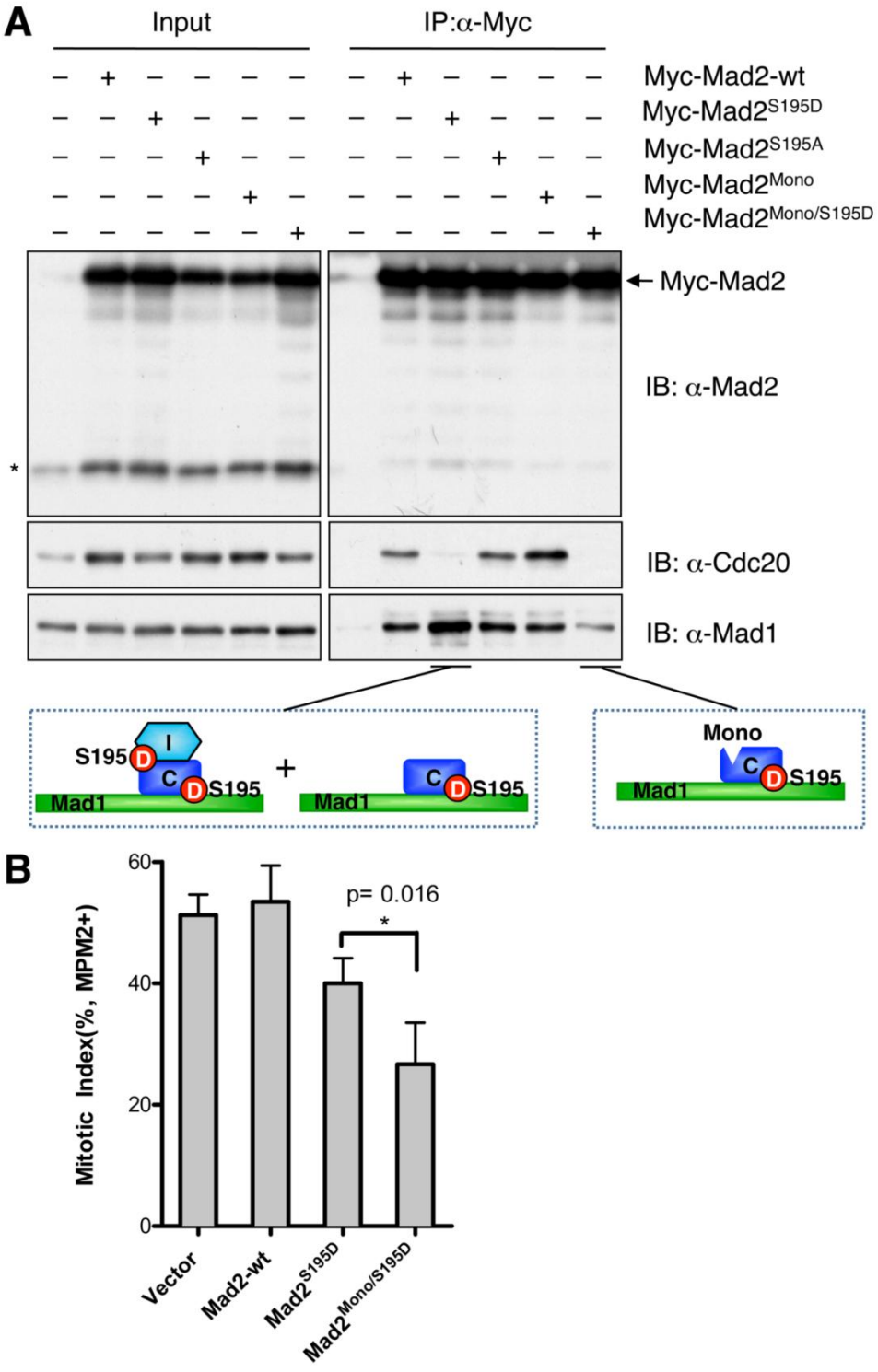

Figure 2-7. Mad2^{S195D} binds to the Mad1–Mad2 core complex, but not to Cdc20. (**A**) HeLa Tet-On cells were transfected with the indicated plasmids and treated with nocodazole.

Lysates of these cells and the a-Myc immunoprecipitates were blotted with the indicated antibodies. The asterisk indicates the position of the endogenous Mad2. (**B**) Overexpression of $Mad2^{Mono/S195D}$ abrogates the spindle checkpoint through Mad1 sequestration. Quantification of mitotic indices of HeLa Tet-On cells transfected with the indicated plasmids and treated with nocodazole. The means and standard deviations of results from three experiments are shown. The p-value was calculated between $Mad2^{S195D}$- and $Mad2^{Mono/S195D}$-transfected samples.

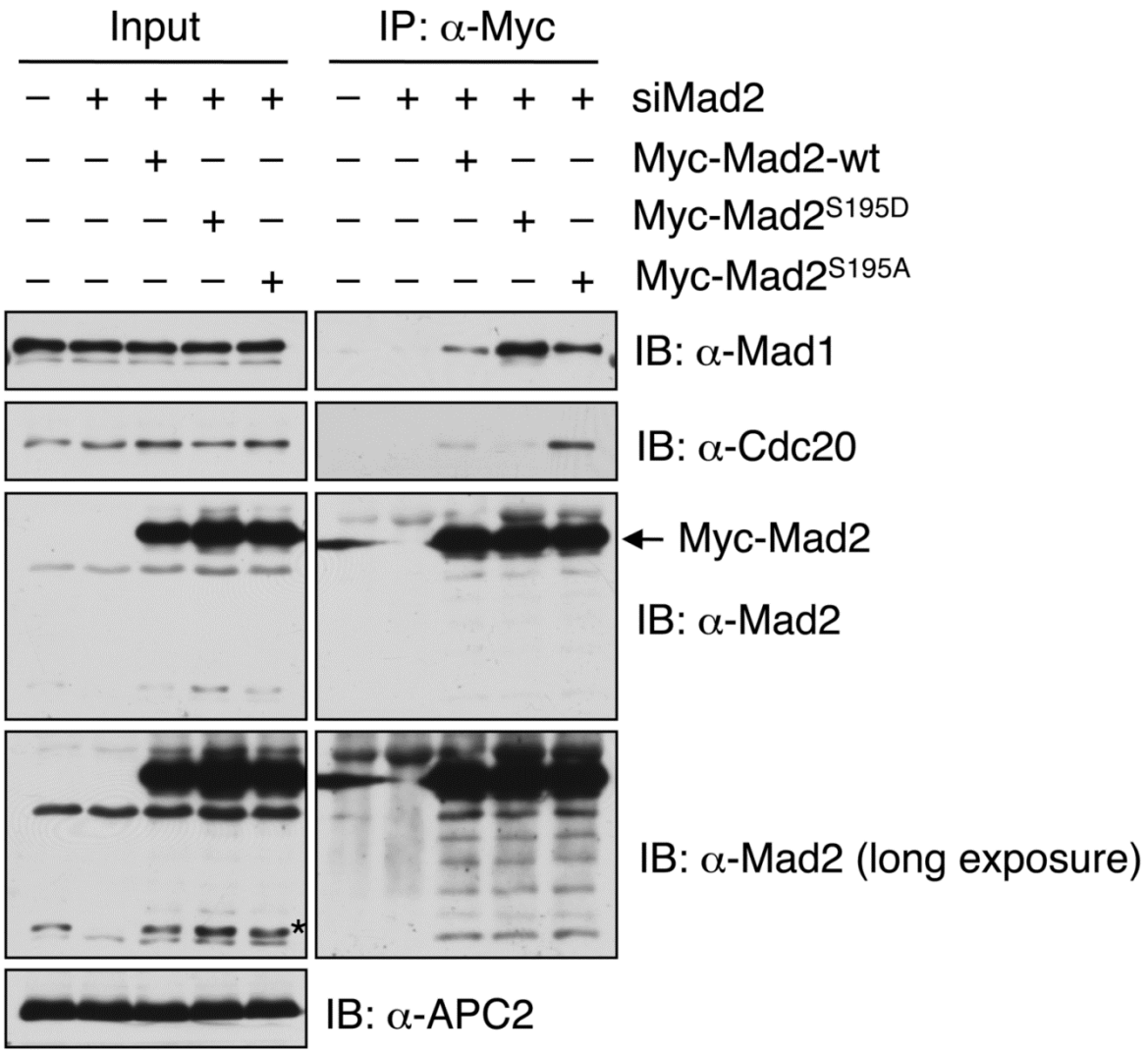

Figure 2-8. Mad1 binding of Mad2^{S195D} does not require the endogenous Mad2. HeLa Tet-On cells were transfected with the indicated siRNA and Mad2 plasmids that contained silent mutations within the siRNA target sequence and treated with nocodazole. Lysates of these cells and the α-Myc immunoprecipitates were blotted with the indicated antibodies. The asterisk indicates the position of the endogenous Mad2 and the exogenous Mad2 that has lost the Myc tag.

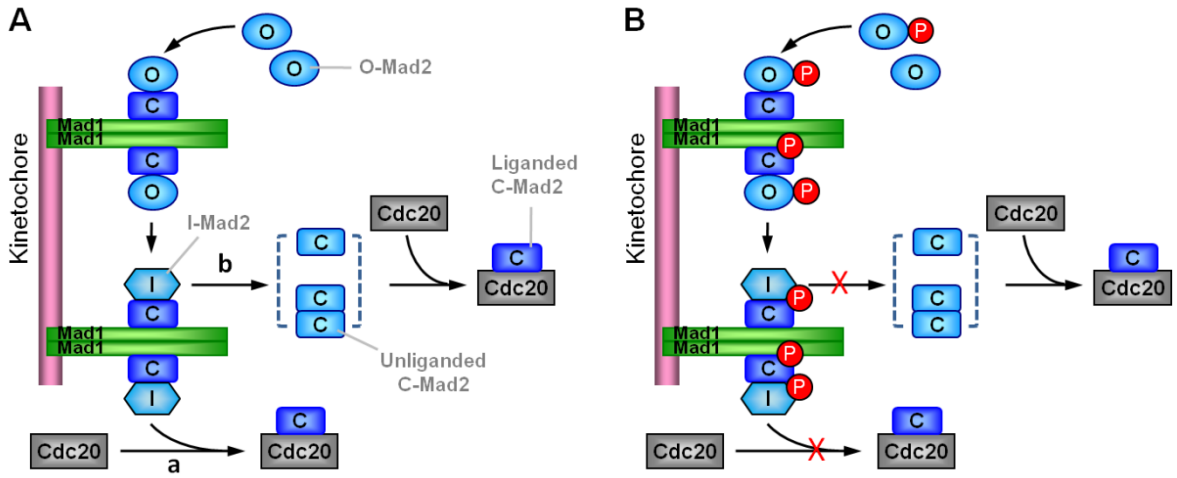

Figure 2-9. Model depicting Mad1-assisted Mad2 conformational activation. (**A**) and the proposed roles of Mad2 phosphorylation or phospho-mimicking mutations (**B**).

CHAPTER III: STRUCTURE OF HUMAN MAD1 C-TERMINAL DOMAIN REVEALS ITS INVOLVEMENT IN KINETOCHORE TARGETING

INTRODUCTION

Aneuploidy is a major form of genomic instability in human cancers and can result from chromosome missegregation in mitosis. The spindle checkpoint is a cell-cycle surveillance system that guards against chromosome missegregation (Bharadwaj and Yu 2004; Qi and Yu 2006; Musacchio and Salmon 2007). Unattached kinetochores that exist intrinsically during normal prometaphase or as a consequence of spindle damage caused by exogenous chemical agents activate the checkpoint. The spindle checkpoint proteins, including Bub1, BubR1, Bub3, Mps1, Mad1, and Mad2, are recruited to unattached kinetochores in a hierarchical fashion and undergo enzymatic and conformational activation. The activated checkpoint proteins collaborate to inhibit APC/C^{Cdc20} (the anaphase-promoting complex/cyclosome bound to its mitotic activator Cdc20) (Yu 2002; Peters 2006; Yu 2007), thereby stabilizing the APC/C substrates, securin and cyclin B1, and delaying anaphase onset until all kinetochores reach proper spindle attachment.

The constitutive Mad1–Mad2 core complex is a downstream component of the kinetochore-targeting hierarchy. Its recruitment to unattached kinetochores requires upstream kinetochore-bound components, including the Ndc80 complex consisting of Ndc80, Nuf2, Spc25, and Spc24 (Martin-Lluesma, Stucke et al. 2002; Bharadwaj, Qi et al. 2004). At the kinetochores, the Mad1–Mad2 core complex catalyzes the

conformational activation of the unusual two-state protein Mad2, which has two natively folded conformers, open-Mad2 (O-Mad2 or N1-Mad2) and closed-Mad2 (C-Mad2 or N2-Mad2) (Luo, Tang et al. 2002; Sironi, Mapelli et al. 2002; Luo, Tang et al. 2004; De Antoni, Pearson et al. 2005; Mapelli, Massimiliano et al. 2007; Mapelli and Musacchio 2007; Luo and Yu 2008; Yang, Li et al. 2008). C-Mad2 in the Mad1–Mad2 core complex recruits cytosolic O-Mad2 through asymmetric dimerization and converts O-Mad2 into intermediate Mad2 (I-Mad2) or unliganded C-Mad2, which then binds to Cdc20. Formation of the Mad2–Cdc20 complex further promotes the binding of BubR1–Bub3 to Cdc20, forming the APC/C-inhibitory mitotic checkpoint complex (MCC) (Kulukian, Han et al. 2009). Thus, the Mad1–Mad2 core complex is a key catalytic engine of the spindle checkpoint.

Despite the importance of kinetochore-bound Mad1 in the spindle checkpoint, the mechanism of its kinetochore targeting is not understood. A C-terminal fragment of yeast Mad1 containing the highly conserved C-terminal domain (CTD) is necessary and sufficient for its kinetochore localization and checkpoint function (Kastenmayer, Lee et al. 2005). By contrast, an N-terminal fragment of *Xenopus* Mad1 lacking the CTD has been shown to localize to kinetochores (Chung and Chen 2002). Finally, mutation of T680, a residue within the CTD and a potential Plk1 phosphorylation site, in human Mad1 has been reported to diminish its kinetochore localization (Chi, Haller et al. 2008). It is thus unclear whether Mad1 has conserved kinetochore-targeting domains. The kinetochore receptor or receptors of Mad1 are also unknown.

In this study, we have determined the crystal structure of the CTD of human Mad1. Unexpectedly, Mad1 CTD has a fold similar to those of the kinetochore-targeting domains of the Ndc80 complex component Spc25 and the yeast monopolin subunit Csm1, despite the lack of obvious sequence similarity. We show that non-overlapping fragments of Mad1 can achieve detectable kinetochore targeting. Deletion of Mad1 CTD diminishes, does not abolish, Mad1 kinetochore targeting. Structure-based mutagenesis identifies a conserved RLK motif in Mad1 CTD critical for Mad1 kinetochore targeting in human cells. Interestingly, the same RLK motif is required for the checkpoint-stimulated Mad1–Bub1 interaction in yeast (Brady and Hardwick 2000). Consistently, Bub1 is required for Mad1 kinetochore targeting in human cells, and depletion of Bub1 by RNA interference (RNAi) does not further reduce the kinetochore targeting of a Mad1 RLK-motif mutant. These results implicate Bub1 as a possible kinetochore receptor for Mad1 CTD. Therefore, Mad1 has an unusually extensive kinetochore-binding interface with multiple quasi-independent contacting sites, one of which involves the CTD.

MATERIALS AND METHODS

Protein purification and crystallization

The coding region of human Mad1$^{597-718}$ was cloned into a modified pET28 vector (EMD Biosciences) that also included a tobacco etch virus (TEV) protease cleavage site. The Mad1 mutants were generated with the QuikChange mutagenesis kit (Stratagene). All constructs were verified by DNA sequencing. The pET28-Mad1$^{597-718}$ plasmid was transformed into the *E. coli* strain BL21(DE3) to produce N-terminal His_6-tagged Mad1$^{597-718}$ protein. Mad1$^{597-718}$ was purified with Ni^{2+}-NTA agarose resin (Qiagen) and cleaved with TEV protease to remove the His_6-tag. The protein was further purified by anion exchange chromatography with a resource Q column followed by size exclusion chromatography with a Superdex 75 column (GE Healthcare). Purified Mad1$^{597-718}$ was concentrated to 18.5 mg/ml in a buffer containing 20 mM Tris (pH 8.0), 100 mM KCl and 1 mM TCEP. The seleno-methionine labeled Mad1$^{597-718}$ was produced using the methionine biosynthesis inhibition method (Van Duyne, Standaert et al. 1993).

Mad1$^{597-718}$ was crystallized at 20˚C using the hanging-drop vapor-diffusion method with a reservoir solution containing 0.1 M sodium cacodylate (pH 6.2), 26% (w/v) PEG 1500 and 1 mM reduced L-Glutathione. The crystals were cryo-protected with the reservoir solution and then flash-cooled in liquid propane. Crystals diffracted to a minimum Bragg spacing (d_{min}) of 1.75 Å, exhibited the symmetry of space group $P6_5$ with cell dimensions of a = 44.8 Å, c = 211.1 Å, and contained one Mad1$^{597-718}$ dimer per asymmetric unit.

Data collection and structure determination

All diffraction data were collected at the beamline 19-ID (SBC-CAT) at the Advanced Photon Source (Argonne National Laboratory, Argonne, Illinois, USA) and processed with HKL3000 (Otwinowski and Minor 1997). Phases were obtained from a selenium-SAD experiment using X-rays at an energy near the selenium K absorption edge. Phenix AutoSol was used to identify the selenium sites and calculate density-modified experimental maps (Adams, Afonine et al. 2010). A total of two refined sites were found, and the experimental density map showed clear features of the protein backbone and well-defined side chains. Automated building with Phenix AutoBuild resulted in a model containing 212 sequence-assigned residues when refined against the experimental phases. The remaining 24 residues were manually built in Coot (Emsley and Cowtan 2004) and refined in Phenix. The final model (R_{work} = 16.0%, R_{free} = 19.7%) contained 236 residues and 287 water molecules. MolProbity was used for structure validation and indicated that all residues were in the Ramachandran favored/allowed regions (Chen, Arendall et al. 2010). Data collection and structure refinement statistics are summarized in **Table 3-1**.

Cell culture and transfection

HeLa Tet-On (Clontech) cells were grown in Dulbecco's modified Eagle's medium (DMEM; Invitrogen) supplemented with 10% fetal bovine serum (FBS). Plasmid transfection was performed with the Effectene reagent (Qiagen) according to

manufacturer's instructions. To establish stable cell lines, HeLa Tet-On cells were transfected with the pTRE2-GFP-Mad1 WT or ΔCTD plasmids or pTRE2-Myc-Mad1-5A WT or R617A plasmids and incubated with 150 μg/ml hygromycin B (Invitrogen). Surviving clones that expressed similar levels of Mad1 WT or mutants were analyzed using live-cell imaging or immunofluorescence. The control siRNA (5'-GACCGUUAGGUACAGAAGAUU-3') and siRNAs targeting human Bub1 (5'-GAGUGAUCACGAUUUCUAAdTdT-3') or Mad1 (5'-GAGCAGAGCAGAUCCGUUCGAAUU-3') were chemically synthesized by Dharmacon. siRNA transfection was performed with Lipofectamine RNAiMAX (Invitrogen) according to manufacturer's protocols.

Live-cell imaging

Cells were grown and transfected in 6-well plates. At 20-24 hrs after transfection, cells were passaged onto chambered coverslips (LabTek), incubated with 2 mM thymidine (Sigma) for 14-16 hrs, and released into fresh media for 4-6 hrs prior to taking images. Differential interference contrast (DIC) and GFP fluorescence images were obtained at 5-min intervals with a DeltaVision deconvolution fluorescence microscope (Applied Precision) equipped with an environmental chamber, a 100x NA 1.4 objective (Olympus), and a CoolSnap HQ^2 camera (Roper Scientific) at 2x2 binning. The images were deconvolved with the Deconvolution tool in *SoftWoRx* (Applied Precision) that used the iterative-constrained algorithm. For 2D-image presentation, five z-series optical sections obtained at 1.5-μm steps were projected by the Max Intensity method.

Presentation images were created with ImageJ (http://rsb.info.nih.gov/ij/) and Photoshop (Adobe).

Immunofluorescence

For interphase Mad1 localization, HeLa Tet-On cells were directly grown in 4-well chambered slides (LabTek). For mitotic Mad1 localization, cells were grown in 6-well plates and incubated with 500 nM nocodazole (Sigma) for 16-18 hrs. Mitotic cells were harvested by shake-off, resuspended in hypotonic solution (55 mM KCl), spun onto slides with Shandon Cytospin 4 (Thermo Fisher). In both cases, cells were permeabilized with PBS containing 0.2% Triton X-100, fixed in 4% paraformaldehyde for 15 min, and incubated with 1 μg/ml of α-GFP (Roche), α-Myc (Roche), or α-Mad1 (generated against purified $Mad1^{481-718}$ protein) and CREST (ImmunoVision) in PBS containing 0.1% Triton X-100 and 3% bovine serum albumin (BSA) for overnight at 4°C. After washing with PBS containing 0.1% Triton X-100, the cells were further incubated with 1 μg/ml fluorescent secondary antibodies (Invitrogen) in PBS containing 0.1% Triton X-100 and 3% BSA for 1 hr at room temperature, washed again with PBS containing 0.1% Triton X-100, and incubated with PBS containing 1μg/ml of 4',6-diamidino-2-phenylindole (DAPI). For co-staining of multiple antibodies, secondary antibodies with Alexa Fluor® 488, 568, or 647 dyes (Invitrogen) were used simultaneously. Images were obtained and processed using a DeltaVision deconvolution fluorescence microscope and *SoftWoRx* (Applied Precision) as described above. For fixed samples, images were acquired with five z-series optical sections at 0.5-μm steps. The 2D images were generated by the

projection with the Sum Intensity method after the deconvolution to quantify the relative intensity of immunofluorescence signals. The intensity of Mad1 signals (labeled with α-GFP, α-Myc, or α-Mad1 antibodies) and CREST signals were measured with ImageJ. A circle that enclosed Mad1 and CREST signals from a single kinetochore or a pair of kinetochores if inseparable was drawn and set as the region of interest (ROI). The integrated density for the selected ROI was measured for both Mad1 and CREST channels. For normalization, the Mad1 intensity was then divided by the corresponding CREST intensity. The average of the normalized Mad1 signals of 20 ROIs chosen at random was used to represent the Mad1 staining in each cell. The graphs and statistics were created with GraphPad Prism (GraphPad Software).

Immunoprecipitation and immunoblotting

Cells were lysed with the Lysis Buffer (50 mM Tris-HCl, pH 8.0, 75 mM KCl, 5 mM $MgCl_2$, 1 mM EGTA, 0.1% Triton X-100, 10 mM NaF, 5 mM β-glycerophosphate, 10% glycerol, 1 mM DTT, and protease inhibitor cocktail from Roche). The lysates were cleared by centrifugation for 30 min at 4°C at top speed in a microcentrifuge. Mouse IgG (Sigma) or α-Myc monoclonal antibodies (Roche) were covalently coupled to Affi-Prep protein A beads (Bio-Rad). The supernatants were incubated with IgG- or α-Myc-coupled beads. The beads were washed with the Lysis Buffer. Proteins bound to the beads were dissolved in SDS sample buffer, boiled, separated by SDS-PAGE, and immunoblotted with α-Myc (Roche), α-Mad1, and α-Mad2 at a concentration of 1 μg/ml or 1:1000 dilution for crude sera.

To test expression levels of plasmid transfection or siRNA efficiency, cells were directly dissolved in SDS sample buffer. The total cell lysates were analyzed by immunoblotting with antibodies against Myc, Bub1(Tang, Bharadwaj et al. 2001), actin (Pierce), or tubulin (Sigma).

Flow cytometry (FACS)

HeLa Tet-On cells stably expressing vector or Myc-Mad1 WT were collected by trypsinization, washed once with PBS, and fixed with cold 70% ethanol. After overnight fixation at -20˚C, cells were washed with PBS and permeabilized with PBS containing 0.25% (v/v) Triton X-100 for 5 min. Cells were then incubated with α-MPM2 (Millipore) followed by an incubation with fluorescent secondary antibodies (Invitrogen) diluted in PBS plus 1% BSA. After washing with PBS, the cells were stained with propidium iodide (Sigma) at a final concentration of 20 μg/ml, and simultaneously treated with 200 μg/ml RNase A (Qiagen). The samples were analyzed with FacsScan (Becton Dickinson) and the FlowJo software (Tree Star).

In vitro binding assay

To assay Mad1-CTD dimerization, same amounts of plasmids encoding Myc- or HA-tagged Mad1-CTD WT or point mutants were translated in reticulocyte lysate in the presence of ^{35}S-methionine. Affi-Prep protein A beads (Bio-Rad) covalently coupled to α-HA monoclonal antibodies (Roche) were incubated with ^{35}S-labeled Mad1-CTD, and

washed three times with TBS containing 0.05% Tween. The bound proteins were separated by SDS-PAGE and analyzed with a phosphor imager (Fujifilm).

RESULTS

Mad1 CTD forms a dimer and has a fold similar to Spc25

Mad1 contains an N-terminal coiled coil domain and a C-terminal globular domain (CTD) (Figure 3-1A). The Mad2-interacting motif (MIM) is located just N-terminal to the CTD. The structure of a 120-residue Mad2-binding fragment of human Mad1 bound to Mad2 had been previously determined (Sironi, Mapelli et al. 2002). Other domains of Mad1 had not been structurally characterized. Because Mad1 CTD was highly conserved from yeast to man, we sought to determine its structure. We expressed and purified a series of CTD-containing human Mad1 fragments with different N-terminal boundaries and examined them using nuclear magnetic resonance (NMR) spectroscopy. Heteronuclear single quantum correlation (HSQC) spectra revealed that the Mad1 CTD fragment containing residues 597-718 was well folded and had no flexible regions (Figure 3-2A). Based on gel filtration chromatography, it had a native molecular mass of about 35 kDa, consistent with it being a homodimer (Figure 3-2B). We next obtained crystals of selenium-methionine-labeled Mad1 CTD that diffracted to 1.75 Å and determined the structure of Mad1 CTD by the single wavelength anomalous dispersion (SAD) method (Table 3-1).

Mad1 CTD is indeed a homodimer and contains a coiled-coil stem and a globular head (Figure 3-1B). Each monomer folds into a long helix (αA), a four-stranded antiparallel β sheet, a short helix (αAB), and two C-terminal helices (αB and αC) (Figure 3-1B and C). The N-terminal segments of two αA helices (one from each monomer) form

the stem. αC and the C-terminal end of αA mediate the dimerization of the globular head. The fold of Mad1 CTD was strikingly similar to those of the kinetochore-targeting C-terminal domains of Spc25 (a subunit of the microtubule-binding Ndc80 kinetochore complex) and Csm1 (a subunit of the yeast monopolin complex) (Figure 3-1B and C) (Wei, Schnell et al. 2006; Ciferri, Pasqualato et al. 2008; Corbett, Yip et al. 2010). This fold was also related to those of the RWD domain and ubiquitin-conjugating enzymes (Nameki, Yoneyama et al. 2004; Burroughs, Jaffee et al. 2008). The fold similarity between Mad1 CTD and the CTDs of Spc25 and Csm1 was unexpected, as they share no obvious sequence similarity. Both CTDs of Mad1 and Csm1 form homodimers while Spc25 forms a heterodimer with the CTD of another Ndc80 subunit Spc24. Spc24 CTD is topologically related, but not identical, to Spc25 CTD (Wei, Schnell et al. 2006; Ciferri, Pasqualato et al. 2008). The Mad1 CTD homodimer is thus structurally similar to the Spc25–Spc24 CTD heterodimer and to the Csm1 homodimer (Figure 3-1B).

Mad1 has multiple quasi-independent kinetochore-binding interfaces

The globular CTD heterodimer of Spc25 and Spc24 mediates the kinetochore targeting of the Ndc80 complex through interactions with the Mis12 complex (Ciferri, Pasqualato et al. 2008; Petrovic, Pasqualato et al. 2010). Similarly, the globular CTD homodimer of Csm1 has also been shown to bind to kinetochores and interact with both the Mis12 complex and CENP-C (Corbett, Yip et al. 2010). The unexpected structural similarity between Mad1 CTD and well-established kinetochore-targeting domains prompted us to test whether the CTD was indeed involved in kinetochore targeting of

human Mad1. On the other hand, previous studies had shown that the N-terminal domain of *Xenopus* Mad1 was critical for kinetochore targeting (Chung and Chen 2002). To systematically define the kinetochore-binding domains of human Mad1, we created truncation mutants of Myc-Mad1-5A and examined their kinetochore localization using immunofluorescence (Figure 3-3). Overexpression of Mad1 caused spindle checkpoint defects by titrating free Mad2 (Figure 3-4A and B) (Chung and Chen 2002), hindering our detection of ectopically expressed Mad1 protein at kinetochores. We thus created a Mad1-5A mutant with the Mad2-interacting motif (MIM) mutated to alanines. Myc-Mad1-5A no longer had detectable binding to Mad2, even though it formed mixed dimers with the endogenous Mad1 (Figure 3-4C). Overexpression of Myc-Mad1-5A did not cause strong spindle checkpoint defects. The Mad1 deletion mutants were thus constructed from Myc-Mad1-5A.

None of the Mad1 fragments retained full kinetochore-targeting function (Figure 3-3). Mad1-ΔCTD had about 50% of the kinetochore-binding activity of the full-length Mad1. Three additional Mad1 fragments, **a**, **b**, and **c** exhibited weak, but detectable, kinetochore localization. Therefore, Mad1 has an extensive kinetochore-binding interface. The fact that non-overlapping Mad1 fragments (**a/c** and **b**) retain residual kinetochore-targeting activity further suggests that Mad1 has multiple quasi-independent kinetochore-binding domains.

Because Mad1-ΔCTD dimerized with the endogenous Mad1 (Figure 3-4C), the kinetochore signal of Mad1-ΔCTD could conceivably belong to this mixed dimer. The kinetochore signal of Myc-Mad1-ΔCTD was, however, still observed in cells depleted of

the endogenous Mad1 by RNAi (Figure 3-5), ruling out this possibility. Mad1 fragments **a**, **b**, and **c** did not dimerize with the endogenous Mad1. The residual kinetochore localization could not be caused by dimerization between the endogenous Mad1 and these fragments.

To confirm the involvement of the CTD in the kinetochore targeting of human Mad1, we next stably transfected GFP-Mad1 or GFP-Mad1-ΔCTD plasmids into HeLa cells and monitored the localization of the GFP-Mad1 fusion proteins using live-cell imaging (Figure 3-6A and B). When cells entered mitosis, Mad1 localized to unattached kinetochores (Figure 3-6A). As mitosis progressed, the number of Mad1-positive kinetochore decreased. At metaphase, all kinetochores became attached to spindle microtubules and lacked Mad1 signals. By contrast, GFP-Mad1-ΔCTD failed to localize to kinetochores during any stages of mitosis (Figure 3-6B). Both GFP-Mad1 and GFP-Mad1-ΔCTD were expressed at similar levels (Figure 3-6C). Importantly, GFP-Mad1-ΔCTD retained the ability to localize to nuclear pores in interphase, ruling out global unfolding of GFP-Mad1-ΔCTD (Figure 3-6D). These results validate a role of the CTD in the kinetochore targeting of Mad1 during unperturbed mitosis of human cells.

It was surprising that Myc-Mad1-ΔCTD retained partial kinetochore targeting in fixed cells while GFP-Mad1-ΔCTD was undetectable by live-cell imaging. A possible explanation was that indirect immunofluorescence on fixed cells was more sensitive than live-cell imaging in detecting the kinetochore localization of Mad1. Consistent with this notion, GFP-Mad1-ΔCTD were indeed detectable at kinetochores in fixed cells (Figure 3-

7). Similar to Myc-Mad1-ΔCTD, the intensity of the GFP-Mad1-ΔCTD kinetochore signal was about 50% of that of GFP-Mad1-WT.

Identification of two classes of Mad1 CTD mutants deficient in kinetochore targeting

To further identify residues within Mad1 CTD critical for kinetochore binding, we performed structure-based mutagenesis and mutated conserved residues that had any exposed surface areas. Some of these residues targeted by mutagenesis were mostly buried. We introduced the Mad1 CTD mutations into full-length GFP-Mad1-5A and performed live-cell imaging experiments to examine their kinetochore localization (Figure 3-8 and 3-9).

Because T680 had been identified as a Plk1 phosphorylation site *in vitro* and had been implicated in Mad1 kinetochore targeting (Chi, Haller et al. 2008), we also mutated T680 to alanine even though T680 was completely buried. Contrary to a published report (Chi, Haller et al. 2008), we observed that the Mad1 T680A mutant retained kinetochore localization. Thus, we did not further pursue a potential regulation of Mad1 kinetochore targeting by Plk1.

Several GFP-Mad1-5A proteins harboring mutations in the CTD indeed failed to localize to kinetochores (Figure 3-8 and 3-9). These mutations could be divided into two classes. Class I mutations, including F629A, Y655A, L677A, F682A, and L709A, affected mostly buried hydrophobic residues (Figure 3-10A and B). Among them, F629, Y655, and L709 were located at the dimer interface. Class II mutations, including

R617A, K619A, and R630A, altered surface-exposed residues in the CTD stem (Figure 3-10A).

Mutations of several conserved surface-exposed residues on αC in the globular head, such as E710, F712, R714, and T716, did not affect the kinetochore targeting of GFP-Mad1-5A (Figure 3-8 and 3-9B). The top face of the globular head of the CTD was thus unlikely a direct kinetochore-binding surface, as we had originally envisioned. We hypothesized that the class I mutations disrupted the structure integrity or dimerization of Mad1 CTD, indirectly diminishing kinetochore binding of Mad1.

To test this hypothesis, we co-translated HA- or Myc-Mad1 CTD *in vitro* in the presence of ^{35}S-methionine and performed immunoprecipitation with anti-HA beads. The wild-type HA-Mad1 CTD efficiently pulled down Myc-Mad1 CTD, confirming that the CTD indeed formed dimers in solution (Figure 3-10C). The Myc-Mad1 CTD bands were more intense than the HA-Mad1 CTD bands, because the former contained six copies of the Myc tag and each Myc tag had a methionine. The HA-Mad1 CTD F629A, Y655A, L677A, F682A, and L709A mutants failed to bind to their Myc-tagged counterparts, indicating that these mutants did not form dimers. Among them, HA-Mad1 CTD F629A and L709A were not efficiently translated or pulled down with the anti-HA beads, suggesting that these mutations were more detrimental to the structural integrity of the Mad1 CTD monomer. Therefore, the class I mutations compromise kinetochore targeting of Mad1 by disrupting the dimerization of Mad1 CTD or its structural integrity or both. We note that Mad1-ΔCTD interacts with the endogenous Mad1 (Figure 3-4C), suggesting that the N-terminal coiled coil domain of Mad1 was sufficient to maintain dimerization of

the full-length Mad1. In the context of full-length Mad1, the CTD mutations are expected to cause local unfolding or splaying of the C-terminal end of Mad1.

In contrast to the class I mutants, the HA-tagged class II mutants (R617A, K619A, and R630A) efficiently pulled down their Myc-tagged counterparts (Figure 3-10C), indicating that these mutants retained their ability to form dimers. Mutations of these residues reduced kinetochore targeting of Mad1, consistent with them being directly involved in kinetochore binding. R617, K619, and R630 are located at the stem, suggesting that the stem of Mad1 CTD is a direct binding site of the kinetochore receptor of Mad1.

Bub1 is required for the proper kinetochore targeting of Mad1

Two of the class II residues, R617 and K619, reside in a conserved RLK motif (Figure 3-8A). In yeast, Mad1 forms a complex with Bub1–Bub3 in nocodazole-arrested mitotic cells, but not in interphase cells (Brady and Hardwick 2000). Interestingly, the RLK motif in yeast Mad1 is required for the checkpoint-stimulated binding between Mad1 and Bub1–Bub3. Cells harboring a Mad1 mutant with this motif mutated are deficient in the spindle checkpoint. The biochemical functions of the Mad1–Bub1–Bub3 interaction are unclear, however. Our results now reveal a requirement of the conserved RLK motif of Mad1 in kinetochore targeting, suggest an underlying basis for the checkpoint defect caused by the mutation of this motif in yeast, and further implicate Bub1 or its associated proteins as conserved kinetochore receptors of Mad1.

There had been conflicting reports in the literature on the requirement of Bub1 in the kinetochore targeting of Mad1 in human cells (Liu, Rattner et al. 2006; Klebig, Korinth et al. 2009). We therefore examined whether Bub1 was required for Mad1 kinetochore localization during unperturbed mitosis of human cells, using live-cell imaging. In cells transfected with the control siRNA, GFP-Mad1-5A localized normally to kinetochores during mitosis (Figure 3-11A). Depletion of Bub1 by RNAi greatly reduced the kinetochore localization of GFP-Mad1-5A. Depletion of Bub1 also diminished the kinetochore localization of the endogenous Mad1 in fixed HeLa cells (Figure 3-11B). Despite the near complete depletion of Bub1 (Figure 3-11C), the intensity of Mad1 staining at the kinetochore was only reduced to about 50% of that in control cells (Figure 3-11D). The reduction of Mad1 staining at the kinetochores was not observed in cells stably expressing RNAi-resistant mCherry-Bub1 (Figure 3-12), indicating that the observed effect of Bub1 RNAi was Bub1-dependent. Thus, Bub1 is required for proper kinetochore targeting of Mad1 in human cells, but it is not the sole kinetochore receptor of Mad1.

If Bub1 targeted Mad1 to kinetochores through an interaction with the RLK motif in the CTD, Bub1 depletion should not further reduce the already weakened kinetochore localization of the RLK-motif mutants. Indeed, depletion of Bub1 significantly reduced the kinetochore localization of Myc-Mad1, but not that of Myc-Mad1 R617A (Figure 3-13). This result placed Bub1 and Mad1 CTD in the same pathway for targeting Mad1 to kinetochores, and strongly implicated Bub1 as a kinetochore receptor for the CTD.

DISCUSSION

The unexpected structural similarity between the C-terminal domain (CTD) of Mad1 and the kinetochore-binding CTDs of Spc25 and Csm1 has led us to identify a role of Mad1 CTD in kinetochore targeting. The Mis12 complex is the kinetochore receptor of the Spc25–Spc24 dimer (Cheeseman, Chappie et al. 2006; Petrovic, Pasqualato et al. 2010). Csm1 interacts with both the Mis12 complex and CENP-C. The lack of apparent sequence similarity between the CTD of Mad1 and those of Spc25 and Csm1, however, suggests that they may not share the same kinetochore receptor. Furthermore, depletion of Ndc80 in human cells diminishes Mad1 kinetochore localization without affecting the kinetochore localization of the Mis12 complex (Martin-Lluesma, Stucke et al. 2002; Kline, Cheeseman et al. 2006). The Mis12 complex is thus unlikely the direct kinetochore receptor of Mad1 CTD.

In yeast, Mad1 forms a mitosis-specific interaction with the Bub1–Bub3 complex (Brady and Hardwick 2000). This interaction requires an RLK motif within Mad1 CTD. Cells harboring a Mad1 mutant with its RLK motif mutated are checkpoint deficient. Strikingly, we have shown here that the same RLK motif in the CTD is required for proper kinetochore targeting of Mad1 in human cells. Furthermore, depletion of Bub1 reduces the kinetochore localization of human Mad1. More importantly, Bub1 depletion does not further reduce the kinetochore localization of the Mad1 R617A mutant, suggesting that Bub1 and the RLK motif of Mad1 act in the same pathway to target Mad1 to kinetochores. These results strongly implicate Bub1 as a conserved kinetochore receptor for Mad1 CTD.

Unfortunately, despite extensive efforts and contrary to a previous report (Seeley, Wang et al. 1999), we have failed to detect a physical interaction between human Mad1 and Bub1 either in cells or *in vitro*. Several non-overlapping Mad1 fragments retain residual kinetochore targeting, indicating that Mad1 has an extensive kinetochore-binding surface with multiple quasi-independent contacting points. Consistently, depletion of Bub1 does not abolish Mad1 kinetochore localization. We propose that Mad1 forms contacts with multiple kinetochore proteins, one of which involves an interaction between Bub1 and Mad1 CTD, either directly or indirectly (Figure 3-14). Because the Mad1 **e** fragment containing the CTD is insufficient for kinetochore binding, the interaction between Mad1 CTD and human Bub1 on its own might be too weak to be detected.

In yeast, a C-terminal fragment of Mad1 is sufficient for kinetochore localization and checkpoint signaling (Kastenmayer, Lee et al. 2005). Binding between yeast Mad1 CTD and Bub1–Bub3 thus makes a more substantial energetic contribution to the Mad1 kinetochore localization and hence might have higher affinity, allowing its detection. Another non-exclusive possibility is that Bub1 as a part of a larger kinetochore complex serves as the receptor for Mad1. The integrity of the Bub1-containing complex might be preserved in yeast cell lysates, but not in human cell lysates, explaining why the Bub1–Mad1 interaction is only observed in yeast.

The kinetochore binding of several checkpoint proteins, such as Bub1, BubR1, and Mps1, can be attributed to small, defined domains (Taylor and McKeon 1997; Stucke, Baumann et al. 2004; Kiyomitsu, Obuse et al. 2007). By contrast, Mad1 uses an extensive, multivalent binding surface to interact with kinetochores. This mode of

kinetochore targeting by Mad1 is unusual and has important implications for checkpoint signaling. In particular, this mechanism rationalizes the graded targeting of Mad1 to kinetochores under different conditions that activate the checkpoint. For example, the concentration of Mad1 at attached but untense kinetochores in Taxol-arrested mitotic human cells is much lower than that at unattached kinetochores in nocodazole-treated cells. Yet, the mitotic arrest of Taxol-treated cells is still dependent on Mad1–Mad2, suggesting that a small amount of Mad1 at the kinetochores is sufficient to sustain the checkpoint. A similar situation exists in cells depleted of the Ndc80 complex (Martin-Lluesma, Stucke et al. 2002).

It is unclear whether the checkpoint-competent, reduced Mad1 kinetochore targeting under these conditions is caused by a distributive, uniform decrease of binding energy across the entire kinetochore-binding interface of Mad1 or by the selective disruption of a subset of discrete interactions between Mad1 and its kinetochore receptors. The current study has laid the foundation and provided the necessary tools for future experiments that will differentiate these two possibilities and establish how Mad1 integrates upstream checkpoint signals.

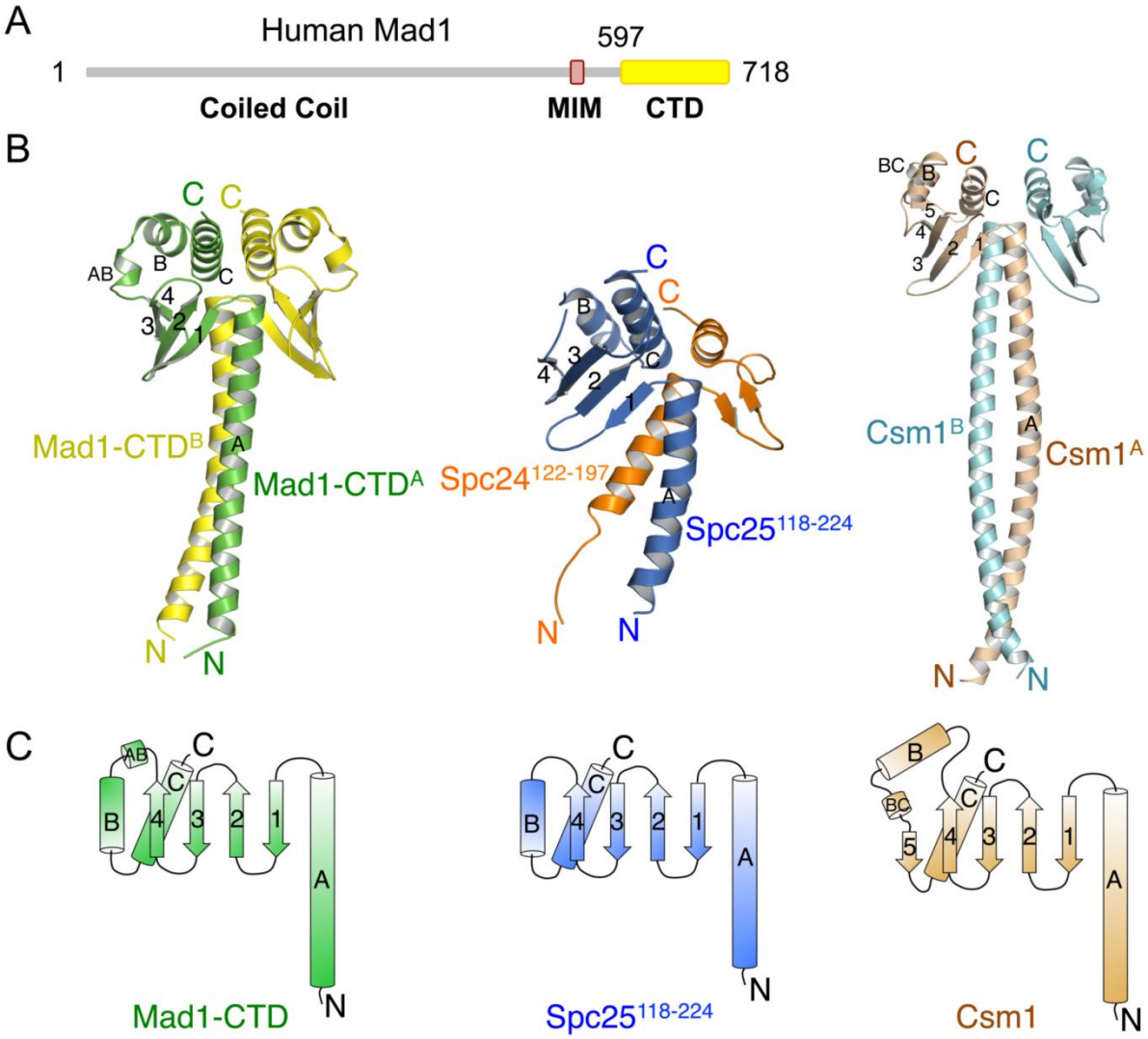

Figure 3-1. Structure of the Mad1 C-terminal domain (CTD) reveals fold similarity to the Ndc80 complex subunit Spc25 and the monopolin subunit Csm1. (**A**) Domain architecture of human Mad1. MIM, Mad2-interacting motif. CTD, C-terminal domain. (**B**) Ribbon diagrams of human Mad1 CTD homodimer (left), the Spc25-Spc24 CTD heterodimer (center; PDB code: 2VE7), and the Csm1 homodimer (right; PDB code: 3N4X). (**C**) Topology diagrams of Mad1 CTD (left), Spc25 CTD (middle) and Csm1 (right). All ribbon diagrams were generated using the program Pymol (http://www.pymol.org).

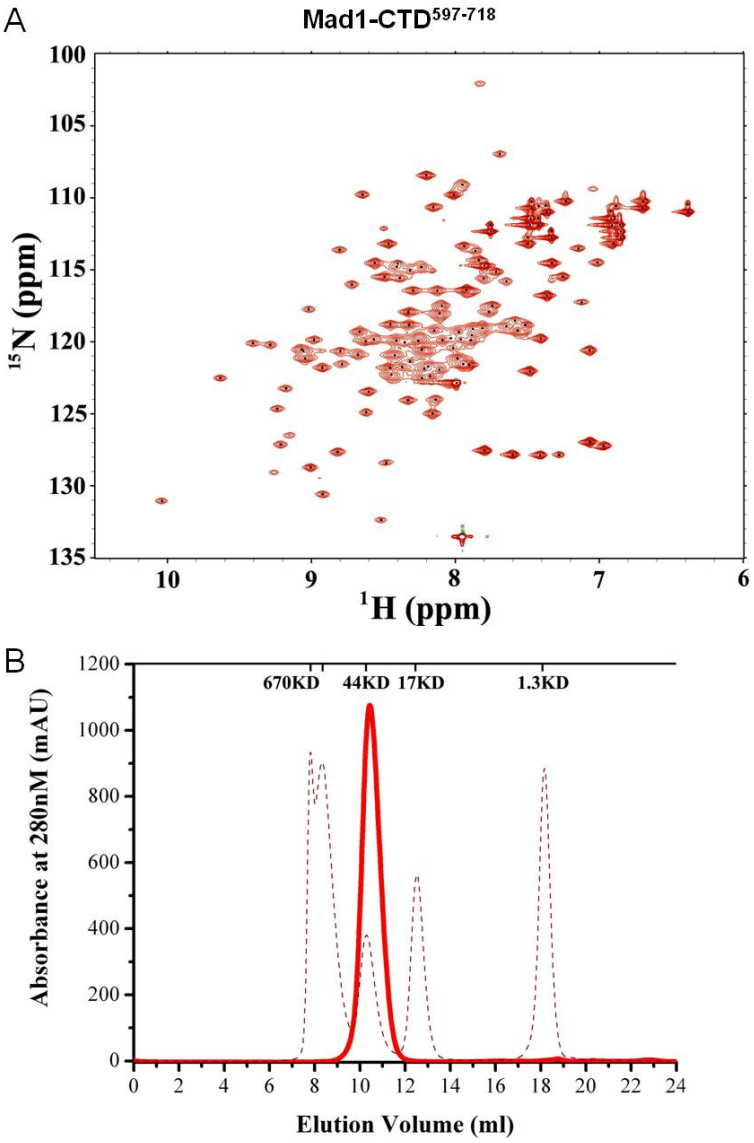

Figure 3-2. The Mad1 C-terminal region is a well-folded domain. (**A**) 2D ^{1}H-^{15}N HSQC spectrum of ^{15}N-labeled Mad1 CTD. (**B**) The UV trace of Mad1 CTD fractionated on a Superdex 75 gel filtration column. The UV trace of molecular mass standards is shown as a dashed line with the molecular masses of the standards indicated at the top of the trace.

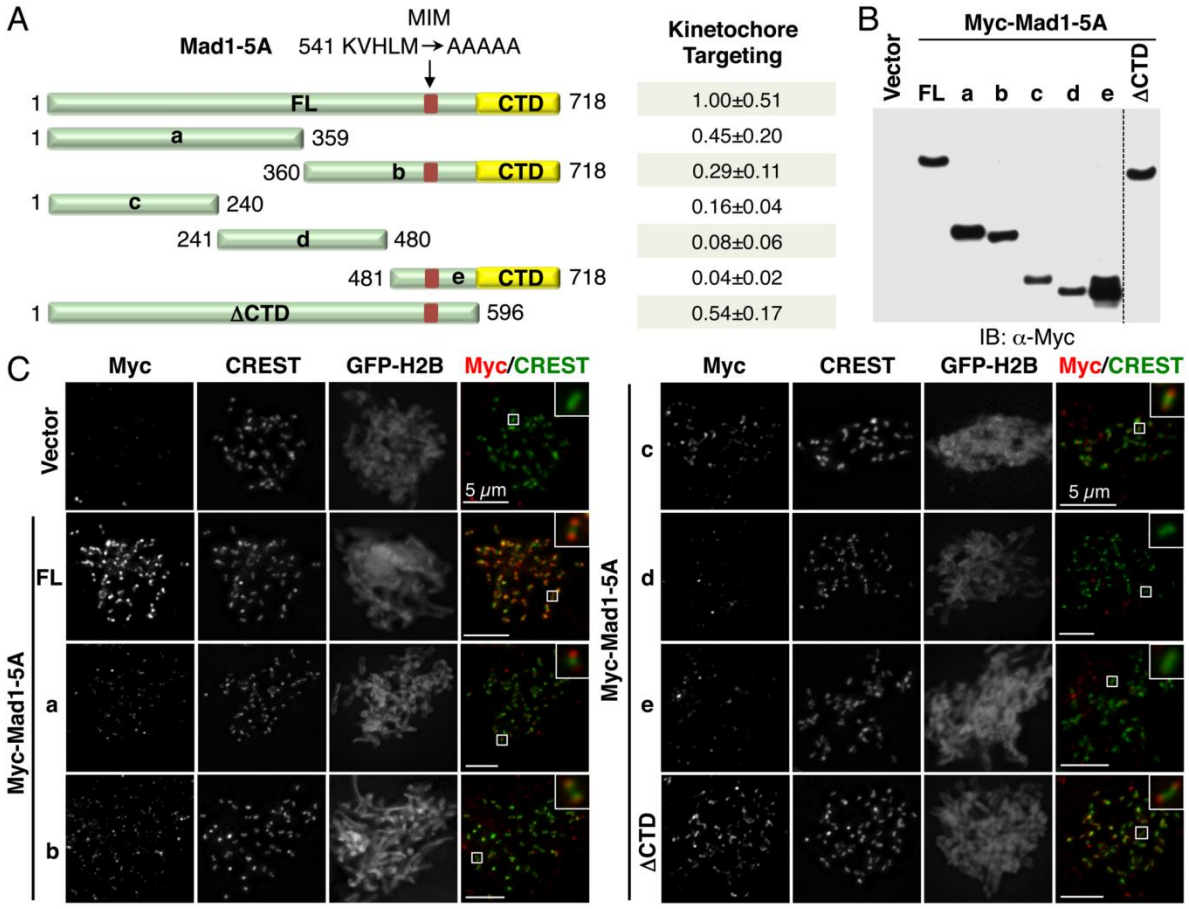

Figure 3-3. Non-overlapping Mad1 fragments exhibit detectable kinetochore binding. (**A**) Schematic drawing of Mad1 fragments used in this study. MIM, Mad2-interacting motif. The full-length Mad1 and fragments **b**, **e**, and ΔCTD had their MIM mutated to five alanines (5A). The relative intensity of the kinetochore signals of these Mad1 mutants was summarized on the right. The mean and standard deviation of Mad1 kinetochore signals from 10 cells for each construct were shown. (**B**) Lysates of HeLa Tet-On cells transfected with plasmids encoding various Mad1 fragments were blotted with anti-Myc. (**C**) Mitotic HeLa Tet-On cells transiently transfected with the indicated Mad1 fragments were stained with antibodies against Myc (red in the overlay) and CREST (green). GFP-H2B was co-transfected with Myc-Mad1 and used as a marker for transfected cells. Scale bars, 5μm.

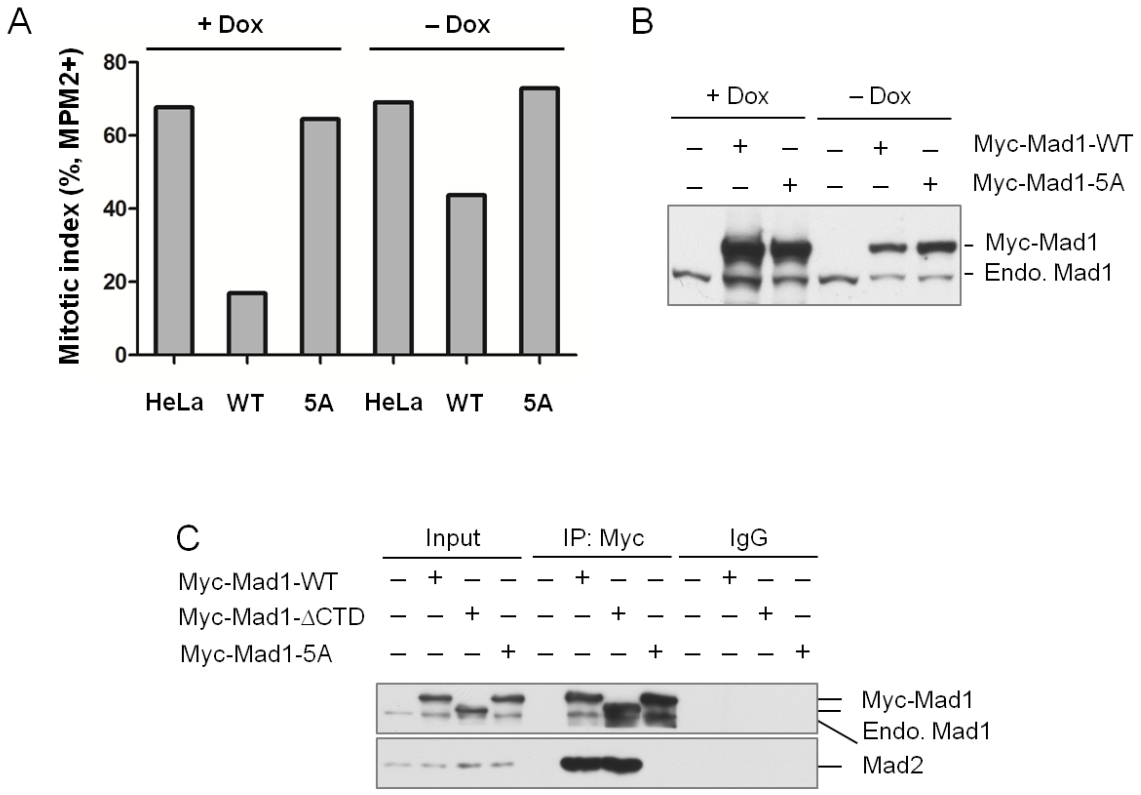

Figure 3-4. Mad1 overexpression inactivates the spindle checkpoint. (**A**) HeLa Tet-On cells stably expressing Myc-tagged Mad1 WT or 5A were treated with thymidine for 14 hrs and released into 300 nM nocodazole for 16 hrs in the absence or presence of 1.0 μg/ml doxycycline (Dox). The parental HeLa Tet-On cells were used as control. The mitotic index was analyzed by MPM2 staining and flow cytometry (FACS). For FACS analysis, cells were collected by trypsinization, washed once with PBS, and fixed with cold 70% ethanol. After overnight fixation at -20˚C, cells were washed with PBS and permeabilized with PBS containing 0.25% (v/v) Triton X-100 for 5 min. Cells were then incubated with α-MPM2 (Millipore) followed by an incubation with fluorescent secondary antibodies (Invitrogen) diluted in PBS plus 1% BSA. After washing with PBS, the cells were stained with propidium iodide (Sigma) at a final concentration of 20 μg/ml, and simultaneously treated with 200 μg/ml RNase A (Qiagen). The samples were analyzed with FacsScan (Becton Dickinson) and the FlowJo software (Tree Star). (**B**) Lysates of cells in (**A**) were blotted with antibodies against Mad1. The positions of Myc-tagged and endogenous (Endo.) Mad1 proteins are labeled. Note that both Myc-Mad1 WT and 5A stable clones had leaky Myc-Mad1 expression in the absence of Dox. (**C**) HeLa Tet-On cells were transfected with the indicated plasmids. The cell lysates, IgG IP

and Myc IP were blotted with antibodies against Mad1 or Mad2. The positions of Myc-tagged and endogenous (Endo.) Mad1 proteins are labeled.

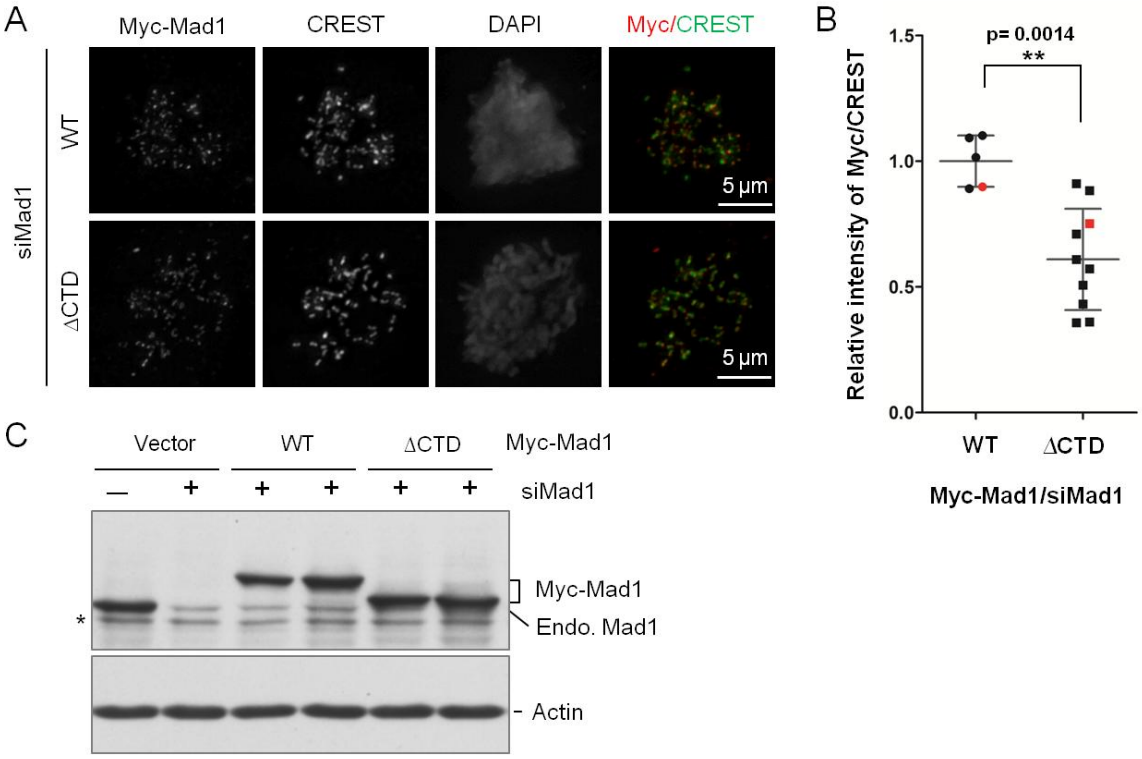

Figure 3-5. The kinetochore localization of Mad1-ΔCTD is independent of the endogenous Mad1. (**A**) Mitotic HeLa Tet-On cells expressing RNAi-resistant Myc-Mad1 WT or ΔCTD were transfected with siMad1 and stained with antibodies against Myc (red), CREST (green), and DAPI. Scale bars, 5 μm. (**B**) Quantification of the normalized intensity of Myc-Mad1 kinetochore signal in cells described in (**A**). In each cell, the fluorescence signal from 20 kinetochores was analyzed and averaged. Each dot indicated a single cell. The red dots belonged to the cells presented in (**A**). The error bars indicated the standard deviation (n=5 for WT; n=10 for ΔCTD). (**C**) HeLa cell lysates and lysates of cells in (**A**) were blotted with antibodies against Mad1 and actin (used as a loading control). The positions of the Myc-tagged and endogenous (Endo.) Mad1 proteins were labeled. The asterisk indicated a cross-reacting band.

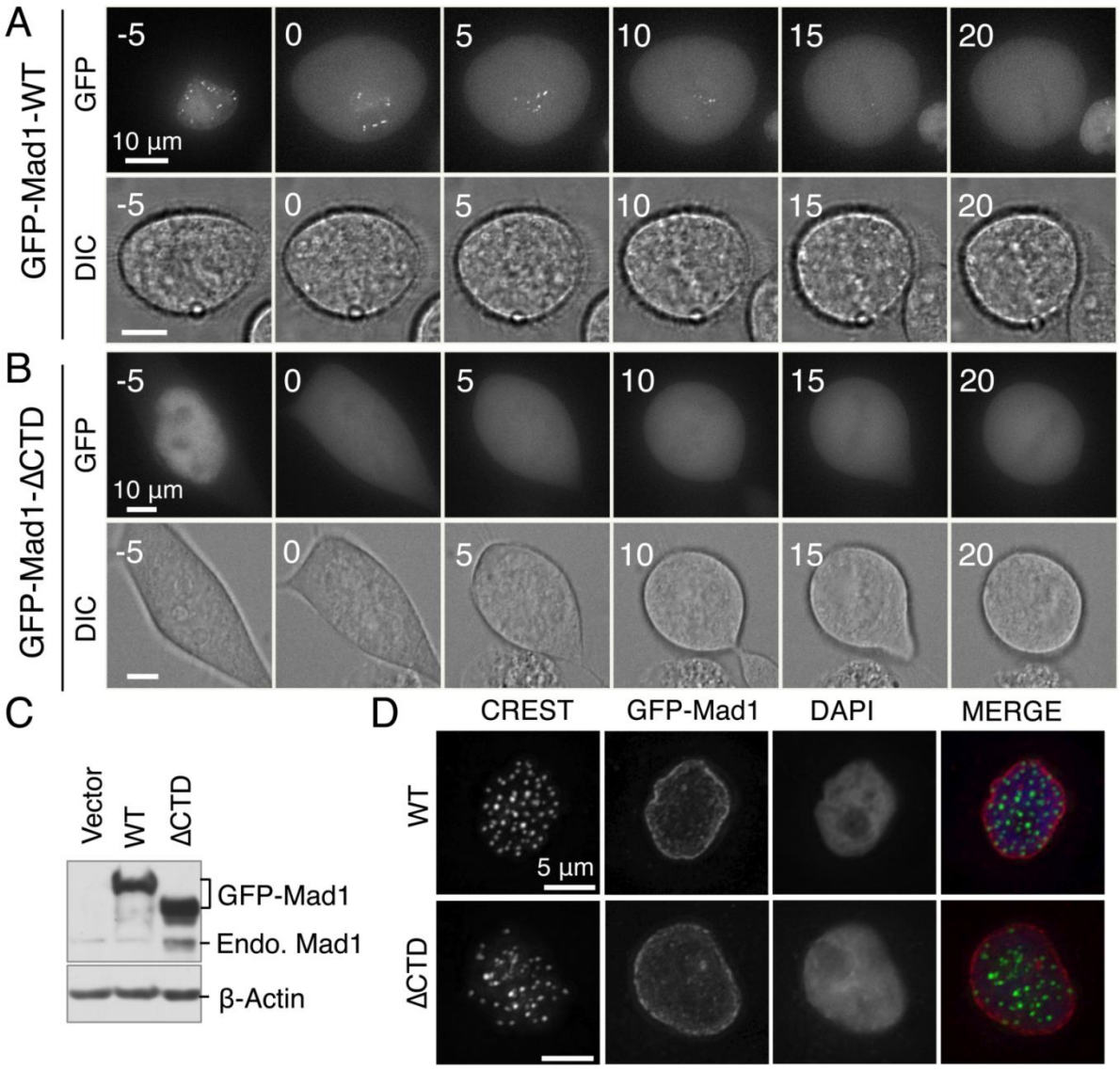

Figure 3-6. The CTD is required for the kinetochore targeting of Mad1 during unperturbed mitosis in human cells. (**A and B**) HeLa Tet-On cells stably expressing GFP-tagged wild-type Mad1 (WT) (**A**) or the ΔCTD mutant (**B**) were analyzed using live-cell imaging. GFP and differential interference contrast (DIC) images of a representative cell at the indicated times (in minutes) were shown. Nuclear envelope break down (NEBD) was set as time 0. Scale bars, 10 μm. (**C**) Lysates of HeLa cells transfected with the empty vector and cells in (**A**) and (**B**) were blotted with anti-Mad1. The positions of GFP-Mad1 or the endogenous (Endo.) Mad1 proteins were indicated. Actin was used as the loading control. (**D**) Interphase HeLa cells stably expressing GFP-

Mad1-WT or ΔCTD were stained with anti-GFP (pseudo-colored red in merge), CREST (green), and DAPI (blue). Scale bars, 5 μm.

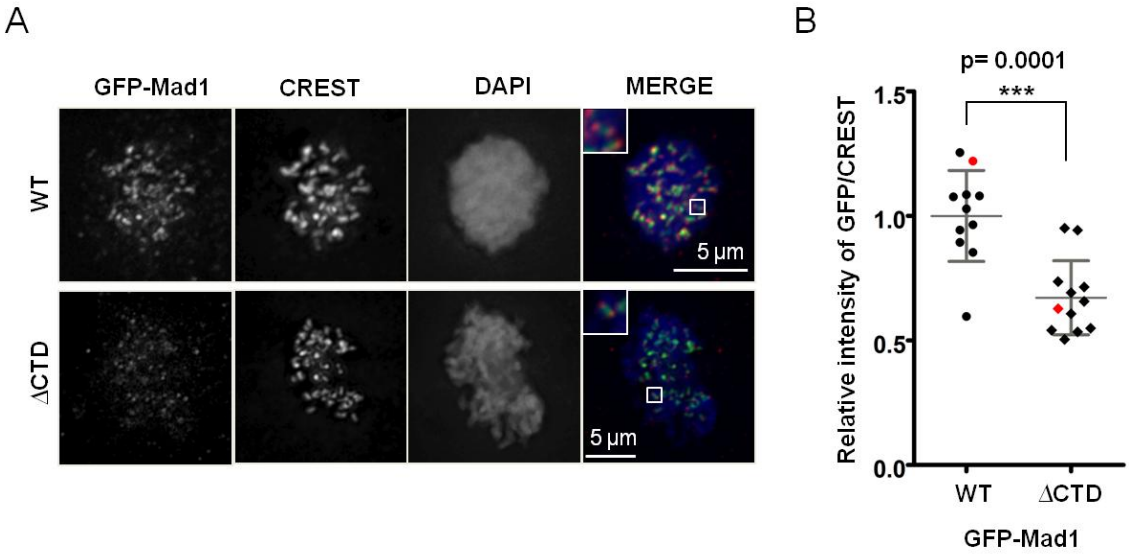

Figure 3-7. GFP-Mad1 ΔCTD exhibits detectable kinetochore binding in fixed cells. (**A**) Mitotic HeLa Tet-On cells stably expressing GFP-Mad1 WT or ΔCTD were stained with DAPI (blue) and antibodies against GFP (red) and CREST (green). Scale bars, 5μm. (**B**) Quantification of the normalized intensity of GFP-Mad1 kinetochore signal in cells described in (**A**). In each cell, the fluorescence signal from 20 kinetochores was analyzed and averaged. Each dot indicated a single cell. The red dots belonged to the cells presented in (**A**). The error bars indicated the standard deviation (n=11 for WT; n=12 for ΔCTD).

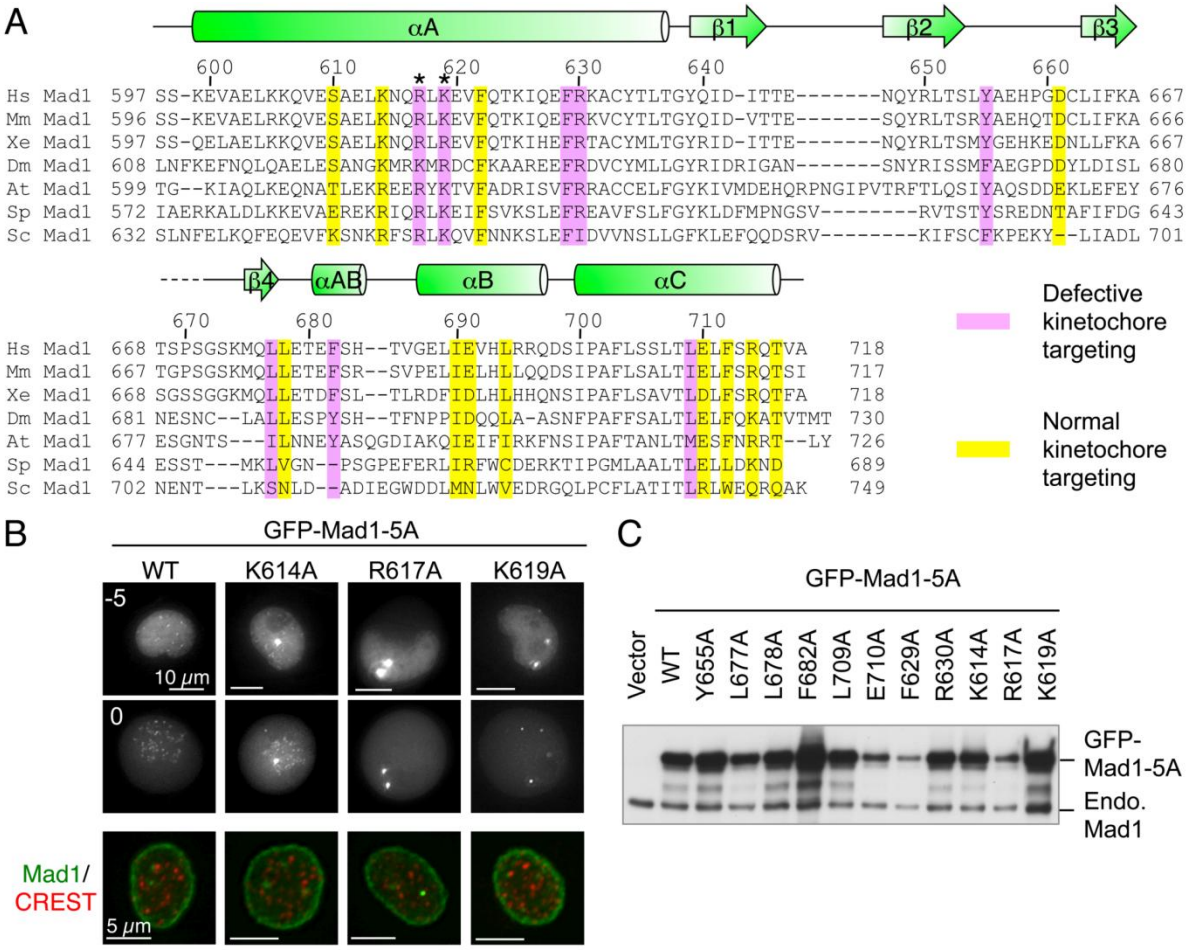

Figure 3-8. Structure-based mutagenesis identifies Mad1 CTD residues critical for kinetochore targeting. (**A**) Sequence alignment of Mad1 CTD from different species with the secondary structural elements shown above. Residues whose mutations did or did not disrupt Mad1 kinetochore targeting were colored purple or yellow, respectively. R617 and K619 in the conserved RLK motif are labeled with asterisks. (**B**) HeLa Tet-On cells expressing the indicated GFP-Mad1-5A mutants were analyzed by time lapse fluorescence microscopy. GFP images of representative cells at NEBD (time 0) and at 5 min before NEBD were shown. Note that a fraction of the overexpressed GFP-Mad1-5A mutant proteins presumably aggregated and formed large foci that were not kinetochores. Scale bars, 10 μm. The right panel showed interphase cells expressing the same Myc-Mad1 mutants stained with anti-Myc (green) and CREST (red). Scale bars, 5 μm. (**C**) Lysates of cells expressing GFP-Mad1-5A and mutants were blotted with anti-Mad1. The positions of GFP-Mad1-5A and the endogenous (Endo.) Mad1 proteins were labeled.

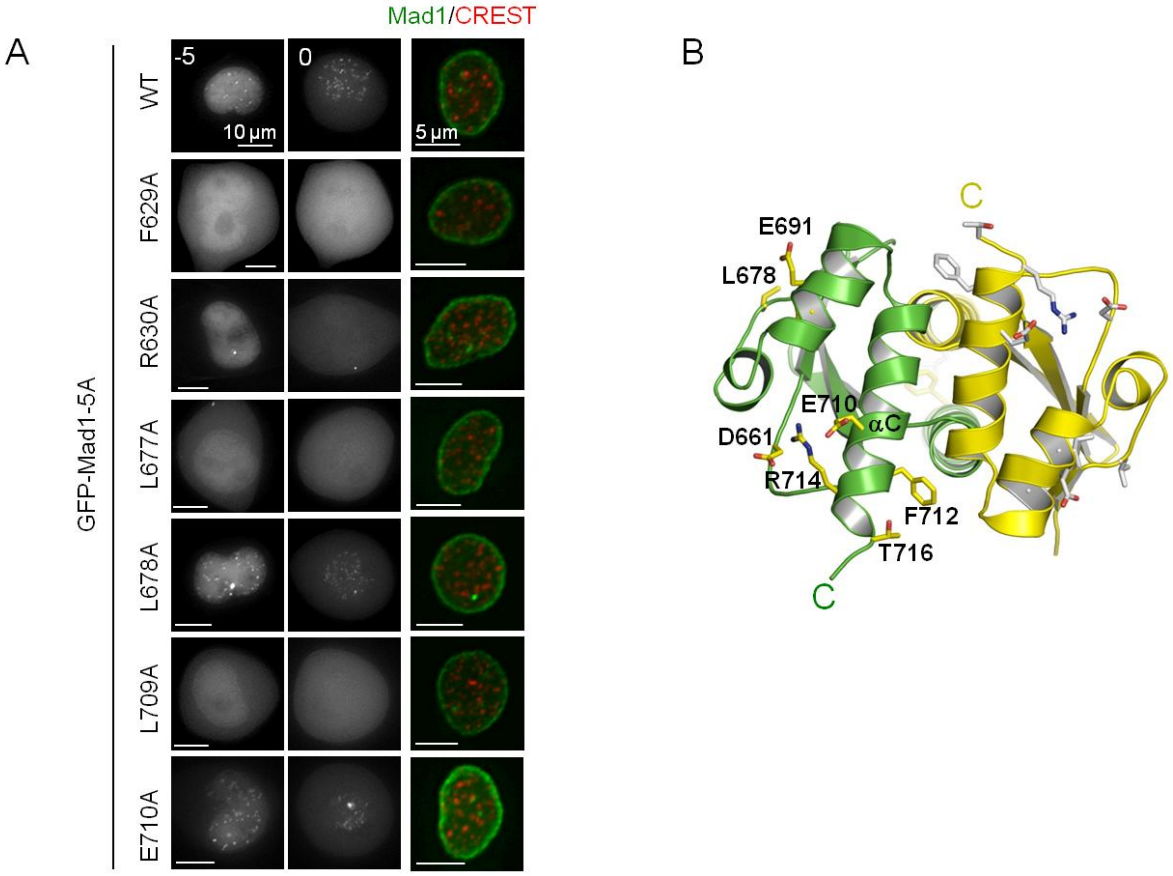

Figure 3-9. Structure-based mutagenesis identifies Mad1 CTD residues critical for kinetochore targeting. (**A**) HeLa Tet-On cells expressing the indicated GFP-Mad1-5A mutants were analyzed by time lapse fluorescence microscopy. GFP images of representative cells at NEBD (time 0) and at 5 min before NEBD were shown. Note that a fraction of the overexpressed GFP-Mad1-5A mutant proteins presumably aggregated and formed large foci that were not kinetochores. Scale bars, 10 µm. The right panel showed interphase cells expressing the same Myc-Mad1 mutants stained with anti-Myc (green) and CREST (red). Scale bars, 5 µm. The same images for WT are also presented in Figure 3-8B. (**B**) Ribbon drawing of Mad1 CTD (top view) with residues not critical for kinetochore targeting in one monomer shown as yellow sticks and labeled. The corresponding residues in the other monomer were shown in grey sticks and not labeled for clarity.

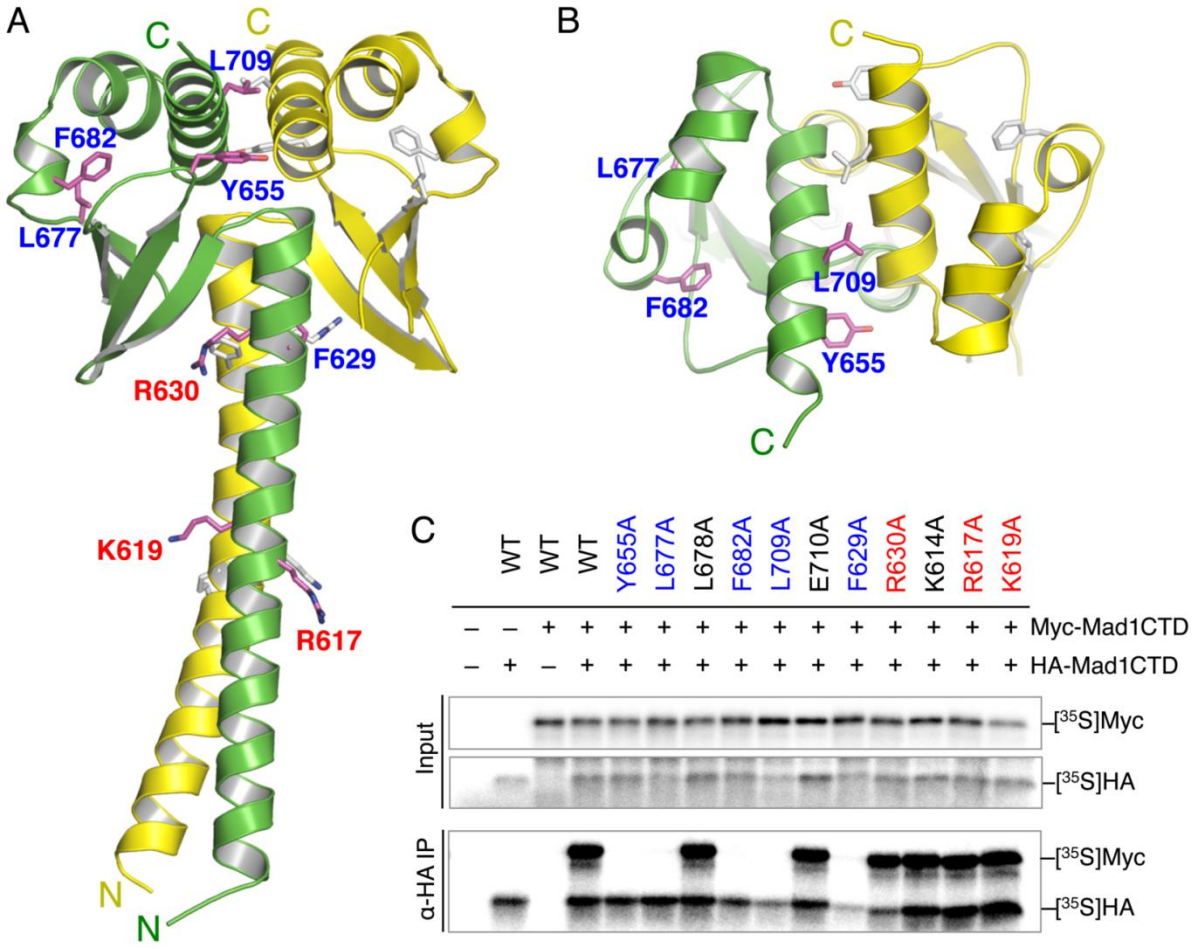

Figure 3-10. Mutations of a conserved RLK motif in Mad1 CTD diminish kinetochore targeting of Mad1 without disrupting CTD dimerization. (**A and B**) Ribbon drawings of Mad1 CTD (**A**, side view; **B,** top view) with residues critical for kinetochore targeting in one monomer shown as purple sticks and labeled. The class I and II residues whose mutations did or did not disrupt dimerization were labeled with blue and red letters, respectively. The corresponding residues in the other monomer were shown in grey sticks and not labeled for clarity. (**C**) In vitro dimerization assays of Mad1 CTD mutants. HA- and Myc-tagged Mad1 CTD proteins were co-translated in vitro in the presence of ^{35}S-methionine. The input (top panel) and anti-HA IP (bottom panel) were separated by SDS-PAGE and analyzed with a phosphor imager.

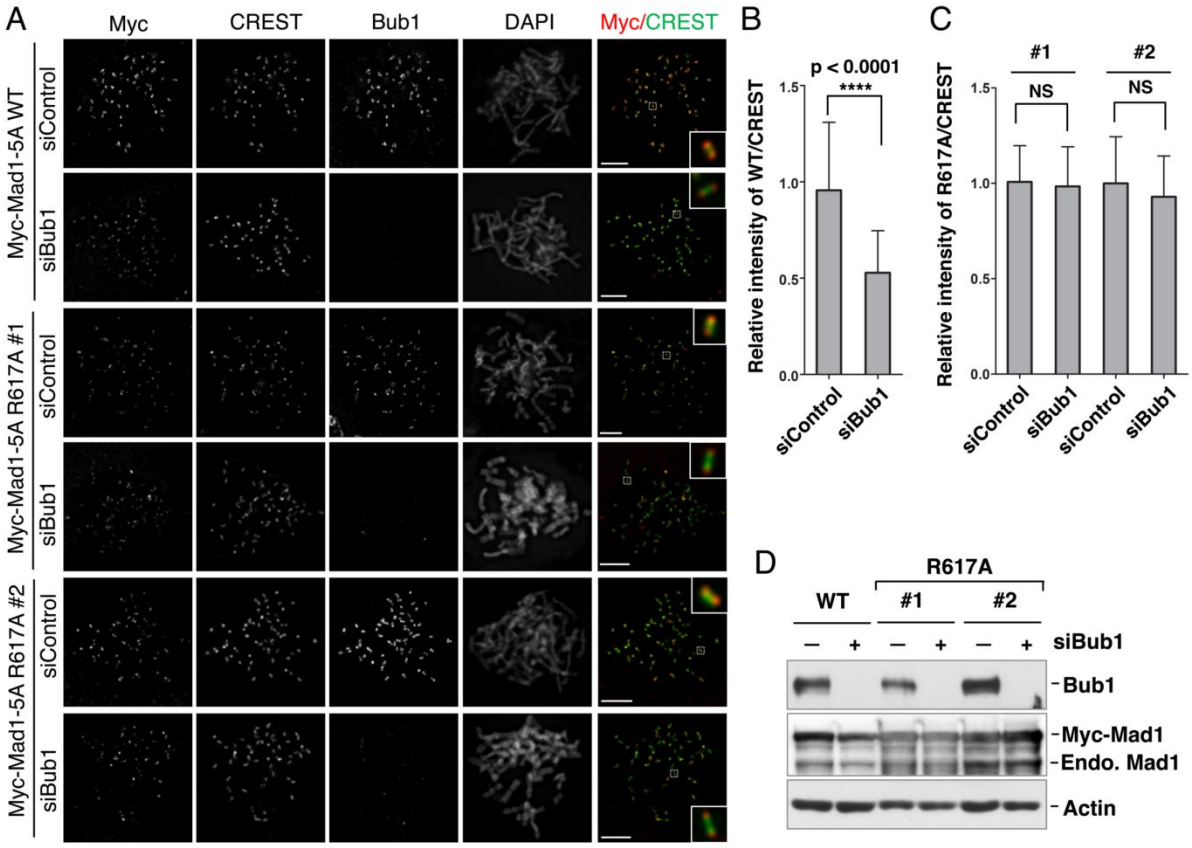

Figure 3-11. Bub1 inactivation does not further reduce the residual kinetochore localization of the Mad1 RLK-motif mutant, R617A. (**A**) HeLa Tet-On cells stably expressing Myc-Mad1-5A WT or R617A (two independent clones, #1 and #2) were transfected with siControl or siBub1. Mitotic cells were stained with antibodies against Myc (red in the overlay), Bub1, CREST (green), and DAPI. Scale bars, 5 μm. (**B** and **C**) Normalized kinetochore intensities of Myc-Mad1-5A WT (**B**) or R617A (**C**) of cells in (**A**). The mean and standard deviation of two independent experiments were shown. NS, not significant. (**D**) Lysates of cells in (**A**) were blotted with antibodies against Bub1, Mad1 and actin (used as a loading control). The positions of the Myc-tagged and endogenous (Endo.) Mad1 proteins were labeled.

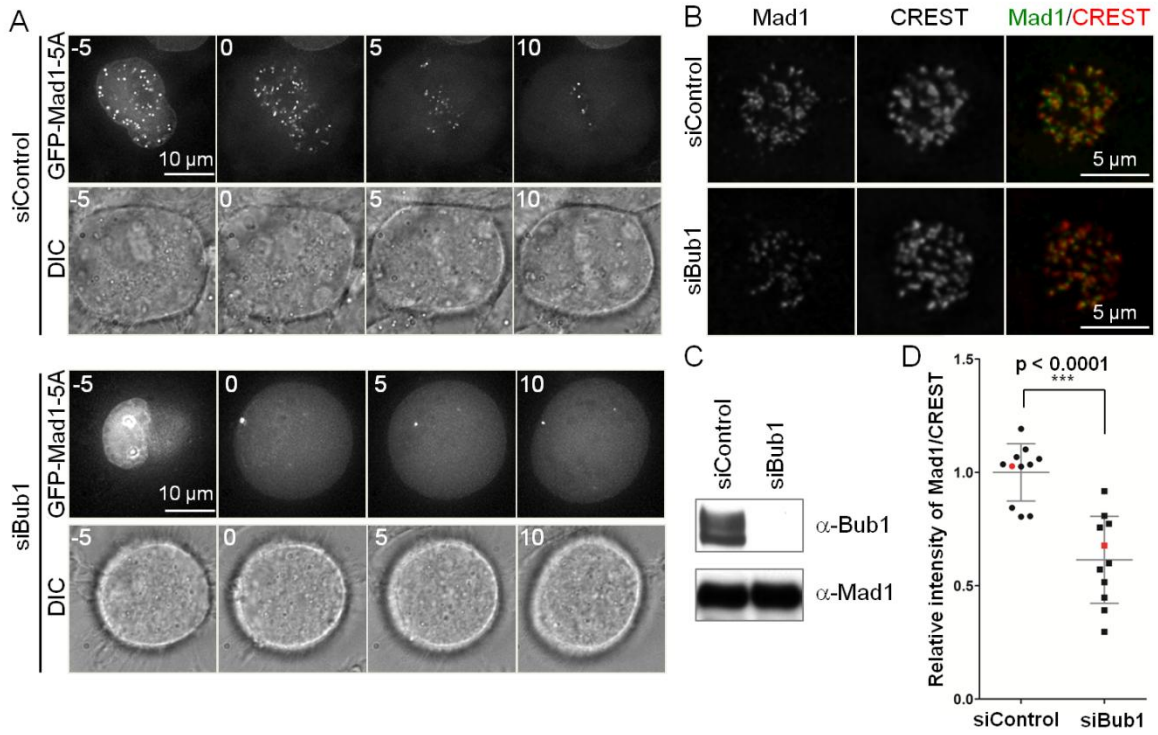

Figure 3-12. Bub1 is required for the kinetochore targeting of Mad1 during unperturbed mitosis in human cells. (**A**) HeLa Tet-On cells expressing GFP-Mad1-5A were transfected with siControl or siBub1 were analyzed using time lapse fluorescence microscopy. GFP and differential interference contrast (DIC) images of a representative cell at the indicated times (in minutes) were shown. Nuclear envelope break down (NEBD) was set as time 0. Scale bars, 10 μm. (**B**) Mitotic HeLa Tet-On cells transfected with siControl or siBub1 were stained with antibodies against Mad1 (green) and CREST (red). Scale bars, 5 μm. (**C**) Lysates of cells in (**B**) were blotted with antibodies against Bub1 and Mad1. (**D**) Quantification of the normalized intensity of Mad1 kinetochore signal in cells described in (**B**). In each cell, the fluorescence signal from 20 kinetochores was analyzed and averaged. Each dot indicated a single cell. The red dots belonged to the cells presented in (**B**). The error bars indicated the standard deviation (n=11).

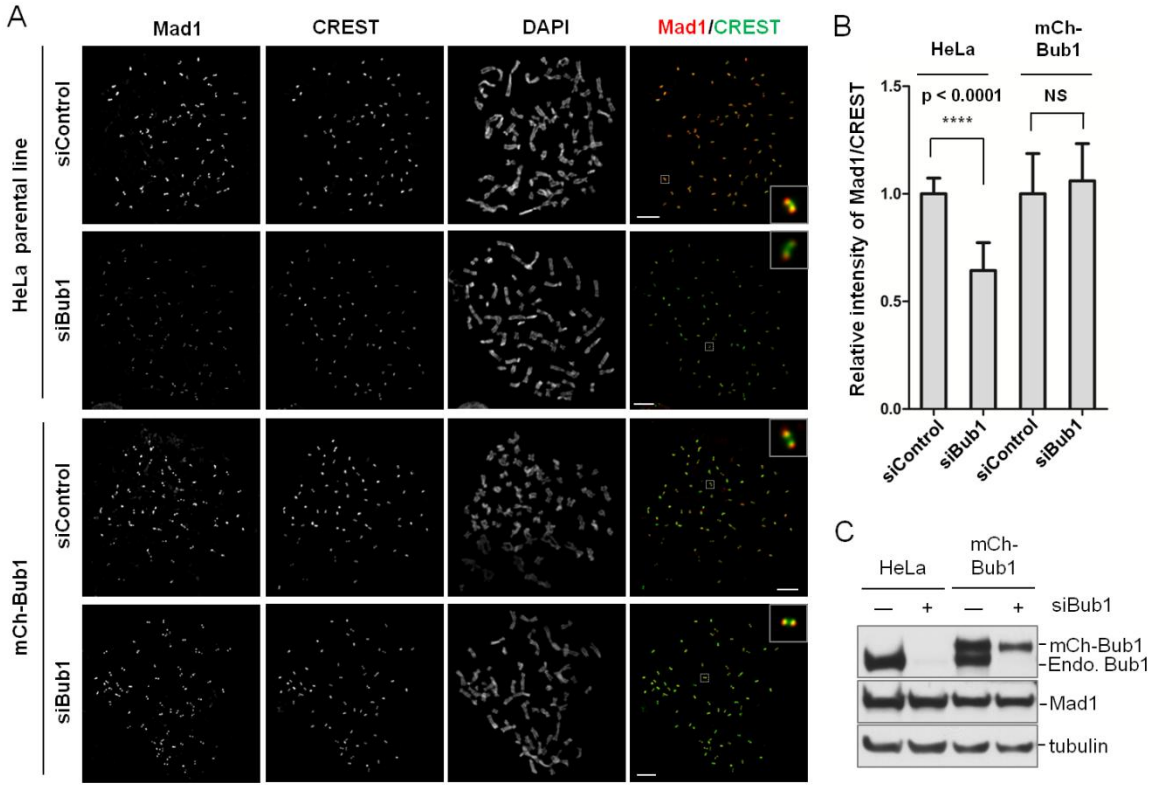

Figure 3-13. The reduction of Mad1 kinetochore localization caused by Bub1 siRNA is rescued by the stable expression of RNAi-resistant Bub1. (**A**) HeLa Tet-On cells stably expressing the RNAi-resistant mutant of mCherry-Bub1 (mCh-Bub1) were transfected with siControl or siBub1. The parental HeLa Tet-On cells were used as the control. Mitotic cells were stained with DAPI and antibodies against Mad1 (red in the overlay) and CREST (green). Scale bars, 5 μm. (**B**) Normalized kinetochore intensities of Mad1. The mean and standard deviation of two independent experiments were shown. NS, not significant. (**C**) Lysates of cells in (**A**) were blotted with antibodies against Bub1, Mad1, and tubulin (used as the loading control). The positions of the mCherry-tagged and endogenous (Endo.) Bub1 proteins were labeled.

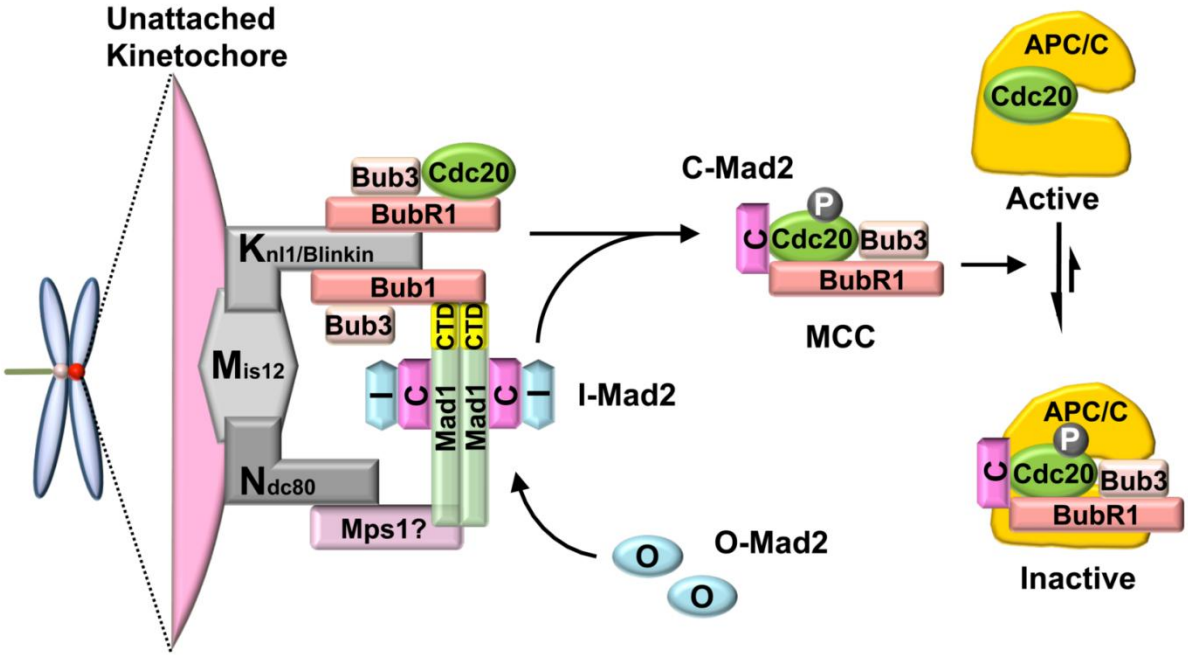

Figure 3-14. A multivalency model for Mad1 kinetochore targeting. In this model, Mad1 is targeted to kinetochores through multiple quasi-independent contact sites with kinetochore receptors. One such contact site is between Bub1 and Mad1 CTD. Bub1–Bub3, BubR1–Bub3, and Mps1 are recruited to kinetochores by the KMN (Knl1/Blinkin–Mis12–Ndc80) network of proteins. Ndc80 and Mps1 are required for proper Mad1 kinetochore targeting. It remains to be established whether the N-terminal region of Mad1 directly contacts Ndc80 or Mps1. At the kinetochores, the Mad1–Mad2 core complex promotes the conformational activation of Mad2, Mad2 binding to Cdc20, and APC/C inhibition.

Table 3-1. Data Collection, Structure Determination, and Refinement

Data Collection	
Crystal	SeMet (Peak)[a]
Space group	$P6_5$
Energy (eV)	12,659.6
Resolution range (Å)	33.96-1.76 (1.79-1.76)
Unique reflections	23,680 (1,202)
Multiplicity	14.8 (11.5)
Data completeness (%)	99.9 (98.6)
R_{merge} (%)[b]	8.1 (67.6)
I/σ(I)	10.2 (3.8)
Wilson B-value (Å^2)	19.83
Phase Determination	
Anomalous scatterer	selenium (2 of 2 possible sites)
Figure of merit (33.96-1.76 Å)	0.47 (0.89 after density modification)
Refinement Statistics	
Resolution range (Å)	33.96 -1.76 (1.80-1.76)
No. of reflections R_{work}/R_{free}	23,583/2,034 (1,423/136)
Data completeness (%)	99.9 (99.0)
Atoms (non-H protein/solvent)	1,914/287
R_{work} (%)	16.0 (23.4)
R_{free} (%)	19.7 (26.8)
R.m.s.d. bond length (Å)	0.011
R.m.s.d. bond angle (°)	1.205
Mean B-value (Å^2) (protein/solvent)	25.8/33.3
Ramachandran plot (%) (favored/disallowed)[c]	100.0/0.0
Maximum likelihood coordinate error	0.40
Missing residues	Chain A: 597, 670-671, 717-718; Chain B: 669-671.

Data for the outermost shell are given in parentheses.

[a]Bijvoet pairs were kept separate for data processing.

[b]$R_{merge} = 100\ \Sigma_h\Sigma_i|I_{h,\ i} - \langle I_h\rangle|/\Sigma_h\Sigma_i I_{h,\ i}$, where the outer sum (h) is over the unique reflections and the inner sum (i) is over the set of independent observations of each unique reflection.

[c]As defined by the validation suite MolProbity.

CHAPTER IV: ASSEMBLY PATHWAYS OF THE SPINDLE CHECKPOINT SENSOR KMN AT KINETOCHORES

INTRODUCTION

The kinetochore is a multilayered protein assembly on centromeric chromatin and acts as a platform on sister chromatids for the attachment of spindle microtubules during mitosis(Cleveland, Mao et al. 2003). The Constitutive Centromere-Associated Network (CCAN) of proteins binds to centromeric chromatin throughout the cell cycle and forms the inner kinetochore(Foltz, Jansen et al. 2006; Okada, Cheeseman et al. 2006; Black and Cleveland 2011; Takeuchi and Fukagawa 2012). It provides the foundation for the mitosis-specific assembly of the outer kinetochore. Among the outer kinetochore proteins, the KMN network, which consists of Knl1 (also known as Blinkin in humans), the Mis12 complex (Mis12C which comprises Dsn1, Nsl1, Mis12, and Nnf1), and the Ndc80 complex (Ndc80C which comprises Ndc80, Nuf2, Spc25, and Spc24), acts as a receptor for spindle microtubules(Cheeseman, Chappie et al. 2006; Cheeseman and Desai 2008). In this network, Mis12C directly binds to both Knl1 and Ndc80C, thus bridging an interaction between the two(Gascoigne and Cheeseman 2013; Petrovic, Mosalaganti et al. 2014).

Accurate chromosome segregation relies on proper kinetochore-microtubule attachment during mitosis, which entails the capturing of a pair of sister kinetochores by microtubules originating from the two opposite spindle poles (a state termed bi-orientation)(Cheeseman and Desai 2008). Unattached or improperly attached

kinetochores activate the spindle checkpoint to delay anaphase onset(Lara-Gonzalez, Westhorpe et al. 2012; Foley and Kapoor 2013; Jia, Kim et al. 2013). Furthermore, the centromeric kinase Aurora B severs improper kinetochore-microtubule attachments through phosphorylating multiple KMN components(Tanaka, Rachidi et al. 2002; Ruchaud, Carmena et al. 2007; Welburn, Vleugel et al. 2010; Lampson and Cheeseman 2011), thus promoting sister-chromatid bi-orientation. After all pairs of sister kinetochores reach bi-orientation, the spindle checkpoint is inactivated to allow synchronous dissolution of sister-chromatid cohesion and equal partition of the separated sister chromatids into the two daughter cells.

In addition to microtubule binding, KMN recruits spindle checkpoint proteins to outer kinetochores during mitosis. Knl1 is the direct kinetochore receptor for the Bub1–Bub3 and BubR1–Bub3 checkpoint complexes(London, Ceto et al. 2012; Shepperd, Meadows et al. 2012; Yamagishi, Yang et al. 2012; Primorac, Weir et al. 2013; Vleugel, Tromer et al. 2013; Krenn, Overlack et al. 2014). Ndc80C is required for the optimal kinetochore targeting of Mps1 and Mad1–Mad2(Martin-Lluesma, Stucke et al. 2002; Stucke, Baumann et al. 2004). Furthermore, Ndc80C inactivation by antibody addition in *Xenopus* egg extracts or by temperature-sensitive mutations in the budding yeast compromises the spindle checkpoint(McCleland, Gardner et al. 2003). These findings suggest a role for KMN components in communicating microtubule-attachment status to the spindle checkpoint.

Despite its importance, our understanding of how KMN is installed at mitotic kinetochores is incomplete. During mitosis, CCAN connects centromeric chromatin and

outer kinetochore through simultaneously engaging both the centromere-defining CENP-A nucleosome and outer kinetochore components, including KMN. Tethering two CCAN components, CENP-T and CENP-C, to non-centromeric loci is sufficient to establish an ectopic functional kinetochore that recruits KMN independently of CENP-A(Gascoigne, Takeuchi et al. 2011). CENP-T and CENP-C directly interact with Ndc80C and Mis12C, respectively(Gascoigne, Takeuchi et al. 2011; Screpanti, De Antoni et al. 2011; Schleiffer, Maier et al. 2012). These findings are seemingly consistent with a simple model in which KMN is anchored to CCAN through the bipartite CENP-C–Mis12C and CENP-T–Ndc80C interactions (Figure. 4-1A; the bipartite recruitment model).

Recent studies have shown, however, that CENP-T and Mis12C bind competitively to overlapping sites on Ndc80C(Bock, Pagliuca et al. 2012; Malvezzi, Litos et al. 2013; Nishino, Rago et al. 2013). CENP-T-bound Ndc80C cannot simultaneously engage Mis12C. Thus, there are two kinetochore complexes containing Ndc80C: CENP-T-bound free Ndc80C and CENP-C-bound intact KMN (Figure. 4-1A; the parallel recruitment model). The CENP-C–Mis12C interaction remains the only well-characterized connection between CCAN and the intact KMN.

The mitosis-specific installation of CENP-T-bound Ndc80C at kinetochores is mediated by the cytoplasm-to-nucleus translocation of Ndc80C shortly before mitotic entry and by Cdk1-dependent phosphorylation of the Ndc80C-binding region of CENP-T(Gascoigne and Cheeseman 2013). The mitosis-specific targeting of CENP-C-bound KMN to kinetochores is not understood, however. In particular, Mis12C resides in the nucleus throughout interphase, but does not localize to kinetochores until

mitosis(Gascoigne and Cheeseman 2013), suggesting that the CCAN–Mis12C interaction is cell cycle regulated. The regulatory mechanism has not been established.

In this study, we investigated the functions of the two outer kinetochore complexes, CENP-C-bound KMN and CENP-T-bound Ndc80C, in the spindle checkpoint in human cells. To avoid complication from checkpoint weakening by partial microtubule occupancy at kinetochores, we treated cells with high concentrations of the microtubule-depolymerizing drug, nocodazole. We found that CENP-C-bound intact KMN is critical for sustaining nocodazole-triggered mitotic arrest whereas CENP-T-bound Ndc80C is dispensable. We developed multiple strategies to inactivate KMN below the threshold required for sustaining an active spindle checkpoint. These KMN-inactivation strategies reveal two parallel, quasi-independent pathways of KMN assembly at kinetochores. In one pathway, Aurora B actively promotes the CCAN–KMN interaction through phosphorylating the Mis12C subunit Dsn1 and strengthening Mis12C binding to CENP-C in mitosis. Strikingly, co-expression of a phospho-mimicking Dsn1 mutant and Ndc80 fused to a nuclear localization signal (NLS) is sufficient to install KMN at interphase kinetochores. In another pathway, CENP-T provides an additional interaction with Ndc80C indirectly through the CENP-H-I-K sub-complex. This function of CENP-T does not require its Ndc80C-binding region. Thus, our results establish KMN as a key coordinator of spindle checkpoint signaling at kinetochores, and reveal the molecular mechanisms of its mitosis-specific attachment to kinetochores.

MATERIALS AND METHODS

Cell culture and transfection

HeLa Tet-On (Clontech) cells were grown in Dulbecco's modified Eagle's medium (DMEM; Invitrogen) supplemented with 10% fetal bovine serum, 6 mM L-glutamine, and 100 μg/ml penicillin and streptomycin. For G1/S arrest, cells were incubated in the growth medium containing 2 mM thymidine (Sigma) for 14-16 hr. For prometaphase arrest, cells were arrested in G1/S with thymidine, washed twice with PBS, and incubated with the growth medium containing 500 nM or 5 μM nocodazole (Sigma) for 11-12 hr. ZM447439 (ZM; Tocris) was added to 4 μM to inhibit Aurora B.

For RNAi experiments, cells were transfected with Lipofectamine RNAiMAX (Invitrogen) and analyzed at 24-72 hr after transfection. In the case of Dsn1 RNAi, a second round of siRNA transfection was performed at 3 days after the initial transfection and a subsequent passage. The predesigned set of four siRNA oligonucleotides was purchased from Thermo Scientific and tested by Western blots or immunostaining to identify the most effective siRNAs. The sequences (from 5' to 3') of siRNAs used in this study are: siControl (UCAUUCCGGAUACUGCGAUUU), siNdc80-4 (GAGUAGAACUAGAAUGUGA), siNdc80-M (AAGUUCAAAAGCUGGAUGAUCUU), siSpc24 (GGACACGACAGUCACAAUC), siSpc25 (CUACAAGGAUUCCAUCAAA), siDsn1 (GUCUAUCAGUGUCGAUUUA), siNsl1 (CAUGAGCUCUUUCUGUUUA), siCENP-C-6 (GAACAGAAUCCAUCACAAA), siCENP-C-9 (CGAAGUUGAUAGAGGAUGA),

siCENP-T-1 (GAAGAACAUCCUACUAACU), siCENP-T-18 (AAGUAGAGCCCUUACACGA), siCENP-H (AGAUUGAUUUGGACAGUAU), siCENP-N (AUACACCGCUUCUGGGUCA), siCdc20 (CGAAAUGACUAUUACCUGA), siCENP-I (GAAGGUGUGUGACAUAUAU), siCENP-L (CCUCAAAGUCUGGACAUUU), siCENP-U-7 (GAAAGCCAUCUGCGAAAUA), siCENP-U-8 (GAAAAUAAGUACACAACGU), siCENP-U-9 (GGGAAGAUAUCUCAUGACA), siCENP-Q-17 (GAGUUAAUGACUGGGAAUA), siCENP-Q-19 (ACAAAGCACACUAACCUAA), and siCENP-Q-20 (UGUCAGAGAAUAAGGUUAG)

Site-directed mutagenesis was performed using the QuikChange kit (Agilent Technologies) to mutate the Aurora B phosphorylation sites (S100 and S109) in Dsn1 and to introduce silent mutations at the siRNA-targeting sites of Dsn1, Ndc80, Spc25, and CENP-T transgenes. The CENP-T mutant with its Ndc80C-binding motif deleted was made with two-step PCR. All constructs were verified by DNA sequencing. Plasmid transfection was performed with the Effectene reagent (Qiagen) when cells reached a confluency of about 60% according to the manufacturer's instructions. For stable cell line generation, HeLa Tet-On cells were transfected with pTRE2 vectors encoding RNAi-resistant Dsn1 WT, S100E/S109E (EE), S100A/S109A (AA), and Δ92-113 tagged at the C-terminus with eGFP, RNAi-resistant Spc25 tagged at the C-terminus with mCherry, RNAi-resistant CENP-T WT or Δ85-99 tagged at the N-terminus with mCherry, or RNAi-resistant Spc25 linked with mCherry followed by RNAi-resistant CENP-T WT. Cells were selected with 150 μg/ml hygromycin (Clontech). The surviving clones were

screened for expression of the desired proteins in the presence of 1 μg/ml doxycycline (Sigma). For all following experiments, 1 μg/ml doxycycline was added to induce expression unless indicated otherwise. For the generation of cell lines with constitutive expression of CENP-A, HeLa Tet-On cells were transfected with pIRES mCherry-CENP-A and selected with 200 ng/ml puromycin (Sigma).

Antibodies, immunoblotting and immunoprecipitation

For the generation of antibodies against human Knl1, CENP-C, and eGFP, GST- or His_6-tagged fragments of Knl1 (residues 1531-1808), CENP-C (residues 1-165), and the full-length eGFP were expressed in bacteria and purified. For the generation of antibodies against human Mis12 complex (Mis12C), Mis12C containing Dsn1, Nsl1, Mis12 and Nnf1 was expressed in bacteria and purified as previously described(Petrovic, Pasqualato et al. 2010). For the generation of the α-Spc24/25 antibody, an Spc24–Spc25 heterodimer containing residues 90-197 of human Spc24 and residues 72-224 of human Spc25 was expressed in bacteria and purified. The proteins were used to immunize rabbits at Yenzym Antibodies, LLC. Production of α-Mad1, α-Mad2, α-APC2, α-Bub1, and α-Ndc80 antibodies was described previously(Bharadwaj, Qi et al. 2004; Kang, Yang et al. 2008; Kim, Sun et al. 2012). The α-Dsn1-pS100 antibody was produced at an in-house facility by immunizing rabbits with a mixture of the pS100 peptide (SWRRApSMKETNC) and the pS109 peptide (TNRRKpSLHPIHC) coupled to haemocyanin (Sigma). The α-Dsn1-pS100 antibody was purified with the pS100 peptide coupled to iodoacetyl-activated agarose beads (Thermo) according to the manufacturer's

protocols. The commercial antibodies used in this study were: α-CENP-T (MBL, D286-3), α-CENP-N (MBL, D285-3), α-CENP-H (MBL, PD031), α-CENP-C (Abcam, ab50974), α-GFP (Roche, 11814460001), α-mCherry (Clontech, 632543), α-Actin (Pierce, MA1-37018), α-Tubulin (Sigma, T4026), CREST (ImmunoVision, HCT-0100), and α-MPM2 (Millipore, 05-368).

For immunoblotting, antibodies were used at a concentration of 1 μg/ml for purified and monoclonal antibodies or at 1:1,000 dilution for crude sera. For immunoprecipitation, anti-Mis12C antibodies were affinity-purified and coupled to Affi-Prep Protein A beads (Bio-Rad) at a concentration of 1 mg/ml. HeLa Tet-On cells were washed once with PBS and resuspended with the lysis buffer [25 mM Tris-HCl, pH 8.0, 75 mM KCl, 5 mM $MgCl_2$, 1 mM EGTA, 0.1% NP-40, 10% (v/v) glycerol, 1 mM dithiothreitol (DTT), 10 mM NaF, 5 mM β-glycerophosphate, 0.5 μM okadaic acid, protease inhibitor cocktail (Roche)] supplemented with 50 units/ml Turbo-nuclease (Accelagen). Cells were lysed with three cycles of freezing and thawing, and kept on ice for 1 hr followed by a 10-min incubation at 37˚C. The lysate was cleared by centrifugation for 20 min at 4˚C at 20,817 g. The antibody beads were incubated with the supernatant for 2 hr at 4˚C with gentle rotation, and then washed four times with the lysis buffer. The proteins bound to beads were dissolved in SDS sample buffer, boiled, separated by SDS-PAGE, and blotted with the desired antibodies. The beads coupled with rabbit IgG (Sigma, I5006) were used as a negative control.

Live-cell imaging

Cells were grown and transfected in 12-well plates, passaged onto chambered coverslips (LabTek), incubated with 2 mM thymidine (Sigma) for 14-16 hr, and released into fresh media for 4-6 hr prior to taking images. GFP or mCherry fluorescence images were acquired at 5-min intervals with a DeltaVision deconvolution fluorescence microscope (Applied Precision) equipped with an environmental chamber and a CoolSnap HQ^2 camera (Roper Scientific). For each time point, 5 z-sections at 2.5-μm intervals were acquired by using a 100X NA 1.4 objective (Olympus) with 2X2 binning. The images were deconvolved with the Deconvolution tool in SoftWoRx (Applied Precision) that used the iterative-constrained algorithm. For 2D image presentation, z-series optical sections were projected by the Max Intensity method. Images were further processed with ImageJ and Photoshop (Adobe).

Immunofluorescence and chromosome spread

For the staining of kinetochore proteins, mitotic cells were harvested by shake-off, washed once with PBS, resuspended in a pre-warmed hypotonic solution (55 mM KCl), and incubated for 15 min at 37˚C. Swollen cells were spun onto slides with a Shandon Cytospin 4 centrifuge (Thermo Fisher), extracted with PBS containing 0.2% Triton X-100, and fixed in 4% paraformaldehyde at room temperature for 5 min. After washing three times with PBS, the fixed cells were incubated with the desired primary antibodies and CREST in PBS containing 0.1% Triton X-100 and 3% BSA for overnight at 4˚C. After washing three times with PBS containing 0.1% Triton X-100, cells were

further incubated with 1 μg/ml fluorescent secondary antibodies (Invitrogen) in PBS containing 0.1% Triton X-100 and 3% BSA for 1 hr at room temperature. Cells were again washed three times with PBS containing 0.1% Triton X-100 and stained with 1 μg/ml 4',6-diamidino-2-phenylindole (DAPI) for 5 min. After the final washes, the slides were mounted and analyzed with the DeltaVision deconvolution fluorescence microscope. Images were acquired with a 100X NA 1.4 or 63X NA 1.42 objectives (Olympus). A series of z-stack images were captured at 0.5 μm intervals for kinetochore images. All images in each experiment were taken with the same light intensity and exposure time. Images were deconvolved as described above, and projected by the Sum Intensity method. To quantify the relative intensity of kinetochore signals, a circle that enclosed CREST signals from a pair of kinetochores was drawn and set as the region of interest (ROI). The integrated density of the gray value for the selected ROI was measured from each channel. The value of object intensity was then divided by the corresponding value of CREST intensity. Twenty ROIs per cell chosen at random were measured. The graphs and statistics were generated with Prism (GraphPad Software).

Flow cytometry

Cells were collected by trypsinization, washed once with PBS, and fixed with cold 70% ethanol for overnight at -20˚C. Cells were washed once with PBS, permeabilized with PBS containing 0.25% Triton X-100 for 5 min, and then incubated with the α-MPM2 antibody diluted in PBS containing 1% BSA for 3 hr. After being washed once with PBS containing 1% BSA, cells were incubated with fluorescent

secondary antibodies (Invitrogen) diluted in PBS plus 1% BSA for 30 min. After one more wash with PBS, cells were stained with propidium iodide (Sigma) at a final concentration of 20 µg/ml, and simultaneously treated with 200 µg/ml RNase A (Qiagen). The samples were analyzed with FACSCalibur (Becton Dickinson) and the FlowJo software (Tree Star).

Protein purification

Mis12C containing Dsn1-WT or EE, $Nsl1^{1-258}$, Mis12 and Nnf1 was expressed in bacteria and purified as previously described. For expression of Mis12C containing Dsn1-WT or EE, the full-length Nsl1, Mis12 and Nnf1, two Strep tags were fused to the C-terminus of Nsl1 separated by a PreScission protease cleavage site. The complex was expressed in bacteria as previously described. Cell pellets were resuspended in buffer A [20 mM Tris-HCl, pH 8.0, 300 mM NaCl, 10% (vol/vol) glycerol, and 2 mM 2-mercaptoethanol] supplemented with a protease inhibitor cocktail (Roche) and TurboNuclease (Accelagen), and lysed with a cell disrupter. The cleared lysate was applied to Strep-Tactin Superflow agarose beads (QIAGEN) pre-equilibrated in buffer A and incubated for 2 hr. Beads were washed with 30 volumes of buffer A, and cleaved with the PreScission protease to remove the Strep tag. The protein was further purified by anion exchange chromatography with a Resource Q column (GE Healthcare) followed by size exclusion chromatography with a Superdex 200 10/300 column (GE Healthcare).

Ndc80C was expressed in insect cells. Cell pellets were resuspended in buffer B [50 mM Tris-HCl, pH 8.0, 150 mM KCl, 0.1% Triton X-100, 5% (vol/vol) glycerol, 10

mM imidazole, and 5 mM 2-mercaptoethanol] supplemented with a protease inhibitor cocktail (Roche) and TurboNuclease (Accelagen), and lysed by a cell disrupter. The cleared lysate was applied to Ni^{2+}-NTA agarose beads (QIAGEN) pre-equilibrated in buffer B and incubated for 2 hr. Beads were washed with 40 volumes of buffer B, and eluted serially with buffer B containing 50 mM, 100 mM, and 250 mM imidazole. The protein was further purified by size exclusion chromatography with a Superdex 200 column (GE Healthcare).

Kinase and protein-binding assays

About 0.1 μg of recombinant Aurora B–INCENP was incubated with 2 μg of Mis12C or MBP substrates for 30 min at 30˚C in 25 μl of the kinase buffer [50 mM Tris-HCl, pH 7.5, 0.2 M NaCl, 1 mM DTT, 10 mM NaF, 5 mM β-glycerophosphate, 0.5 μM okadaic acid, protease inhibitor cocktail (Roche), 0.1 mM ATP, and 0.1 μCi/μl γ-^{32}P-ATP]. Reaction mixtures were quenched with the SDS sample buffer, separated on SDS-PAGE, and analyzed using a phosphorimager (Fuji). For testing the specificity of the α-Dsn1-pS100 antibody, kinase assays on Mis12C-WT and Mis12C-EE were performed with cold ATP, and samples were analyzed by immunoblotting.

For protein-binding assays, purified Mis12C were immobilized on Ni^{2+}-NTA beads (Qiagen) pre-equilibrated in the binding buffer [25 mM Tris-HCl, pH 8.0, 75 mM KCl, 5 mM $MgCl_2$, 1 mM EGTA, 0.1% NP-40, 10% (v/v) glycerol, 1 mM DTT, 10 mM NaF, 5 mM β-glycerophosphate and protease inhibitor cocktail (Roche)], and incubated with the blocking solution (the binding buffer containing 5% non-fat milk). The ^{35}S-

methionine-labeled CENP-C^{1-71} proteins was produced with coupled in vitro transcription and translation of the pCS2-myc-CENP- C^{1-71} vectors in reticulocyte lysate using the TNT SP6 kit (Promega), and incubated with the Mis12C-bound beads in the blocking solution for 1 hr at room temperature. The beads were washed three times with the binding buffer, and the bound proteins were separated by SDS-PAGE and analyzed with a phosphorimager (Fuji). For binding between CCAN sub-complexes and Mis12C/Ndc80C, Myc-, HA- or untagged-CCAN subunits in desired combinations were co-translated in reticulocyte lysate in the presence of ^{35}S-methionine and assayed as described above.

Microscale thermophoresis (MST) measurements were performed with a Monolith NT.115 instrument (NanoTemper) at 24˚C. The fluorescein-labeled CENP-C^{1-28} peptide (5FAM-MAASGLDHLKNGYRRRFCRPSRARDINT) at a fixed concentration (200 nM) was mixed with increasing concentrations of Mis12C-WT or -EE in PBS containing 0.1% NP-40. The samples were loaded into hydrophilic capillaries (NanoTemper) after a 90-min incubation at room temperature. Measurements were performed with 20% LED power and 40% IR-laser power per manufacturer's instructions. Data analyses were performed using the PALMIST software.

RESULTS

Simultaneous depletion of multiple KMN components causes strong spindle checkpoint defects

We first revisited the role of Ndc80C (which consisted of four subunits: Ndc80, Nuf2, Spc25, and Spc24) in the spindle checkpoint in human cells. Consistent with earlier reports(Martin-Lluesma, Stucke et al. 2002; Bharadwaj, Qi et al. 2004), depletion of a single Ndc80C subunit in human cells caused kinetochore-microtubule attachment defects and checkpoint-dependent mitotic arrest (data not shown). Moreover, these cells also underwent prolonged mitotic arrest in the presence of high concentrations of nocodazole (Figure. 4-1B,C). A previous study showed that a more complete depletion of Ndc80 or Nuf2 in human cells caused them to escape from mitotic arrest triggered by inactivation of a microtubule-binding protein(Meraldi, Draviam et al. 2004). We found that the Ndc80 siRNA (siNdc80-M) used in that study was insufficient to allow cells to escape from nocodazole-mediated mitotic arrest (Figure. 4-2A). Furthermore, siNdc80-M was not as efficient in reducing Ndc80 protein levels as siNdc80-4 (which was used throughout this study) (Figure. 4-2B). Thus, depletion of a single subunit of Ndc80C reduces the levels of intact Ndc80C below the threshold needed for proper kinetochore-microtubule attachment. The small amount of residual Ndc80C is still above the threshold needed for spindle checkpoint signaling when all kinetochores are unattached.

We reasoned that simultaneous depletion of multiple subunits of a given protein complex might more efficiently reduce the concentration of the intact complex, as

compared to the depletion of each subunit alone. Indeed, HeLa cells transfected with a mixture of siNdc80, siSpc25, and siSpc24 (termed siNdc80C) failed to arrest in mitosis in the presence of nocodazole, whereas cells transfected with siSpc25 and siSpc24 still did (Figure. 4-1B,C). As expected, we observed the greatest decrease of protein levels of Ndc80C subunits when cells were transfected with siNdc80C (Figure. 4-1D). Importantly, transient transfection of RNAi-resistant Ndc80-Myc partially restored the mitotic arrest in cells transfected with siNdc80C (Figure. 4-1E and Figure. 4-2C). Therefore, Ndc80C is required for sustaining spindle checkpoint signaling, even when microtubule is depolymerized and all kinetochores are unattached. Because the spindle checkpoint can be activated by a few unattached kinetochores within the cell(Rieder, Cole et al. 1995; Collin, Nashchekina et al. 2013; Dick and Gerlich 2013; Heinrich, Geissen et al. 2013; Subramanian and Kapoor 2013), the kinetochore proteins that initiate checkpoint signaling have to be reduced to exceedingly low levels to reveal their requirement for mitotic arrest in the absence of the mitotic spindle.

There are two distinct Ndc80C-containing outer kinetochore complexes: CENP-T-bound Ndc80C or CENP-C-bound KMN (Figure. 4-1A). To address which complex was critical for spindle checkpoint signaling, we depleted Mis12C, which consisted of Dsn1, Nsl1, Mis12, and Nnf1, and was only present in the latter complex, from HeLa cells, and investigated the ability of these cells to undergo mitotic arrest in the presence of nocodazole. Depletion of both Dsn1 and Nsl1 with a mixture of siDsn1 and siNsl1 (termed siMis12C) caused a major defect in mitotic arrest, whereas depletion of either protein alone did not (Figure. 4-3A,B). The mitotic-arrest deficiency produced by

siMis12C was rescued by the inducible, stable expression of RNAi-resistant Dsn1-GFP (Figure. 4-1F,G, and Figure. 4-3C). These results indicate that Mis12C is indispensable for the spindle checkpoint, and suggest that CENP-C-bound KMN is required for the spindle checkpoint.

CENP-T-bound Ndc80C is insufficient to sustain checkpoint signaling

To examine the effect of Mis12C depletion on the localization of Ndc80C and vice versa, we transfected cells with siMis12C or siNdc80C together with siCdc20 to prevent mitotic exit, and visualized Mis12C and Ndc80 by immunofluorescence (Figure. 4-1H,I and Figure. 4-3D,E). Transfection of siMis12C reduced the kinetochore signal of Mis12C to background levels. The kinetochore signal of Ndc80 was reduced about 2-fold (Figure. 4-1H,I). In contrast, the signals of CENP-C and CENP-T at kinetochores were not greatly reduced. These results are consistent with earlier studies, and suggest that there are multiple pools of Ndc80C at kinetochores. The remaining signal of Ndc80 at kinetochores in siMis12C cells presumably belongs to CENP-T-bound Ndc80C. Because siMis12C cells fail to undergo mitotic arrest in nocodazole, this pool of Ndc80C is insufficient to maintain the spindle checkpoint.

The kinetochore signal of Ndc80 was undetectable in cells treated with siNdc80C (Figure. 4-3D,E). While depletion of Ndc80C did not alter the kinetochore localization of CENP-C or CENP-T, the kinetochore signal of Mis12C was reduced by 2-fold. This finding was surprising, as CENP-C is the major kinetochore receptor of Mis12C, and Ndc80C binding to Mis12C does not affect the binding of Mis12C to CENP-C in

vitro(Screpanti, De Antoni et al. 2011). The fact that Ndc80C contributes the kinetochore localization of Mis12C thus suggests that, aside from the CENP-C–Mis12C interaction, attachment of intact KMN to kinetochores involves an additional Ndc80C-dependent mechanism.

Aurora B regulates the kinetochore targeting of KMN during mitosis

Partial inactivation of Ndc80C through transfecting cells with siNdc80 alone does not cause mitotic arrest deficiency in the presence of nocodazole. Likewise, although the Aurora B activity is required for the mitotic arrest exerted by the microtubule-stabilizing drug Taxol, it is largely dispensable for the mitotic block caused by nocodazole(Hauf, Cole et al. 2003). We tested whether Aurora B inhibition by ZM447439 (ZM) in siNdc80-transfected cells allowed them to escape from nocodazole-mediated mitotic arrest. Consistent with previous reports(Santaguida, Vernieri et al. 2011; Saurin, van der Waal et al. 2011), we found that Aurora B inhibition in Ndc80 RNAi cells caused them to escape from nocodazole-induced mitotic arrest (Figure. 4-4A, B). The mitotic escape of cells treated with siNdc80 and ZM was partially rescued by the transient expression of RNAi-resistant Ndc80-Myc (Figure. 4-4C-E). Thus, Aurora B had a rather direct role in the spindle checkpoint, in addition to its proposed role in creating transient, unattached kinetochores through destabilizing the connection between kinetochores and Taxol-stabilized microtubules.

We decided to investigate the mechanism underlying the synergy between Aurora B inhibition and Ndc80 depletion in abolishing the spindle checkpoint. We found that

several checkpoint proteins, including Bub1, BubR1, Mad1, and Mad2, were absent from kinetochores in siNdc80/ZM-treated cells that were maintained in mitosis by the proteasome inhibitor MG132 (Figure. 4-4F and data not shown). Because KMN is required for the kinetochore localization of these checkpoint proteins, we examined the localization of KMN in these cells. Aurora B inhibition or siNdc80 alone diminished the kinetochore staining of Knl1 and Mis12C about 2-fold (Figure. 4-4G,H and Figure. 4-5A-E). Aurora B inhibition did not alter CENP-C and -T localization (Figure. 4-5A-C). To our surprise, Aurora B inhibition in Ndc80 RNAi cells abolished the kinetochore localization of Knl1 and Mis12C. These results indicate that, when Ndc80C is compromised, the kinetochore targeting of Knl1 and Mis12C requires Aurora B. Thus, a critical microtubule-independent function of Aurora B in the spindle checkpoint is to cooperate with Ndc80C to target Knl1, Mis12C, and downstream checkpoint proteins to kinetochores.

We noticed that there were detectable Ndc80 kinetochore signals in siNdc80-treated cells (Figure. 4-4I). This residual Ndc80 signal was abolished by Aurora B inhibition. Because this residual Ndc80 signal was barely above background, quantification of the intensity of the Ndc80 signal in siNdc80 cells did not show significant differences with or without Aurora B inhibition (Figure. 4-5F). These results again suggest that the spindle checkpoint requires a very small amount of Ndc80C (presumably as a part of KMN) at kinetochores.

Aurora B contributes to KMN kinetochore targeting through Dsn1 phosphorylation

Consistent with the fact that Aurora B inhibition reduced the kinetochore localization of KMN without affecting CENP-C and -T localization, Aurora B inhibition weakened the binding between KMN and CENP-C and -T in co-immunoprecipitation (IP) assays (Figure. 4-6A). We next sought to identify the relevant Aurora B substrates in this process. Aurora B phosphorylated Dsn1 of recombinant Mis12C in vitro (Figure. 4-6B). Consistent with previous studies(Yang, Wu et al. 2008; Welburn, Vleugel et al. 2010), our mass spectrometry analysis identified S100 and S109 in Dsn1 as the major Aurora B phosphorylation sites (data not shown). The functions of these phosphorylation events were controversial, however(Yang, Wu et al. 2008; Welburn, Vleugel et al. 2010). We made a phospho-specific antibody against phospho-S100 Dsn1 (Figure. 4-7A), and confirmed that this phosphorylation in human cells was indeed dependent on the Aurora B activity (Figure. 4-6C,D). Phospho-S100 Dsn1 localized to kinetochores (Figure. 4-6D). Thus, Dsn1 is a kinetochore substrate of Aurora B.

We constructed HeLa cell lines that stably expressed Dsn1-WT-GFP, the phospho-deficient Dsn1-S100A/S109A (AA)-GFP, and the phospho-mimicking Dsn1-S100E/S109E (EE)-GFP in a doxycycline-inducible manner (Figure. 4-7B), and monitored the kinetochore localization of these Dsn1-GFP proteins (Figure. 4-6E). Similar to that of the endogenous Mis12C, the kinetochore signal of Dsn1-WT-GFP was reduced by ZM (Figure. 4-6E and Figure. 4-7C). The kinetochore signal of the phospho-mimicking Dsn1-EE-GFP was slightly stronger than that of Dsn1-WT-GFP, and was not reduced by ZM. The kinetochore signal of Dsn1-AA-GFP was similar to that of Dsn1-WT-GFP in ZM-treated cells, and was not further reduced by ZM. The intensities of the

kinetochore signals of Knl1 were similarly affected in these samples (Figure. 4-6E and Figure. 4-7D). These results indicate that Dsn1 is a critical substrate of Aurora B at the CCAN–KMN interface. Phosphorylation of Dsn1 by Aurora B contributes to KMN kinetochore localization in mitosis.

To test whether Dsn1 phosphorylation by Aurora B is required for chromosome alignment, we monitored mCherry-CENP-A expressing cells using live-cell imaging with or without the depletion of endogenous Dsn1 (Figure. 4-8A,B). As expected, depletion of Dsn1 in mCherry-CENP-A cells produced severe chromosome alignment defects. Despite not achieving proper chromosome alignment, these cells initiated anaphase, indicating that they also had a weakened spindle checkpoint. Expression of Dsn1-WT-GFP rescued the chromosome alignment defects caused by siDsn1 (Figure. 4-8C). The chromosome alignment was also rescued by Dsn1-AA-GFP expression, although the metaphase plate of siDsn1 cells expressing Dsn1-AA-GFP tended to become unfocused at later time points before starting anaphase in these cells (Figure. 4-8C,D). Thus, consistent with a previous report(Welburn, Vleugel et al. 2010), phosphorylation of Dsn1 by Aurora B is largely dispensable for chromosome alignment.

To test whether Dsn1 phosphorylation by Aurora B is required for the spindle checkpoint, we transfected cells with siMis12C and measured the mitotic index in the presence of nocodazole, with or without inducing the expression of Dsn1-WT-GFP or Dsn1-AA-GFP (Figure. 4-8E,F). While Dsn1-WT was able to rescue the mitotic escape caused by Mis12C depletion, Dsn1-AA was partially defective in rescuing the phenotype.

Thus, Aurora B-dependent phosphorylation contributes to, but is not required for, the spindle checkpoint.

Phospho-mimicking Dsn1 mutation and forced nuclear localization of Ndc80 suffice to install KMN at interphase kinetochores

We monitored the subcellular localization of Dsn1-WT-GFP and Dsn1-EE-GFP using live-cell imaging. As expected, Dsn1-WT-GFP localized to kinetochores during mitosis, but not in interphase (Figure. 4-9A,B). In contrast, Dsn1-EE-GFP constitutively localized to kinetochores throughout the cell cycle. Dsn1-EE-GFP was sufficient to target Knl1 to kinetochores during interphase (Figure. 4-9B), but was insufficient to recruit Ndc80 or Mad1, which remained localized at the cytosol and nuclear pores, respectively (Figure. 4-10A). Consistently, Dsn1-EE-GFP, but not Dsn1-WT-GFP, co-immunoprecipitated with CENP-C and -T in cells arrested at the G1/S boundary (Figure. 4-10B). Therefore, although Dsn1 phosphorylation by Aurora B is not strictly required for Mis12C kinetochore localization in mitosis, untimely phosphorylation is likely sufficient to target the Knl1–Mis12C complex to kinetochores in interphase.

An elegant, previous study showed that co-expression of a phospho-mimicking mutant of CENP-T and an Ndc80 protein fused to the nuclear localization signal (NLS) was sufficient to install Ndc80C, but not Mis12C, at interphase kinetochores(Gascoigne and Cheeseman 2013). That study clearly demonstrated that the mitosis-specific kinetochore targeting of CENP-T-bound Ndc80C relied on two processes: Cdk1-dependent phosphorylation of CENP-T and the nuclear translocation of Ndc80C. We

tested whether forced nuclear targeting of Ndc80 enabled the kinetochore targeting of Ndc80C in Dsn1-EE cells in interphase. Similar to endogenous Ndc80, ectopically expressed Ndc80-mCherry remained in the cytosol in Dsn1-EE cells (Figure. 4-9C). As expected, Ndc80-NLS-mCherry was enriched in the nucleus in Dsn1-WT cells (Figure. 4-9D). Strikingly, Ndc80-NLS-mCherry localized to interphase kinetochores in Dsn1-EE cells. Other components of Ndc80C, Spc24/25, were also found at interphase kinetochores in cells expressing both Dsn1-EE and Ndc80-NLS (Figure. 4-9E). These results suggest that Aurora B-dependent phosphorylation of Dsn1 and nuclear translocation of Ndc80C are key regulatory events during mitosis-specific assembly of KMN at kinetochores.

Dsn1 phosphorylation by Aurora B strengthens the CENP-C–Mis12C interaction

The simplest model to explain the interphase kinetochore targeting of Dsn1-EE is that Dsn1 phospho-mimicking mutations strengthened the Mis12C–CCAN interaction. Among CCAN components, CENP-C is the direct binding partner of Mis12C(Screpanti, De Antoni et al. 2011). We first tested whether Dsn1-EE had additional binding partners in CCAN. Recombinant Mis12C containing either Dsn1-WT or -EE (Mis12C-WT or -EE) failed to bind to several CCAN sub-complexes obtained through in vitro translation, including CENP-L-M-N, CENP-T-W-S-X, CENP-H-I-K, and CENP-O-P-Q-U-R (Figure. 4-11A). Consistently, the interphase kinetochore localization of Dsn1-EE was abolished in CENP-C RNAi cells (Figure. 4-9F), but was still detectable in cells transfected with siCENP-T, -I, -L, -N, or -U (Figure. 4-11B). Therefore, CENP-C is still

the major CCAN receptor for Dsn1-EE and, by inference, the phosphorylated form of Dsn1, in interphase cells.

We next compared the CENP-C-binding affinities of recombinant Mis12C-WT and -EE. His_6-tagged Mis12C containing Dsn1-EE (Mis12C-EE) pulled down more ^{35}S-labeled CENP-C^{1-71} (Figure. 4-9G). The interaction between CENP-C and Mis12C-EE was not further enhanced by Ndc80C. We then quantitatively measured the binding affinities of Mis12C-WT and -EE towards a fluorescently labeled CENP-C peptide (residues 1-28) with microscale thermophoresis. Consistent with the in vitro pull-down assay, the dissociation constant (K_d) of the Mis12C-WT–CENP-C^{1-28} interaction was 2.1 ± 0.4 μM whereas the K_d between Mis12C-EE and CENP-C^{1-28} was 0.74 ± 0.15 μM (Figure. 4-10C). These results suggest that Dsn1-EE and, quite possibly, phosphorylated Dsn1 bind to CENP-C more tightly than Dsn1-WT, although we do not know whether the three-fold higher affinity suffices to explain the interphase targeting of Mis12-EE.

The two Aurora B phosphorylation sites of Dsn1, S100 and S109, reside in a basic motif conserved in vertebrate Dsn1 proteins (Figure. 4-9H). To test whether this motif of Dsn1 mediated CENP-C binding, we created a Dsn1 mutant with this motif deleted (Δ91-113). Surprisingly, Dsn1-Δ91-113-GFP behaved like Dsn1-EE-GFP. It localized to kinetochores properly during mitosis, and showed premature kinetochore localization during interphase (Figure. 4-9I). Consistently, similar amounts of CCAN components, including CENP-C, -T and -N, were associated with Dsn1-WT, -EE or Δ91-113 in mitotic cell lysates, whereas the CCAN interaction with Dsn1-AA was weaker (Figure. 4-9J). Therefore, phospho-S100/S109 residues of Dsn1 do not create a direct CCAN-

binding motif. We speculate that this basic motif of Dsn1 might mask the CENP-C-binding site of Mis12C through an autoinhibitory mechanism. Phosphorylation of this motif, as well as phospho-mimicking or deletion mutations, might release this autoinhibition and expose the binding site for CENP-C, thus enhancing the Mis12C–CCAN interaction. This Aurora B-dependent mechanism for strengthening the Mis12C–CCAN interaction is likely conserved in budding yeast(Akiyoshi, Nelson et al. 2013).

Taken together, our results so far indicate that Aurora B contributes to the kinetochore targeting of KMN through phosphorylating Dsn1 and strengthening the CENP-C–Mis12C interaction. During normal mitosis, Aurora B is not strictly required for the kinetochore localization of KMN. Aurora B becomes critical, however, when the Ndc80C function is compromised. Thus, two pathways install the intact KMN at kinetochores during mitosis: an Aurora B-dependent CENP-C–Mis12C pathway, and an Aurora B-independent, Ndc80C-dependent pathway.

CENP-T contributes to KMN kinetochore targeting independently of its Ndc80C-binding region

We next examined whether this Aurora B-independent, Ndc80C-dependent pathway involved CENP-T-bound Ndc80C. Similar to Aurora B inhibition in siNdc80 cells, Aurora B inhibition in siCENP-T cells caused mitotic arrest deficiency in the presence of nocodazole, whereas Aurora B inhibition had marginal effects on siCENP-C cells (Figure. 4-12A and Figure. 4-13A). Moreover, Aurora B inhibition and siCENP-T greatly reduced Mis12C and Ndc80 kinetochore signals without affecting CENP-C

signals (Figure. 4-12B,C and Figure. 4-13B-D). These results were seemingly consistent with a model in which CENP-T-bound Ndc80C was involved in the Aurora B-independent, Ndc80C-dependent pathway of KMN attachment to kinetochores.

We wondered how this pool of Ndc80C might contribute to KMN attachment. One possibility was that CENP-T-bound Ndc80C might be an obligatory intermediate in the KMN assembly pathway. Ndc80C might first be recruited by CENP-T to kinetochores and then be passed on to Mis12C in a relay mechanism (Figure. 4-12D). To test this hypothesis, we created an Spc25-mCherry–CENP-T fusion protein (Spc25–CENP-T) and a CENP-T mutant with its Ndc80C-binding region deleted (CENP-T Δ85-99), and tested their functions in human cells. Both proteins localized normally to kinetochores throughout the cell cycle (Figure. 4-14A-C). Expression of Spc25–CENP-T rescued or partially rescued the mitotic accumulation of log-phase cells depleted of CENP-T or Spc25, indicating that the fusion protein was functional (Figure. 4-12E,F). Spc25–CENP-T did not restore the nocodazole-induced mitotic arrest of siSpc25 cells treated with ZM (Figure. 4-12G), again consistent with the notion that the CENP-T-bound pool of Ndc80C was insufficient for checkpoint signaling. Unexpectedly, Spc25–CENP-T rescued the mitotic arrest deficiency of siCENP-T cells treated with ZM in the presence of nocodazole (Figure. 4-12H). Even more surprisingly, expression of the Ndc80C-binding-deficient CENP-T Δ85-99 rescued the checkpoint defect of siCENP-T cells (Figure. 4-12H). CENP-T Δ85-99 also restored or partially restored Mis12C or Ndc80C signals at kinetochores (Figure. 4-12I and Figure. 4-14D,E). These results were inconsistent with the relay model of KMN assembly described above, and suggest that

CENP-T has a role in KMN attachment independently of its direct interaction with Ndc80C.

CENP-T indirectly contributes to KMN kinetochore attachment through CENP-H-I-K

Because CENP-T is required for the proper localization of other CCAN components including the CENP-H-I-K sub-complex(Hori, Amano et al. 2008), we tested whether CENP-T contributed to KMN kinetochore targeting indirectly through maintaining the integrity of CCAN (Figure. 4-15A). We first systematically depleted various CCAN components and tested whether their depletion synergized with Aurora B inhibition to cause mitotic arrest deficiency in the presence of nocodazole. While depletion of CENP-N, CENP-U, or CENP-Q did not have significant effects (Figure. 4-16A-C), depletion of CENP-H synergized with Aurora B inhibition to produce checkpoint defects (Figure. 4-15B and Figure. 4-16D,E). A previous study showed that CENP-I depletion and Aurora B inhibition also caused cells to escape from nocodazole-induced mitotic arrest(Matson, Demirel et al. 2012). Moreover, CENP-H depletion and Aurora B inhibition greatly reduced Mis12C and Ndc80C kinetochore localization, without affecting CENP-C localization (Figure. 4-15C-F). Taken together, these results implicate CENP-H-I-K in Aurora B-independent KMN attachment to kinetochores.

We next tested whether CENP-H-I-K physically interacted with Ndc80C. Purified recombinant His_6-Ndc80C efficiently pulled down in vitro translated ^{35}S-labeled CENP-H-I-K (Figure. 4-15G). This Ndc80C–CENP-H-I-K interaction was not blocked by

Mis12C, suggesting that Ndc80C can bind simultaneously to Mis12C and CENP-H-I-K. In contrast to a previous report that implicated CENP-H in Ndc80 binding(Mikami, Hori et al. 2005), we found that CENP-I on its own bound efficiently to Ndc80C, and it could also bridge an interaction between Ndc80C and CENP-H-K only when both CENP-H and -K were present (Figure. 4-16F).

We then examined the potential interdependence between CENP-T and CENP-H in their kinetochore localization. Consistent with a previous report(Hori, Amano et al. 2008), depletion of CENP-H did not substantially reduce CENP-T kinetochore signals (Figure. 4-15F, right panel). Despite being incomplete, depletion of CENP-T reduced the kinetochore signals of CENP-H by two-fold (Figure. 4-15H,I). Importantly, expression of either CENP-T or CENP-T Δ85-99 restored the CENP-H kinetochore localization. Taken together, our results are consistent with a model in which CENP-T recruits CENP-H-I-K to kinetochores. CENP-H-I-K then contributes to Aurora B-independent KMN attachment to kinetochores through physically interacting with Ndc80C (Figure. 4-15A).

Two quasi-independent pathways install KMN at mitotic kinetochores

Our results so far suggest that two quasi-independent pathways attach KMN to kinetochores in mitosis (Figure. 4-17A). In pathway I, Aurora B phosphorylates Dsn1 and promotes the CENP-C–Mis12C interaction. In pathway II, CENP-T anchors CENP-H-I-K at kinetochores, which interacts with Ndc80C to promote KMN kinetochore targeting. It is well established that Aurora B inhibition alone is insufficient to abrogate the nocodazole-triggered mitotic arrest(Santaguida, Vernieri et al. 2011; Saurin, van der

Waal et al. 2011). Thus, without the proper function of pathway I, pathway II is sufficient to maintain kinetochore KMN at a level above the threshold needed for checkpoint signaling. We wondered whether pathway I could also transduce checkpoint signals when pathway II was compromised. Expression of the phospho-mimicking Dsn1 EE, but not Dsn1 WT, partially restored nocodazole-induced mitotic arrest (Figure. 1-17B) and the Ndc80 kinetochore signals (Figure. 1-17C-E) in siCENP-T cells treated with ZM. Therefore, the two pathways of KMN attachment to kinetochores are quasi-independent. They are not strictly dependent on each other for checkpoint signaling. When microtubules are depolymerized, only inactivation of both pathways can reduce the kinetochore level of KMN to below that required for checkpoint signaling.

DISCUSSION

KMN as a kinetochore spindle checkpoint sensor

Inactivation of certain KMN components causes spindle checkpoint defects in various organisms(McCleland, Gardner et al. 2003; Kiyomitsu, Obuse et al. 2007). Its components recruit key spindle checkpoint proteins, including Bub1–Bub3 and BubR1–Bub3, to kinetochores. Despite this circumstantial evidence, KMN has not been definitively shown to be a spindle checkpoint sensor in human cells, however. A major reason for this lack of definitive evidence stems from the high sensitivity of the spindle checkpoint. A few unattached kinetochores within a mitotic cell can engage the spindle checkpoint and cause prolonged mitotic arrest. Because a human cell contains 92 kinetochores (more than 100 for the aneuploid HeLa cell) during mitosis, the function of the kinetochore sensor has to be reduced to below a few percent of the wild-type level to reveal a strong checkpoint defect. This level of inactivation is difficult to attain experimentally, as KMN is a well-established kinetochore receptor for spindle microtubules, and is essential for cell viability. Insufficient inactivation of KMN often causes chromosome misalignment and checkpoint-dependent mitotic delay in human cells, complicating the analysis.

Through simultaneously targeting multiple components of two KMN sub-complexes, Mis12C or Ndc80C, we have suppressed both the kinetochore targeting and function of KMN in human cells below the thresholds needed to sustain a prolonged mitotic arrest, even when all kinetochores are unattached due to nocodazole-induced

microtubule depolymerization. This mitotic arrest deficiency can be rescued by the ectopic expression of RNAi-resistant Mis12C or Ndc80C transgenes, ruling out dominant RNAi off-target effects. Our results clearly demonstrate a requirement for KMN in spindle checkpoint signaling. Being the kinetochore receptor for both microtubules and spindle checkpoint proteins, KMN is ideally suited to coordinate the generation and extinction of checkpoint signals.

The strategy of depleting multiple subunits of a given protein complex by RNAi to achieve more complete inactivation should be generally applicable. This strategy remains especially useful for protein complexes that are essential for cell viability, as simple deletion of their coding genes by new techniques, such as CRISPR(Mali, Esvelt et al. 2013), is not feasible.

Pathways to install KMN at mitotic kinetochores

Our study further reveals two parallel pathways that install KMN at kinetochores during mitosis in human cells: the Aurora B-dependent CENP-C–Mis12C pathway and the CENP-T-dependent CENP-I–Ndc80C pathway (Figure. 1-17A). Either pathway is sufficient to install enough KMN at kinetochores to sustain prolonged mitotic arrest when microtubules are depolymerized. Inactivation of both pathways through Aurora B inhibition and partial depletion of CCAN or KMN components reduces KMN levels at kinetochores to below the threshold needed to sustain checkpoint signaling, lending further support for KMN being a critical sensor of the spindle checkpoint. Our model is consistent with an earlier study that demonstrated the synergistic effects of depleting both

Knl1 and CENP-H-I-K in abolishing kinetochore functions in human cells(Cheeseman, Hori et al. 2008), although that study did not explicitly examine the spindle checkpoint.

We have further shown that Aurora B-dependent phosphorylation of Dsn1 is a major regulatory mechanism for mitosis-specific attachment of KMN at kinetochores. Strikingly, expression of the phospho-mimicking Dsn1 mutant, in conjunction with forced nuclear targeting of Ndc80, suffices to install the intact KMN at interphase kinetochores. In contrast, expression of phospho-mimicking CENP-T and forced nuclear targeting of Ndc80 only installs Ndc80C, but not Knl1 or Mis12C, at interphase kinetochores(Gascoigne and Cheeseman 2013), consistent with the notion that CENP-T and Mis12C bind competitively to Ndc80C. Interestingly, forced nuclear targeting of Ndc80 alone (in the absence of phospho-mimicking Dsn1) is insufficient to install Ndc80C at interphase kinetochores, indicating that the CENP-I–Ndc80C interaction on its own cannot install Ndc80C on interphase kinetochores. Because the CENP-I–Ndc80C pathway by itself can maintain a KMN pool at mitotic kinetochores in the absence of Aurora B activity, this result suggests the existence of additional, unidentified mechanisms that promote this pathway during mitosis. Further defining the CENP-I–Ndc80C interaction and its mitotic regulation remain important challenges for the future.

The mechanism by which CENP-T recruits CENP-H-I-K to kinetochores also remains to be established. CENP-T forms a complex with CENP-W, CENP-S, and CENP-X(Nishino, Takeuchi et al. 2012). All subunits of the CENP-T-W-S-X complex have histone-like folds. CENP-T-W-S-X can form an octamer that binds to

DNA(Takeuchi, Nishino et al. 2014). It is possible that CENP-H-I-K interacts with the nucleosome-like structure formed between CENP-T-W-S-X and centromeric DNA.

Roles of Aurora B in mitotic regulation

Our results clearly demonstrate a role of Aurora B in mitosis-specific attachment of KMN to kinetochores through strengthening the CENP-C–Mis12C connection. On the other hand, this is not the only function of Aurora B in the spindle checkpoint, as expression of the phospho-mimicking Dsn1 mutant in HeLa cells treated with Taxol fails to rescue the mitotic arrest deficiency caused by Aurora B inhibition (data not shown). Aurora B phosphorylates other substrates at outer kinetochores, including Ndc80 and Knl1(Welburn, Vleugel et al. 2010). These phosphorylation events likely contribute to the spindle checkpoint directly or indirectly. In addition, Aurora B is required for the kinetochore localization and activation of the checkpoint kinase Mps1, although the key substrates of Aurora B in that process have not been identified(Saurin, van der Waal et al. 2011; Nijenhuis, von Castelmur et al. 2013).

Finally, Aurora B as a part of the chromosome passenger complex dissociates from the mitotic centromeres during anaphase(Ruchaud, Carmena et al. 2007). Aurora B-dependent phosphorylation of Dsn1 is expected to decline at that stage. It will be interesting to test whether the CENP-I–Ndc80C interaction becomes more critical for KMN attachment to CCAN and for chromosome movement during anaphase.

CONCLUSION

The maturation of the outer kinetochore during mitosis is one of the most fascinating events in cell biology. Shortly after mitotic entry, tens of outer kinetochore proteins, including the KMN network, assemble onto the inner kinetochore in a hierarchical fashion. KMN then serves as the kinetochore receptor for both microtubules and spindle checkpoint proteins, and has been postulated to coordinate spindle checkpoint signaling. In this study, we have established KMN as a key kinetochore sensor of the spindle checkpoint in human cells. We have further delineated two parallel pathways that anchor KMN to kinetochores. Our findings highlight a role of Aurora B in mitosis-specific KMN attachment to kinetochores, and identify the CENP-I–Ndc80C interaction as a new molecular tether between CCAN and KMN.

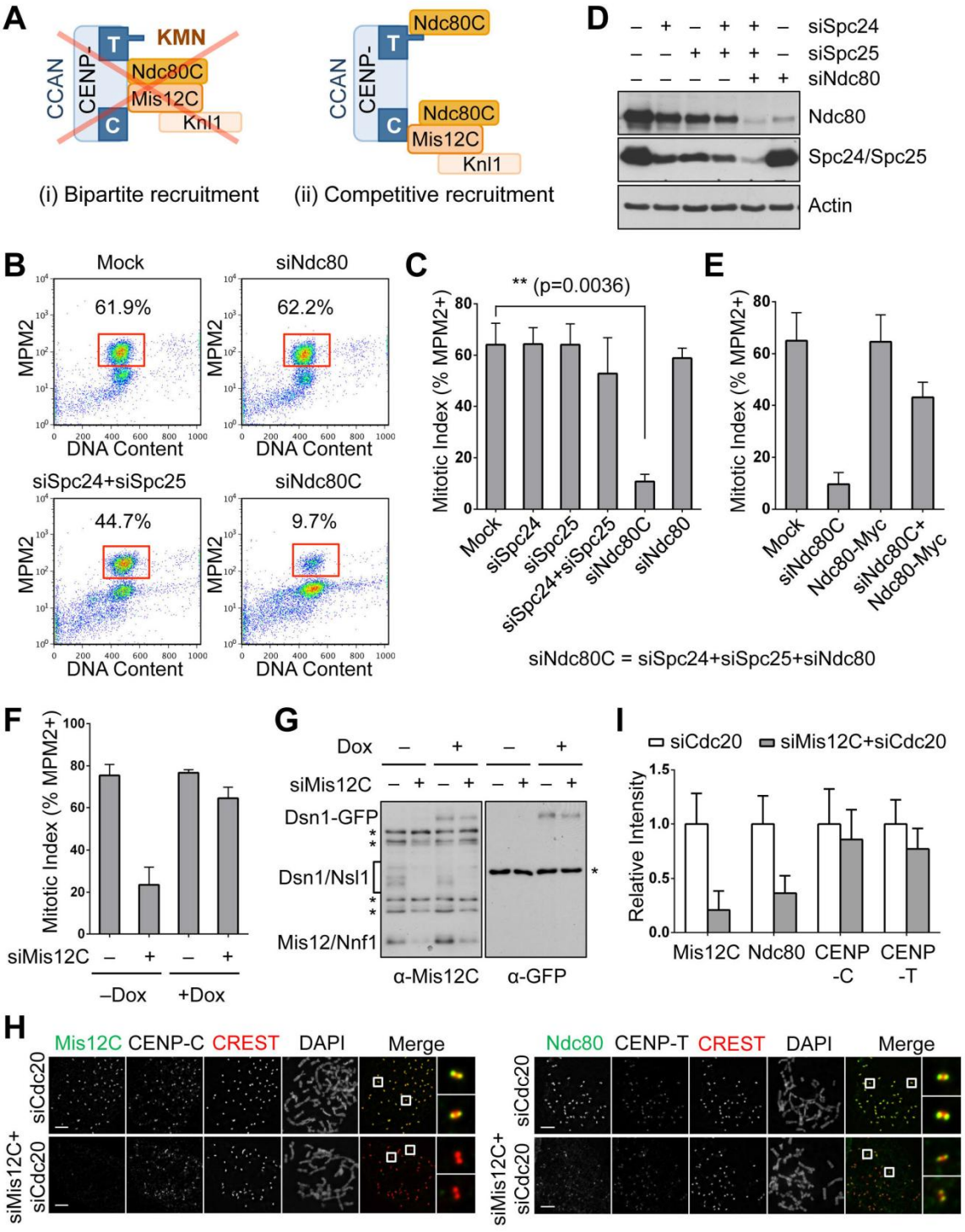

Figure 4-1. KMN is required for the spindle checkpoint in human cells. (**A**) Two models of KMN attachment to kinetochores. Recent reports support the competitive

recruitment model. (**B**) HeLa Tet-On cells transfected with the indicated siRNAs, treated with thymidine for 14 hr, released into nocodazole-containing medium for 15 hr, and stained with propidium iodide (DNA content) and MPM2. Cells were subjected to flow cytometry (FACS) analysis. Mitotic cells defined as cells with 4C DNA content and high MPM2 staining are boxed, with their percentages indicated above. (**C**) HeLa Tet-On cells were mock transfected or transfected with the indicated siRNAs targeting Ndc80C subunits and analyzed by flow cytometry as described in **B**. The means and standard deviations (SD) of three independent experiments are shown. (**D**) Lysates of cells in **c** were blotted with the indicated antibodies. (**E**) HeLa Tet-On cells were first transfected with vector or RNAi-resistant Ndc80-Myc and were then mock transfected or transfected with siNdc80C (the mixture of siSpc24, siSpc25, and siNdc80-4). The mitotic index of the cells was determined as described in **B**. The means and standard deviations (SD) of three independent experiments are shown. (**F**) HeLa Tet-On cells stably expressing Dsn1-WT-GFP were mock transfected or transfected with siMis12C (the mixture of siDsn1 and siNsl1) in absence (–) or presence (+) of doxycycline (Dox). Cells were treated with thymidine for 14 hr, released into nocodazole-containing medium for 15 hr, and analyzed by flow cytometry. The mitotic index of each sample is quantified as described in **B**. Representative plots are shown in Figure. 4-3C. The means and standard deviations (SD) of three independent experiments are shown. (**G**) Lysates of cells in **F** were blotted with the indicated antibodies. Asterisks indicate non-specific bands. (**H**) HeLa Tet-On cells were transfected with the indicated siRNAs, treated with thymidine for 14 hr, and released into nocodazole-containing medium. Mitotic cells were collected by shake-off and stained with the indicated antibodies and DAPI. The CREST staining was colored red in the merged images whereas Mis12C or Ndc80 staining was colored green. The boxed regions were magnified and shown in the rightmost column. Scale bars, 5 μm. (**I**) Quantification of the normalized intensities of the indicated staining in **H**. The intensities of 40 kinetochores per cell in 10 cells per condition were measured. The means and SDs are shown.

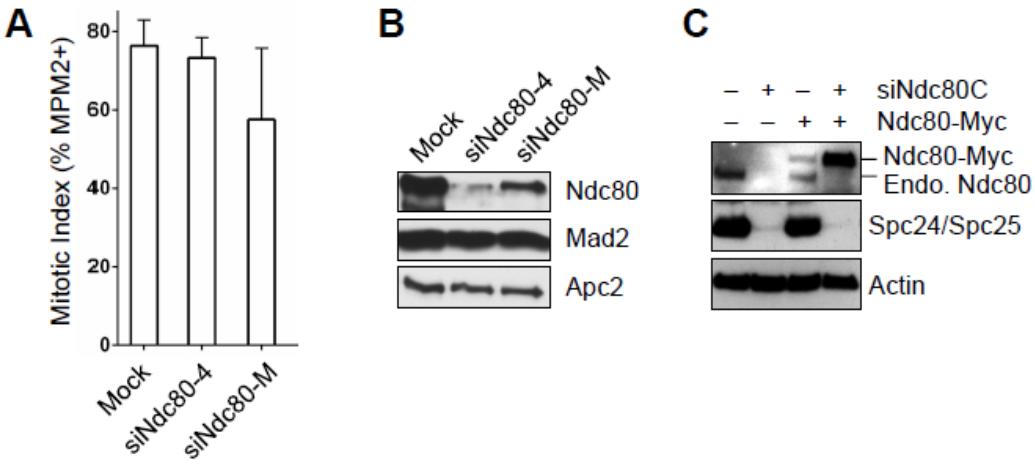

Figure 4-2. Depletion of Ndc80 alone from HeLa cells does not cause mitotic arrest deficiency in the presence of nocodazole. (**A**) HeLa Tet-On cells were mock transfected or transfected with the indicated siRNAs. Cells were treated with thymidine for 14 hr and released into nocodazole-containing medium for 15 hr. Their mitotic index was determined by FACS. Means and SDs of three independent experiments are shown. (**B**) Lysates of cells in (**A**) were blotted with the indicated antibodies. (**C**) Lysates of cells described in Figure. 4-1E were blotted with the indicated antibodies.

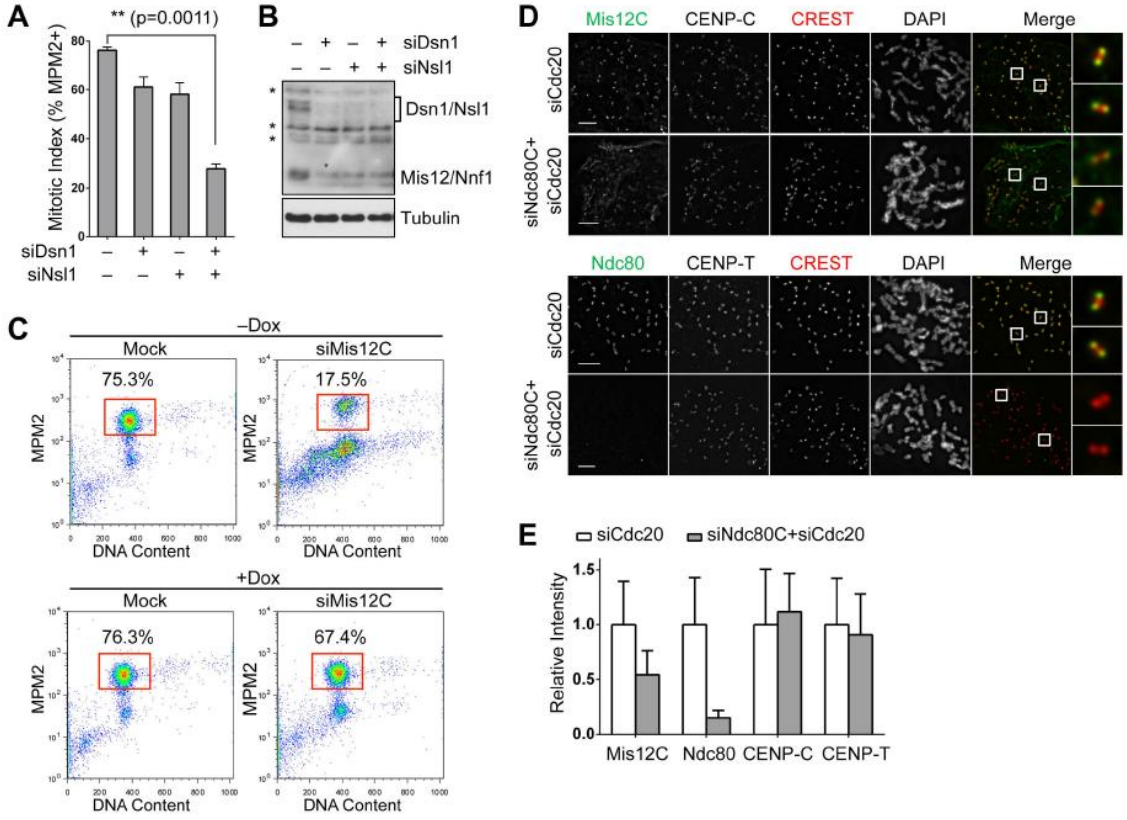

Figure 4-3. Complete depletion of Mis12C or Ndc80C causes spindle checkpoint defects. (**A**) HeLa Tet-On cells were mock transfected or transfected with the indicated siRNAs. Cells were treated with thymidine for 14 hr and released into nocodazole-containing medium for 15 hr. Their mitotic index was determined by FACS. Means and SDs of three independent experiments are shown. (**B**) Lysates of cells in **A** were blotted with the indicated antibodies. Asterisks indicate non-specific bands. (**C**) Representative FACS plots of experiments in Figure. 4-1F. (**D**) HeLa Tet-On cells were transfected with the indicated siRNAs, treated with thymidine for 14 hr, and released into nocodazole-containing medium. Mitotic cells were collected by shake-off and stained with the indicated antibodies and DAPI. The CREST staining was colored red in the merged images whereas Mis12C or Ndc80 staining was colored green. The boxed regions were magnified and shown in the rightmost column. Scale bars, 5 μm. (**E**) Quantification of the normalized intensities of the indicated staining in **D**. The intensities of 40 kinetochores per cell in 10 cells per condition were measured, with means and SDs shown.

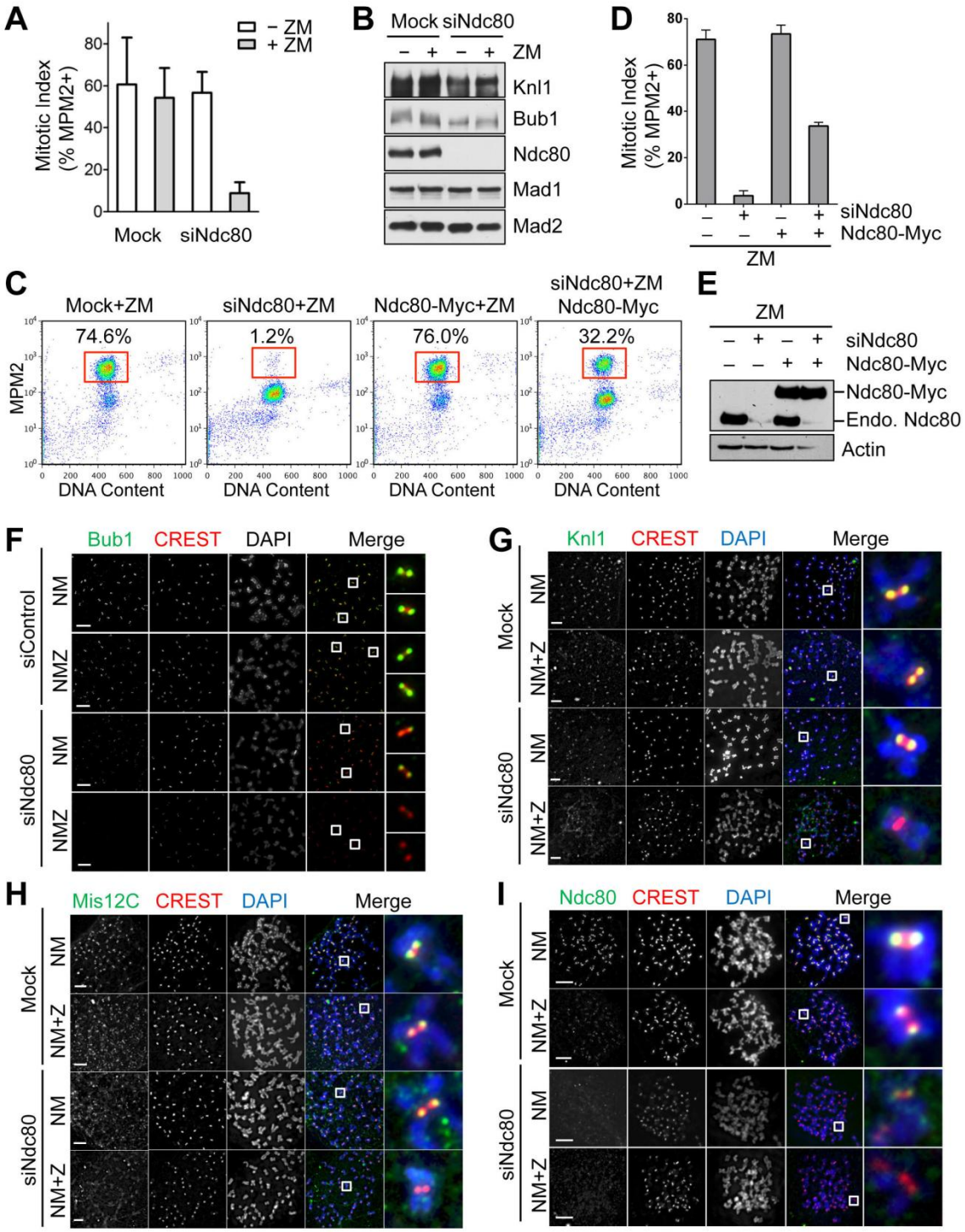
A
Mitotic Index (% MPM2+)
80
60
40
20
0
Mock
siNdc80
– ZM
+ ZM
B
Mock siNdc80
– + – +
ZM
Knl1
Bub1
Ndc80
Mad1
Mad2
D
Mitotic Index (% MPM2+)
80
60
40
20
0
siNdc80
Ndc80-Myc
ZM
C
Mock+ZM
siNdc80+ZM
Ndc80-Myc+ZM
siNdc80+ZM Ndc80-Myc
74.6%
1.2%
76.0%
32.2%
MPM2
DNA Content
E
ZM
siNdc80
Ndc80-Myc
Ndc80-Myc
Endo. Ndc80
Actin
F
Bub1
CREST
DAPI
Merge
siControl
siNdc80
NM
NMZ
G
Knl1
CREST
DAPI
Merge
Mock
siNdc80
NM
NM+Z
H
Mis12C
CREST
DAPI
Merge
Mock
siNdc80
NM
NM+Z
I
Ndc80
CREST
DAPI
Merge
Mock
siNdc80
NM
NM+Z

Figure 4-4. Aurora B is critical for the spindle checkpoint and kinetochore targeting of KMN in cells with compromised Ndc80C. (**A**) HeLa Tet-On cells were mock transfected or transfected with siNdc80 for 10 hr, treated with thymidine for 14 hr, released into nocodazole-containing medium for 12 hr, treated with ZM447439 (ZM) for 2 hr, and analyzed by flow cytometry. The percentages of mitotic cells (defined as MPM2-positive cells with 4C DNA contents) were plotted. The means and standard deviations (SD) of three independent experiments are shown. (**B**) Lysates of cells in **A** were blotted with the indicated antibodies. (**C**) HeLa Tet-On cells were first transfected with vector or RNAi-resistant Ndc80-Myc, and were then mock transfected or transfected with siNdc80 for 10-12 hr. Cells were treated with thymidine for 14 hr, released into nocodazole-containing medium for 12 hr, treated with ZM for 2 hr, and analyzed with flow cytometry. Representative flow cytometry plots are shown, with the mitotic cells boxed and their percentages indicated. (**D**) Quantification of the mitotic indices of cells in **C**. The means and standard deviations (SD) of three independent experiments are shown. (**E**) Lysates of cells in **c** were blotted with the indicated antibodies. (**F-I**) HeLa Tet-On cells were mock transfected or transfected with the indicated siRNAs, and arrested in mitosis with nocodazole (N). Mitotic cells were collected by shake-off, and each sample was divided into two fresh wells. One well was incubated with the proteasome inhibitor MG132 (M) for 2 hr (NM) while the other well was treated with both MG132 and ZM for 2 hr (NM+Z). Cells were stained with DAPI, CREST, and anti-Bub1 (**F**), anti-Knl1 (**G**), anti-Mis12C (**H**) or anti-Ndc80 (**I**) antibodies. The channels included in the merged images were labeled with their respective colors. The boxed regions were magnified and shown in the rightmost column. Scale bars, 5 μm. Quantifications of the relative intensities of KMN in (**G-I**) are included in Figure. 4-5D-F.

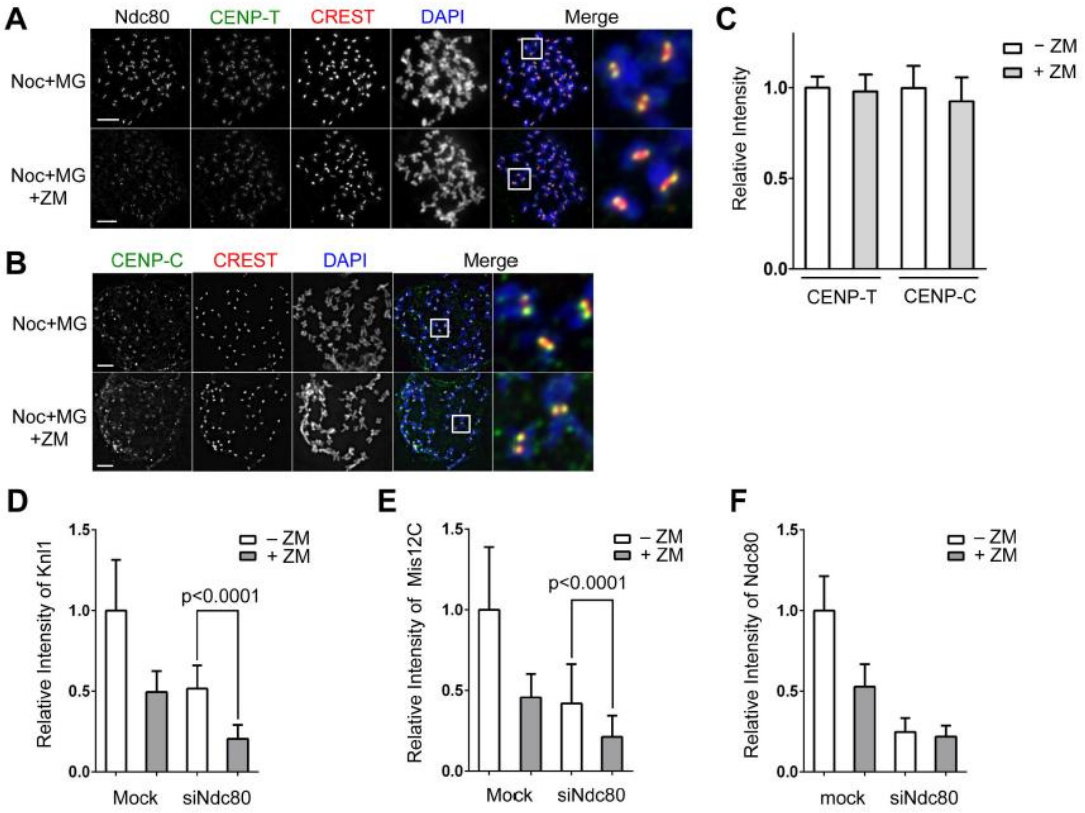

Figure 4-5. Aurora B inhibition reduces KMN kinetochore targeting without affecting CENP-T and -C. (**A**) HeLa cells were arrested in mitosis with nocodazole (Noc) and MG132 (MG), treated with ZM447439 (ZM), and stained with DAPI (blue in merge), CREST (red), α-Ndc80, and α-CENP-T (green). The boxed regions were magnified and shown in the rightmost column. Scale bars, 5 μm. (**B**) HeLa cells were treated as in **A** and stained with DAPI (blue in merge), CREST (red), and α-CENP-C (green). The boxed regions were magnified and shown in the rightmost column. Scale bars, 5 μm. (**C**) Quantification of the normalized intensities of the CENP-T and -C staining of cells in **A,B**. The means and SDs of two independent experiments (with 40 kinetochores per cell and 19-30 cells per condition measured in each experiment) are shown. (**D-F**) Quantification of the relative intensities of KMN staining in Figure. 4-4G-I. The intensities of 40 kinetochores per cell in 10 cells per condition were measured, with means and SDs shown.

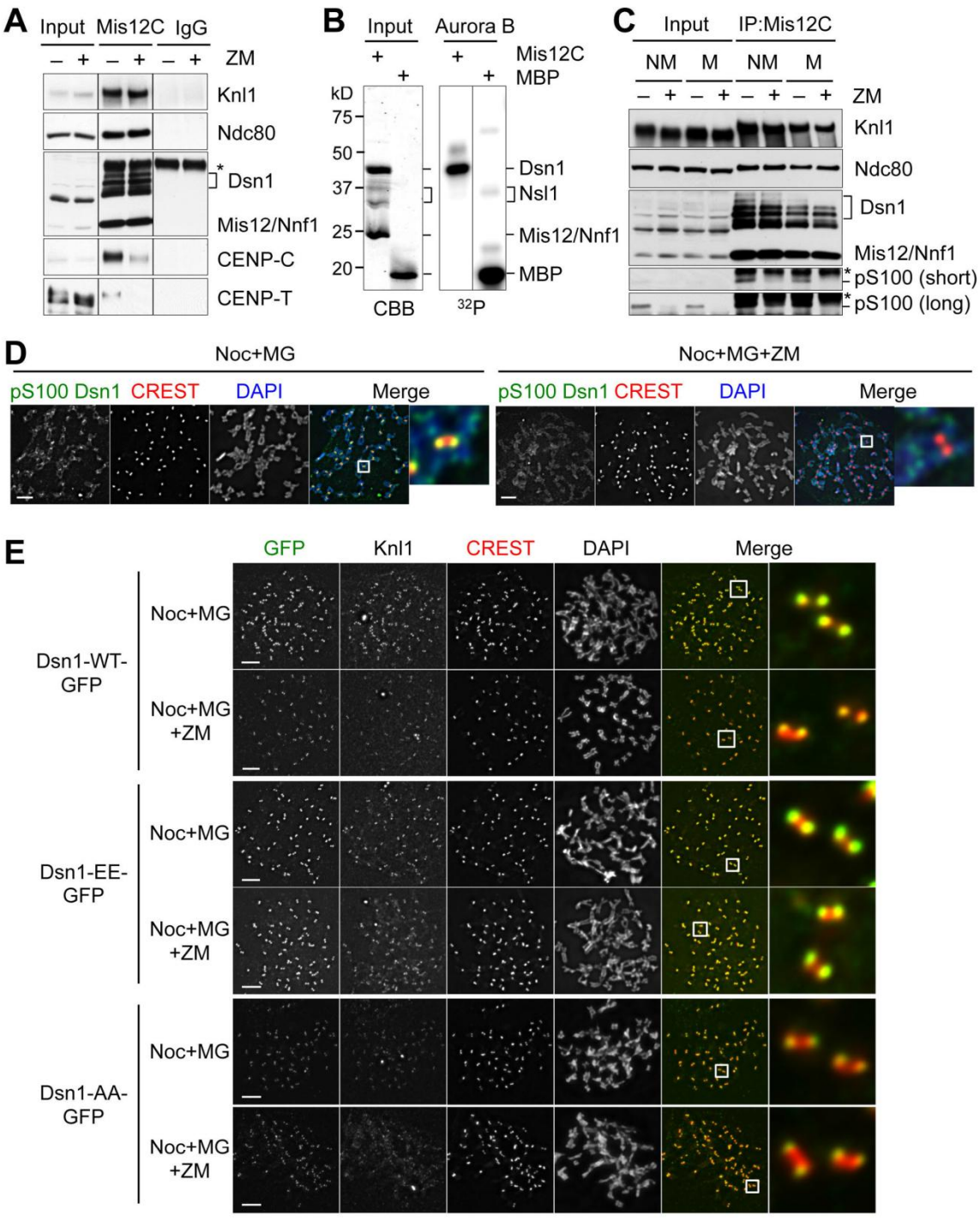

Figure 4-6. Aurora B phosphorylates Dsn1 and strengthens the CCAN–KMN interaction. (**A**) HeLa Tet-On cells arrested in mitosis with nocodazole were incubated

without (–) or with (+) ZM447439 (ZM) in the presence of MG132 for 2 hr before lysis. Lysates were immunoprecipitated with IgG or the α-Mis12C antibody. The whole cell lysates (Input), α-Mis12C IP (Mis12C), and IgG IP were blotted with the indicated antibodies. The asterisk indicates the IgG heavy chain in the IP samples. Dsn1 migrated as multiple bands presumably due to phosphorylation. Mis12 and Nnf1 co-migrated. (**B**) Recombinant Mis12C was incubated with recombinant Aurora B–INCENP and γ-^{32}P-ATP, separated by SDS-PAGE, and analyzed with a phosphorimager. Mis12 and Nnf1 co-migrated. Nsl1 underwent proteolysis. Myelin basic protein (MBP*)* was used as a positive control for Aurora B activity. (**C**) HeLa cells were arrested in mitosis with nocodazole and MG132 (NM) or simply MG132 (M) and then treated with (+) or without (–) ZM447439 (ZM). Lysates and α-Mis12C IP of these cells were blotted with the indicated antibodies. Two exposures of the anti-pS100 Dsn1 blot were shown. Asterisks indicate IgG heavy chain in the IP samples. (**D**) HeLa Tet-On cells were arrested in prometaphase with nocodazole (Noc) and incubated with MG132 (MG) alone or with MG132 and ZM447439 (ZM) for 2 h, and then stained with DAPI (blue in the merge), CREST (red), and α-pS100 Dsn1 (green). The boxed regions were magnified and shown in the rightmost column. Scale bars, 5 μm. (**E**) Cells stably expressing Dsn1-WT, S100E/S109E (EE), or S100A/S109A (AA)-GFP were transfected with siDsn1, treated as in **D**, and stained with the indicated antibodies. The Dsn1-GFP and CREST signals were colored green and red, respectively, in the merge. The boxed regions were magnified and shown in the rightmost column. Scale bars, 5 μm. Quantification of the relative intensities of GFP and Knl1 is included in Figure. 4-7C,D.

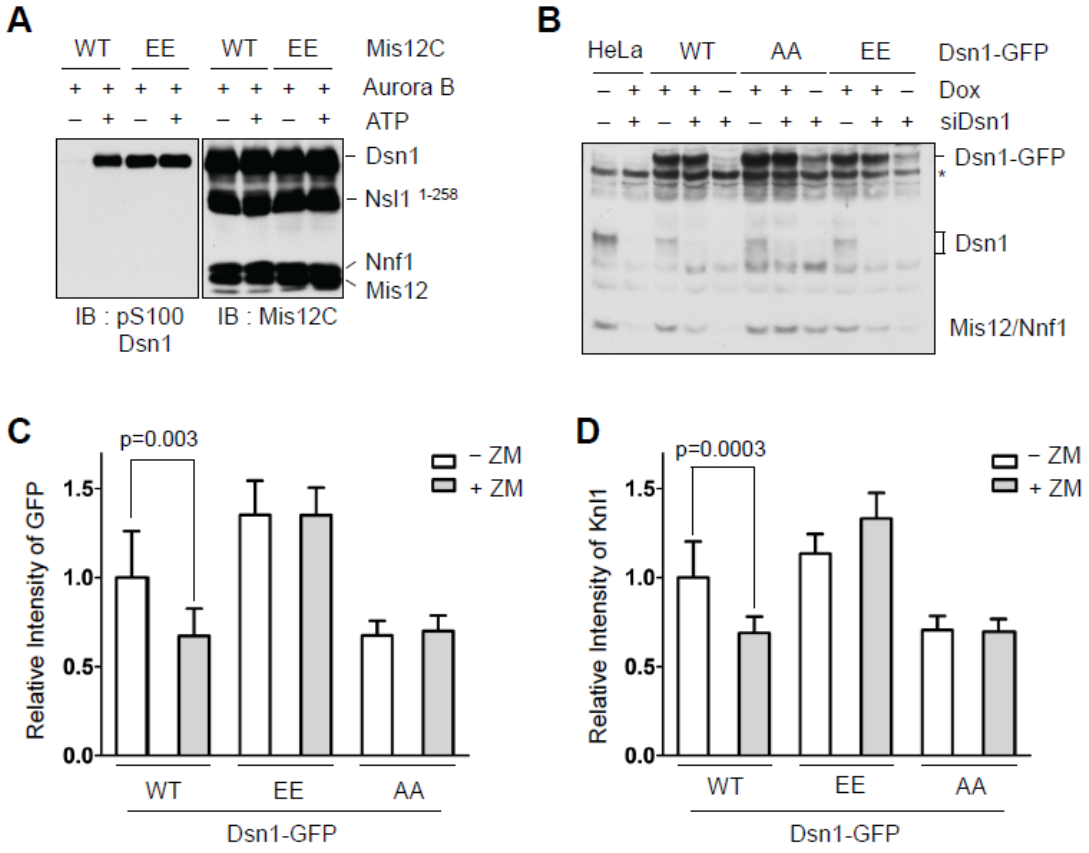

Figure 4-7. Aurora B-dependent phosphorylation of Dsn1 promotes its kinetochore targeting. (**A**) Recombinant Mis12C containing Dsn1-WT or Dsn1-EE was incubated with Aurora B–INCENP with (+) or without (–) cold ATP. Samples were separated by SDS-PAGE and blotted with the indicated antibodies. Note that the phospho-mimicking Dsn1 mutant was strongly recognized by α-pS100 Dsn1. (**B**) HeLa Tet-On parental cells and cells stably expressing Dsn1-WT-GFP, Dsn1-S100A/S109A (AA)-GFP, or Dsn1-S100E/S109E (EE)-GFP were cultured in the absence (–) or presence (+) of doxycycline (Dox) and were either mock transfected (–) or transfected with (+) siDsn1. Cell lysates were blotted with α-Mis12C. In the absence of Dox, Dsn1-AA-GFP and Dsn1-EE-GFP lines had leaky expression. The asterisk indicates a non-specific band that serves as a loading control. (**C,D**) Quantification of the normalized intensities of Dsn1-GFP (**C**) and Knl1 (**D**) of cells in Figure. 4-6E. The means and SDs of the intensities of 10 cells per condition (with 40 kinetochores analyzed per cell) are shown.

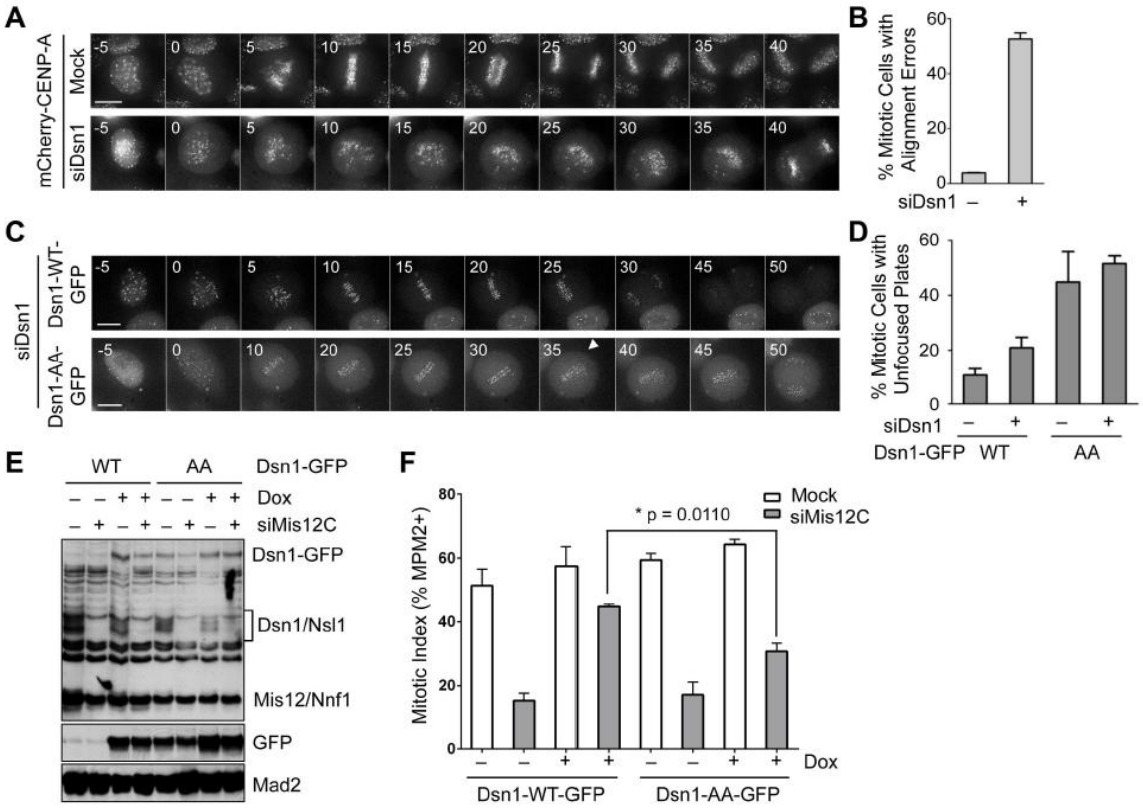

Figure 4-8. Dsn1 phosphorylation is largely dispensable for chromosome alignment, but contributes to spindle checkpoint signaling. (**A**) HeLa Tet-On cells stably expressing mCherry-CENP-A were mock transfected or transfected with Dsn1 siRNA, and analyzed by time lapse microscopy. mCherry images of representative cells at the indicated times (in minutes) with nuclear envelope breakdown (NEBD) as the reference point (time 0) were shown. Scale bars, 10 μm. (**B**) Quantification of the percentage of mitotic cells in **A** with chromosome alignment defects. The means and SDs of two independent experiments (with 22-83 cells counted in each sample) are shown. (**C**) HeLa Tet-On cells stably expressing Dsn1-WT-GFP or Dsn1-AA-GFP were transfected with siDsn1 and analyzed as in **A**. Scale bars, 10 μm. (**D**) Quantification of the percentage of mitotic cells in **C** with unfocused metaphase plate (marked with arrowhead). The means and SDs of three independent experiments (with 8-32 cells counted per condition) are shown. Cells that underwent spindle rotations during mitosis were excluded from the analysis. (**E**) HeLa Tet-On cells stably expressing Dsn1-WT-GFP or Dsn1-AA-GFP were mock transfected or transfected with siMis12C (the combination of siDsn1 and siNsl1) in the absence (–) or presence (+) of doxycycline (Dox). Cells were treated with thymidine for 14 hr, and released into nocodazole-containing medium for 15 hr. Lysates of these

cells were blotted with the indicated antibodies. (**F**) The mitotic index of cells in **E** was determined by FACS, with means and SDs of three independent experiments shown.

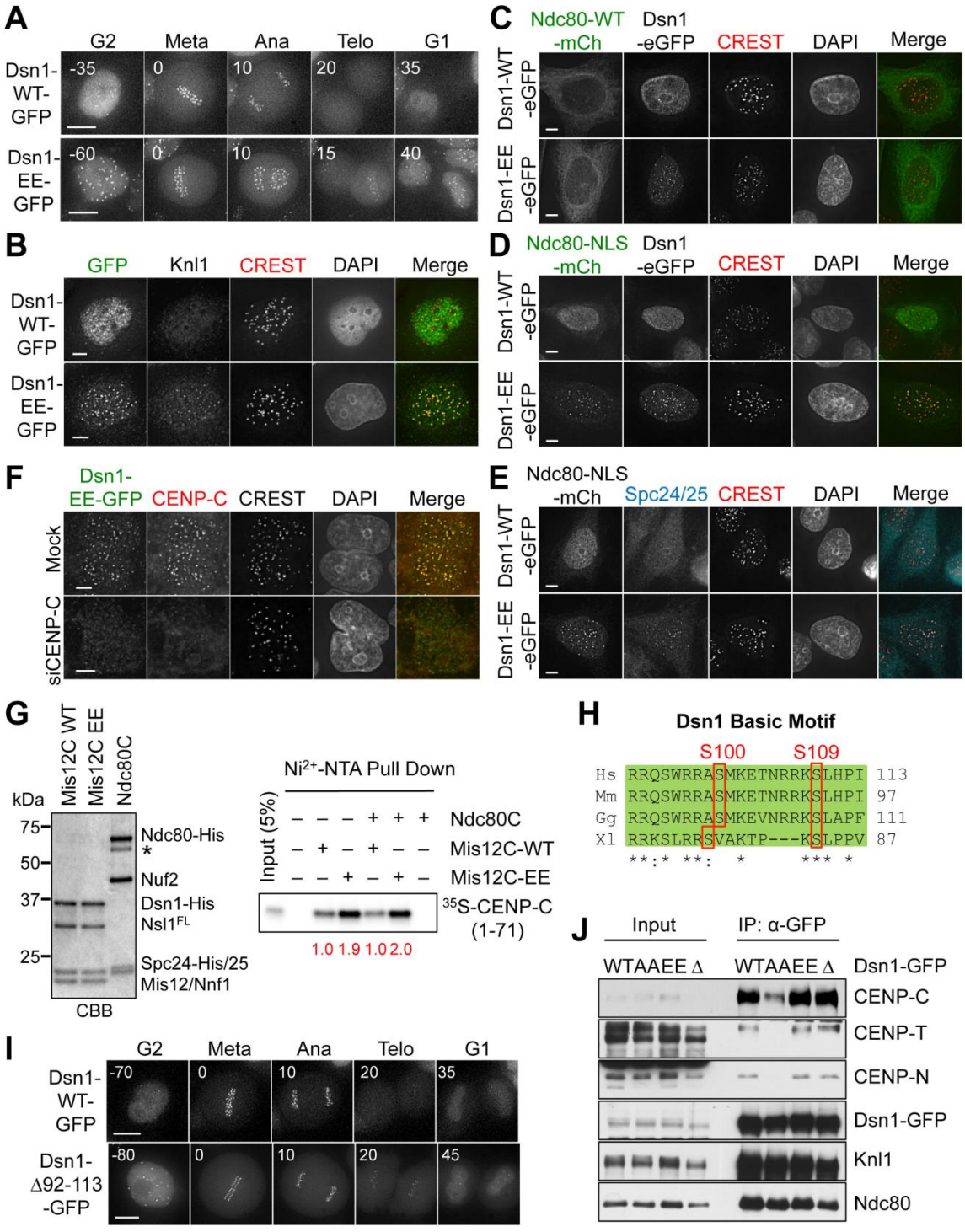
A
G2
Meta
Ana
Telo
G1
Dsn1-WT-GFP
-35
0
10
20
35
Dsn1-EE-GFP
-60
0
10
15
40
B
GFP
Knl1
CREST
DAPI
Merge
Dsn1-WT-GFP
Dsn1-EE-GFP
C
Ndc80-WT -mCh
Dsn1 -eGFP
CREST
DAPI
Merge
Dsn1-WT -eGFP
Dsn1-EE -eGFP
D
Ndc80-NLS -mCh
Dsn1 -eGFP
CREST
DAPI
Merge
Dsn1-WT -eGFP
Dsn1-EE -eGFP
E
Ndc80-NLS -mCh
Spc24/25
CREST
DAPI
Merge
Dsn1-WT -eGFP
Dsn1-EE -eGFP
F
Dsn1-EE-GFP
CENP-C
CREST
DAPI
Merge
Mock
siCENP-C
G
Mis12C WT
Mis12C EE
Ndc80C
kDa
75
50
37
25
Ndc80-His *
Nuf2
Dsn1-His
Nsl1FL
Spc24-His/25
Mis12/Nnf1
CBB
Ni2+-NTA Pull Down
Input (5%)
Ndc80C
Mis12C-WT
Mis12C-EE
35S-CENP-C (1-71)
1.0 1.9 1.0 2.0
H
Dsn1 Basic Motif
S100
S109
Hs RRQSWRRASMKETNRRKSLHPI 113
Mm RRQSWRRASMKETNRRKSLHPI 97
Gg RRQSWRRASMKEVNRRKSLAPF 111
Xl RRKSLRRSVAKTP---KSLPPV 87
I
G2
Meta
Ana
Telo
G1
Dsn1-WT-GFP
-70
0
10
20
35
Dsn1-Δ92-113-GFP
-80
0
10
20
45
J
Input
IP: α-GFP
WTAAEE Δ
WTAAEE Δ
Dsn1-GFP
CENP-C
CENP-T
CENP-N
Dsn1-GFP
Knl1
Ndc80

Figure 4-9. Phospho-mimicking Dsn1 mutation and forced nuclear localization of Ndc80 suffice to install KMN at interphase kinetochores. (**A**) HeLa Tet-On cells stably expressing Dsn1-WT-GFP or Dsn1-EE-GFP were analyzed by time lapse microscopy. GFP images of representative cells at the indicated times (in minutes) from G2 to the next G1 phase were shown. Metaphase was used as the reference point (time 0). Scale bars, 10 μm. (**B**) Interphase cells stably expressing Dsn1-WT-GFP or Dsn1-EE-GFP were stained with DAPI, α-Knl1, α-GFP (green in the merge), and CREST (red). Scale bars, 5 μm. (**C-E**) HeLa Tet-On cells stably expressing Dsn1-WT-GFP or Dsn1-EE-GFP were transfected with plasmids encoding Ndc80-WT-mCherry or Ndc80-NLS-mCherry, and stained with the indicated antibodies and DAPI. Scale bars, 5 μm. (**F**) HeLa Tet-On cells stably expressing Dsn1-EE-GFP were mock transfected or transfected with CENP-C siRNA, arrested in thymidine, and stained with DAPI, α-GFP (green in merge), α-CENP-C (red), and CREST. Scale bars, 5 μm. (**G**) Recombinant Mis12C and Ndc80C were stained with Coomassie brilliant blue (CBB, left panel). The asterisk indicates a degradation band of Ndc80. Recombinant Mis12C containing Dsn1-WT (Mis12C-WT) or Dsn1-EE (Mis12C-EE) was pre-incubated with or without recombinant Ndc80C and immobilized on Ni^{2+}-NTA beads and incubated with ^{35}S-methionine labeled CENP-C fragment (residues 1-71). The bound proteins and 5% input were separated by SDS-PAGE and analyzed with a phosphorimager (right panel). The relative band intensity of autoradiography is indicated at the bottom. (**H**) Sequence alignment of the basic motif encompassing the two Aurora B phosphorylation sites in Dsn1 proteins from different species (Hs, *Homo sapiens*; Mm, *Mus musculus*; Gg, *Gallus gallus*; Xl, *Xenopus laevis*). (**I**) HeLa Tet-On cells stably expressing Dsn1-WT-GFP or Dsn1-Δ92-113-GFP were analyzed by time lapse microscopy as described in **A**. Scale bars, 10 μm. (**J**) HeLa Tet-On cells stably expressing Dsn1-WT, -AA, -EE, or -Δ92-113-GFP were arrested in mitosis with nocodazole. Lysates and α-GFP IP of these cells were blotted with the indicated antibodies.

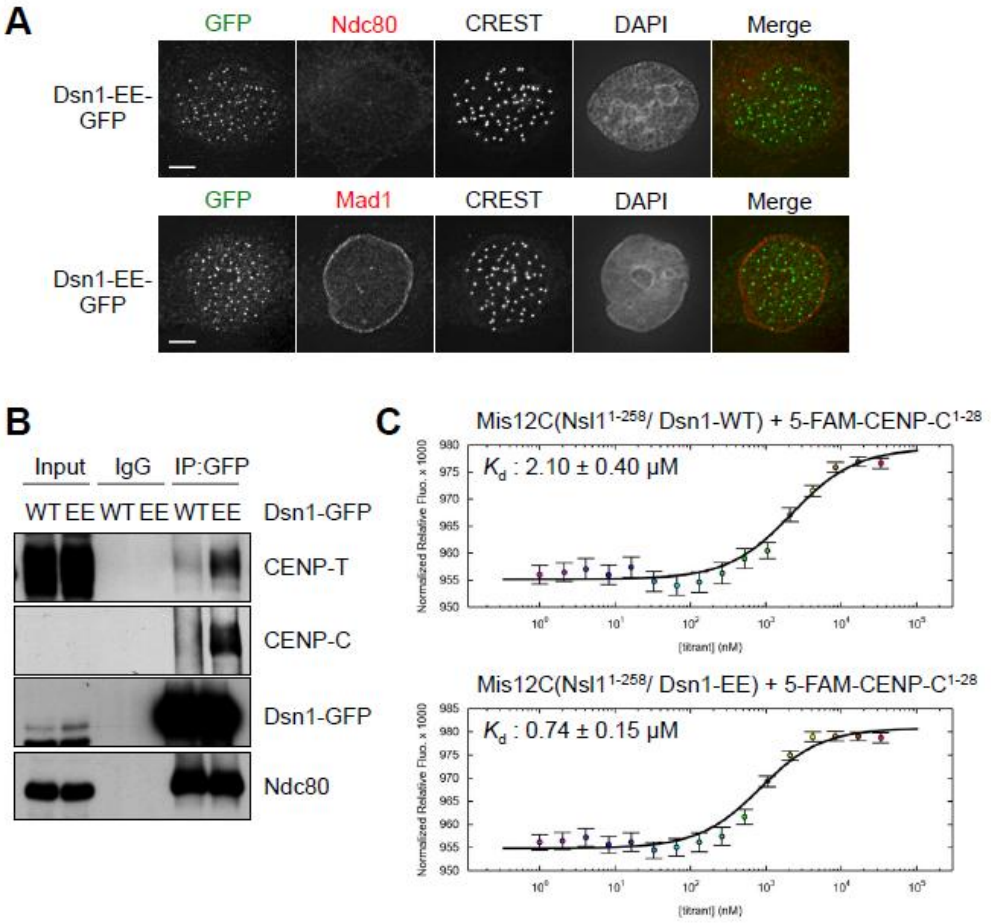

Figure 4-10. Phospho-mimicking Dsn1-EE enhances the CENP-C–Mis12C interaction. (**A**) Interphase HeLa cells expressing Dsn1-EE-GFP were stained with DAPI, α-Ndc80 or α-Mad1 (red in merge), α-GFP (green), and CREST. Scale bars, 5 μm. (**B**) HeLa Tet-on cells stably expressing Dsn1-WT-GFP or Dsn1-EE-GFP were treated with thymidine for 14 hr. Lysates were immunoprecipitated with IgG or the α-GFP antibody. The cell lysates (Input), α-Mis12C IP (Mis12C), and IgG IP were blotted with the indicated antibodies. (**C**) MST titration curves of the binding reactions between a fluorescently labeled CENP-C peptide and Mis12C containing Dsn1 WT (top panel) or EE (bottom panel) with the K_d indicated.

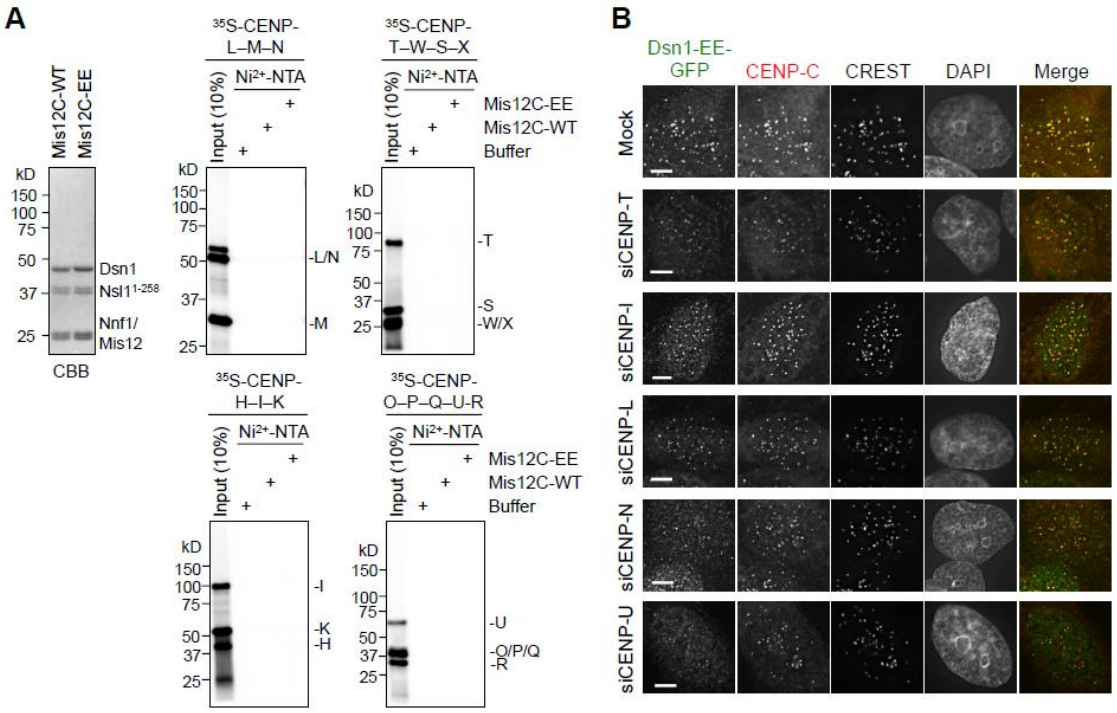

Figure 4-11. CENP-C is the major kinetochore receptor for phospho-mimicking Dsn1 in interphase cells. (**A**) Components of several CCAN sub-complexes, including CENP-L−M−N, CENP-T−W−S−X, CENP-H−I−K, and CENP-O−P−Q−U−R were co-translated in reticulocyte lysate in the presence of ^{35}S-methionine. Recombinant Mis12C containing Dsn1-WT (Mis12C-WT) or Dsn1-EE (Mis12C-EE) was immobilized on Ni^{2+}-NTA beads and incubated with the ^{35}S-labeled CCAN proteins. The bound proteins and 10% input were separated by SDS-PAGE and analyzed with a phosphorimager. Coomassie brilliant blue (CBB) staining of recombinant Mis12C used in the binding assays was shown in the top leftmost panel. (**B**) HeLa Tet-On cells stably expressing Dsn1-EE-GFP were either mock transfected or transfected with siRNAs against the indicated CENPs, arrested in thymidine, and stained with DAPI, CREST, α-GFP (green in merge), and α-CENP-C (red). Scale bars, 5 μm.

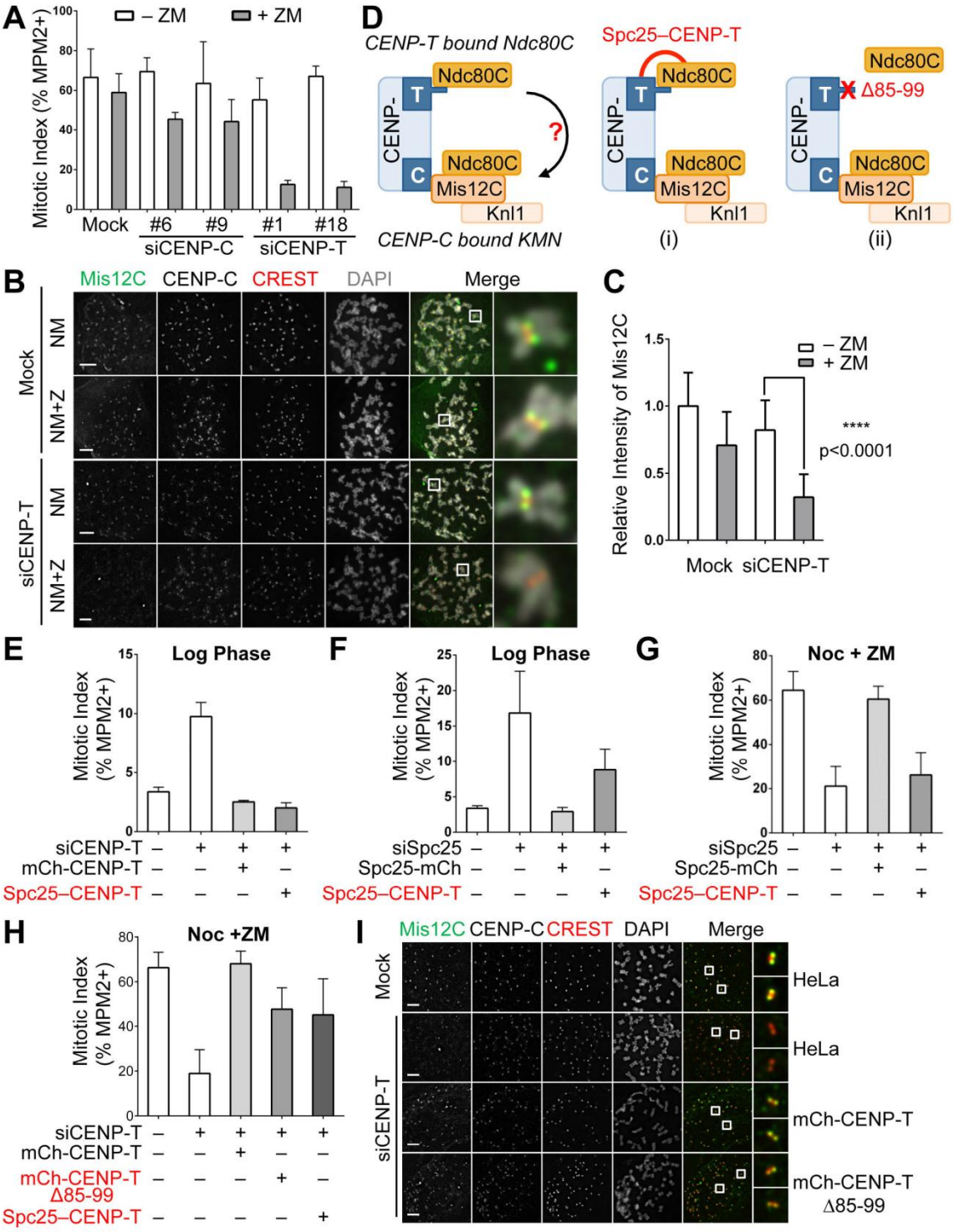
A
– ZM
+ ZM
Mitotic Index (% MPM2+)
Mock
#6
#9
#1
#18
siCENP-C
siCENP-T
D
CENP-T bound Ndc80C
Ndc80C
CENP-
T
C
Mis12C
Knl1
CENP-C bound KMN
Spc25–CENP-T
Δ85-99
(i)
(ii)
B
Mis12C
CENP-C
CREST
DAPI
Merge
Mock
siCENP-T
NM
NM+Z
C
Relative Intensity of Mis12C
****
p<0.0001
Mock
siCENP-T
E
Log Phase
siCENP-T
mCh-CENP-T
Spc25–CENP-T
F
Log Phase
siSpc25
Spc25-mCh
G
Noc + ZM
H
Noc +ZM
mCh-CENP-T Δ85-99
I
HeLa
mCh-CENP-T
mCh-CENP-T Δ85-99

Figure 4-12. CENP-T contributes to KMN kinetochore targeting independently of Aurora B and direct Ndc80C binding. (**A**) HeLa Tet-On cells were mock transfected or transfected with the indicate siRNAs, treated with thymidine for 14 he, released into nocodazole-containing medium for 12 hr, and treated with ZM for 2 hr. The mitotic index of these cells was determined by flow cytometry. The means and SDs of three experiments are shown. (**B**) HeLa Tet-On cells were mock transfected or transfected with siCENP-T and arrested in mitosis by nocodazole. Mitotic cells were collected by shake-off. Each sample was divided into two fresh wells. One well was incubated with MG132 (MG) for 2 hr (NM) while the other well was treated with both MG and ZM for 2 hr (NM+Z). Cells were stained with indicated antibodies and DAPI. The boxed regions of the merged images of the selected channels were magnified and shown in the rightmost column. Scale bars, 5 μm. (**C**) Quantification of the relative kinetochore intensities of Mis12C in **B**. The intensities of 40 kinetochores per cell in 10 cells per condition were measured. The means and SDs are shown. (**D**) Schematic drawing of the two Ndc80C pools at kinetochores and our strategies to perturb the CENP-T-bound Ndc80C pool. (**E,F**) HeLa Tet-On parental cells or cells stably expressing Spc25-mCherry, Spc25-mCherry-CENP-T, or mCherry-CENP-T were mock transfected or transfected with siCENP-T or siSpc25, and harvested after 48 hr for flow cytometry analysis to determine their mitotic index. The means and SDs of three experiments are shown. (**G**) HeLa Tet-On parental cells or cells stably expressing Spc25-mCherry or Spc25-mCherry-CENP-T were mock transfected or transfected with siSpc25, treated with thymidine for 14 hr, released into nocodazole-containing medium for 12 hr, and treated with ZM for 2 hr (Noc+ZM). Their mitotic index was determined by flow cytometry. Means and SDs of three experiments are shown. (**H**) HeLa Tet-On cells or cells stably expressing mCherry-CENP-T, mCherry-CENP-T Δ85-99, or Spc25-mCherry-CENP-T were mock transfected or transfected with siCENP-T, treated with thymidine for 14 hr, released into nocodazole-containing medium for 12 hr, and treated with ZM for 2 hr. Their mitotic index was determined by flow cytometry. Means and SDs of three experiments are shown. (**I**) HeLa Tet-On cells or cells stably expressing mCherry-CENP-T or mCherry-CENP-T Δ85-99 were arrested in mitosis by nocodazole, incubated with ZM and MG132 for 2 hr, and stained with the indicated antibodies and DAPI. The boxed regions of the merged images were magnified and shown in the rightmost column. Scale bars, 5 μm.

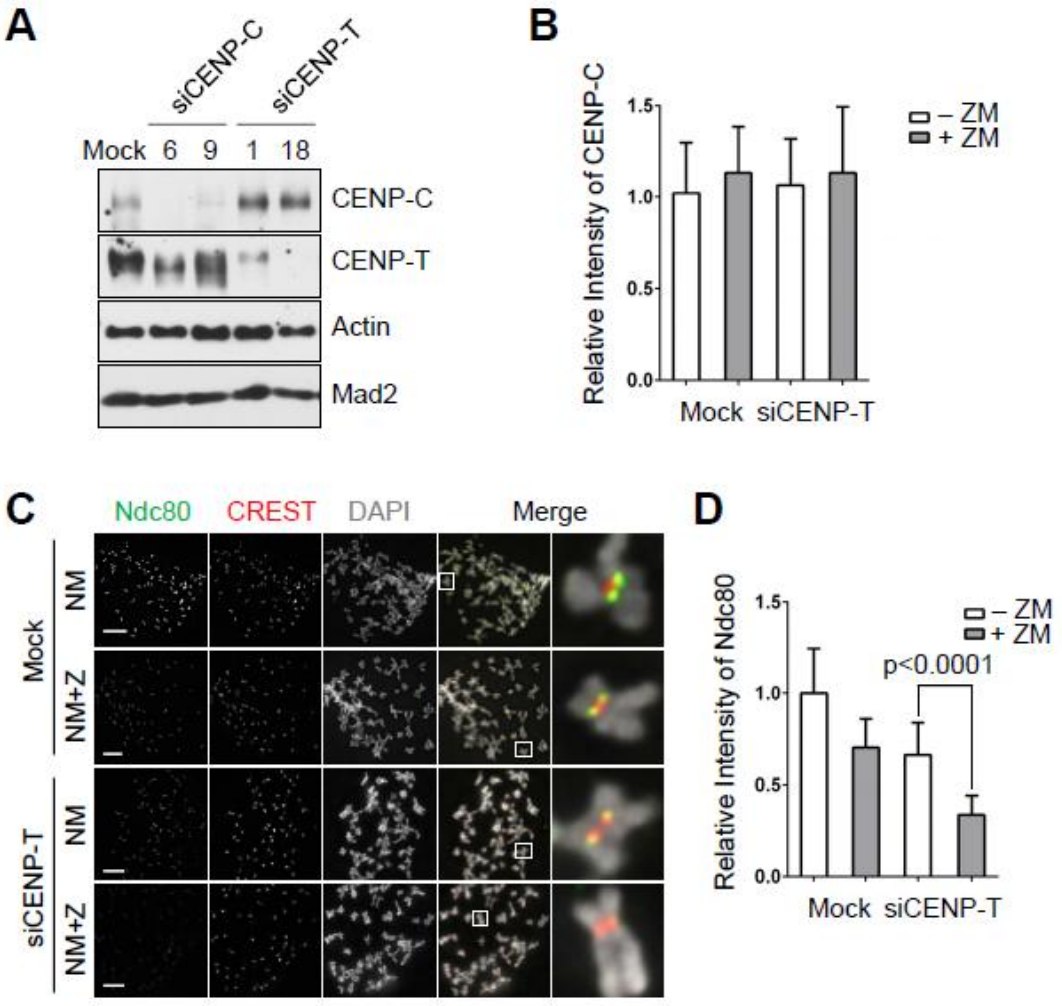

Figure 4-13. Depletion of CENP-T and Aurora B inhibition greatly reduce Ndc80 kinetochore localization without affecting CENP-C. (**A**) Lysates of cells analyzed in Figure. 4-12A were blotted with the indicated antibodies. (**B**) Quantification of the relative intensities of CENP-C of cells in Figure. 4-12B. Means and SDs of the intensities of 10 cells per condition (with 40 kinetochores analyzed per cell) are shown. (**C**) Cells in Figure. 4-12B were stained with the indicated antibodies and DAPI. The boxed regions of the merged images of the selected channels were magnified and shown in the rightmost column. Scale bars, 5 μm. (**D**) Quantification of the relative kinetochore intensities of Ndc80 in **C**. The intensities of 40 kinetochores per cell in 10 cells per condition were measured, with means and SDs shown.

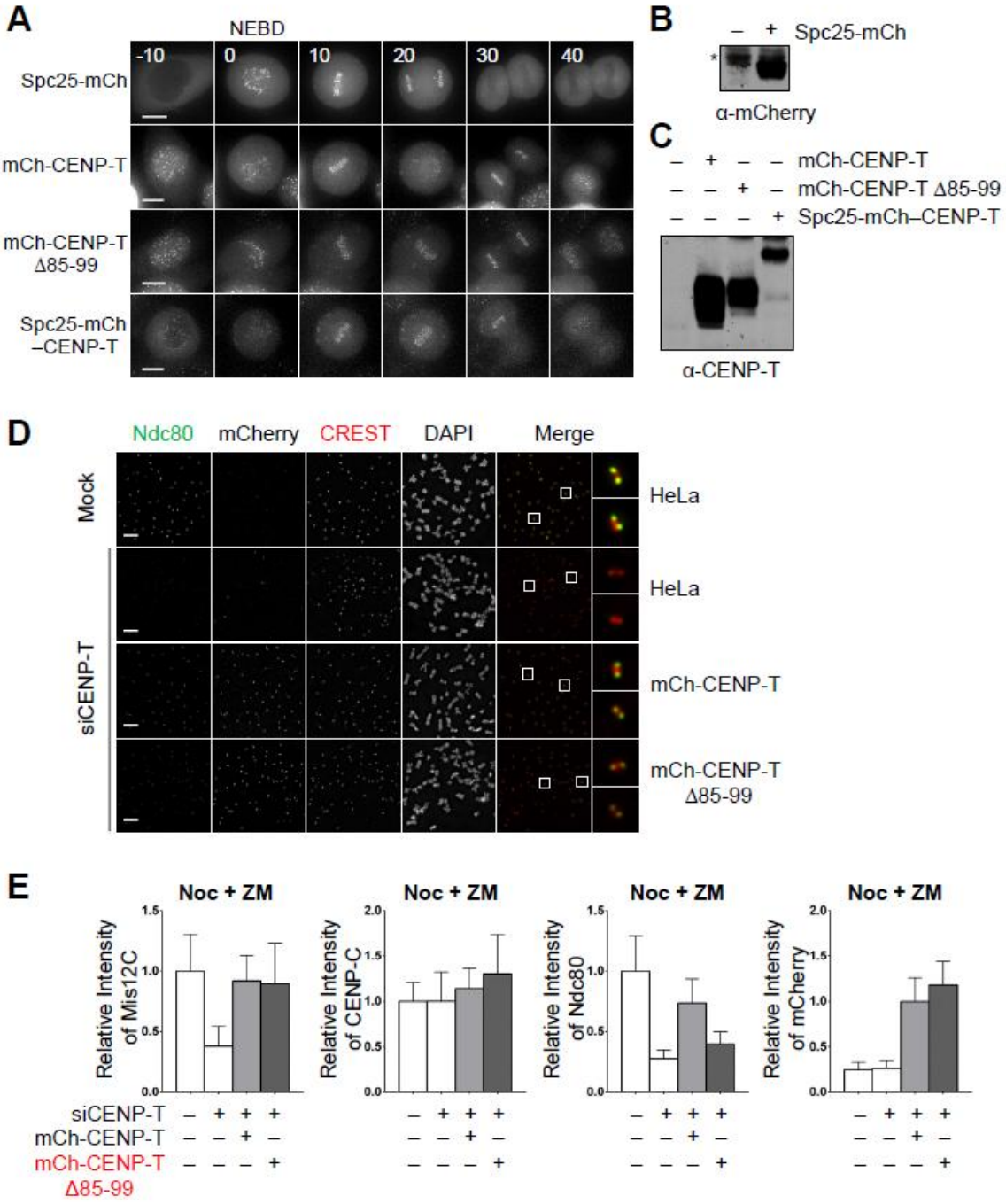

Figure 4-14. Ndc80-binding-deficient CENP-T mutant supports Mis12C kinetochore targeting in the presence of Aurora B inhibition. (**A**) HeLa Tet-On cells stably expressing Spc25-mCherry (mCh), mCherry-CENP-T, mCherry-CENP-T Δ85-99, or

Spc25-mCh-CENP-T were analyzed by time lapse microscopy. mCherry images of representative cells at the indicated times (in minutes) were shown. Nuclear envelope breakdown (NEBD) was used as the reference point (time 0). Scale bars, 10 μm. (**B,C**) Parental HeLa cells or cells expressing the indicated mCherry proteins were cultured in the presence of 1 μg/ml doxycycline. Cell lysates were blotted with α-mCherry (**B**) or α-CENP-T (**C**). The asterisk indicates a non-specific band. (**D**) HeLa Tet-On parental cells or cells stably expressing mCherry-CENP-T or mCh-CENP-T Δ85-99 were mock transfected or transfected with siCENP-T, treated with thymidine for 14 hr, released into nocodazole-containing medium for 12 hr, treated with ZM and MG132 for 2 hr, and stained with the indicated antibodies and DAPI. The boxed regions of the merged images were magnified and shown in the rightmost column. Scale bars, 5 μm. (**E**) Quantification of the relative intensities of the indicated proteins stained in **D** and Figure. 4-12I. The intensities of 40 kinetochores per cell in 10 cells per condition were measured, with means and SDs shown.

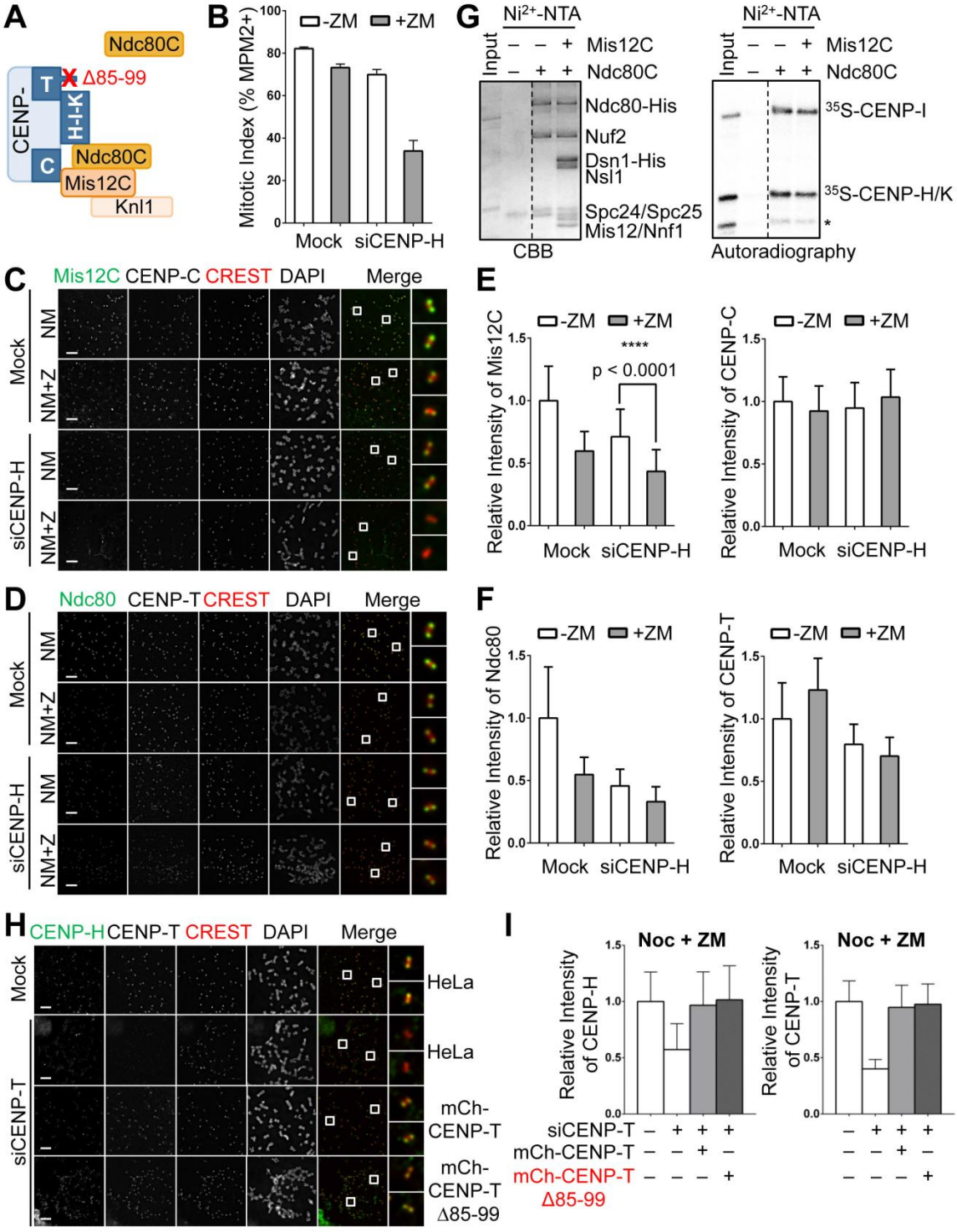
A
Ndc80C
CENP-
T
Δ85-99
H-I-K
C
Ndc80C
Mis12C
Knl1
B
-ZM
+ZM
Mitotic Index (% MPM2+)
Mock
siCENP-H
G
Ni2+-NTA
Input
Mis12C
Ndc80C
Ndc80-His
Nuf2
Dsn1-His
Nsl1
Spc24/Spc25
Mis12/Nnf1
CBB
35S-CENP-I
35S-CENP-H/K
Autoradiography
C
Mis12C CENP-C CREST DAPI Merge
Mock
siCENP-H
NM
NM+Z
E
Relative Intensity of Mis12C
Relative Intensity of CENP-C
****
p < 0.0001
D
Ndc80 CENP-T CREST DAPI Merge
F
Relative Intensity of Ndc80
Relative Intensity of CENP-T
H
CENP-H CENP-T CREST DAPI Merge
siCENP-T
HeLa
mCh-CENP-T
mCh-CENP-T Δ85-99
I
Noc + ZM
Relative Intensity of CENP-H
Relative Intensity of CENP-T
siCENP-T
mCh-CENP-T
mCh-CENP-T Δ85-99

Figure 4-15. CENP-T promotes KMN kinetochore targeting indirectly through CENP-H-I-K. (**A**) Model for how CENP-T contributes to KMN assembly independently of its direct binding to Ndc80C. (**B**) HeLa Tet-On cells were mock transfected or transfected with siCENP-H, treated with thymidine for 14 hr, released into nocodazole-containing medium for 12 hr, and treated with or without ZM for 2 hr. Their mitotic index was determined by flow cytometry. Means and SDs of three experiments are shown. (**C,D**) HeLa Tet-On cells were mock transfected or transfected with siCENP-H and arrested in mitosis by nocodazole. Cells were further incubated with MG132 (MG) for 2 hr (NM) or with both MG and ZM for 2 hr (NM+Z), and stained with the indicated antibodies and DAPI. The merged images were shown in indicated colors. The boxed regions were magnified and shown in the rightmost column. Scale bars, 5 μm. (**E,F**) Quantification of the relative intensities of the indicated proteins stained in **C,D**. The intensities of 40 kinetochores per cell in 10 cells per condition were measured, with means and SDs shown. (**G**) Recombinant Ndc80C was pre-incubated with or without recombinant Mis12C and immobilized on Ni^{2+}-NTA beads and incubated with ^{35}S-methionine labeled CENP-H-I-K. The bound proteins and 5% input were separated by SDS-PAGE, stained with Coomassie brilliant blue (left panel), and analyzed with a phosphorimager (right panel). CENP-H and -K co-migrate. The asterisk indicates a CENP-K fragment. (**H**) HeLa Tet-On parental cells or cells stably expressing mCherry-CENP-T or mCh-CENP-T Δ85-99 were mock transfected or transfected with siCENP-T, treated with thymidine for 14 hr, released into nocodazole-containing medium for 12 hr, treated with ZM and MG132 for 2 hr, and stained with the indicated antibodies and DAPI. The boxed regions of the merged images were magnified and shown in the rightmost column. Scale bars, 5 μm. (**I**) Quantification of the relative intensities of the indicated proteins stained in **H**. The intensities of 40 kinetochores per cell in 10 cells per condition were measured, with means and SDs shown.

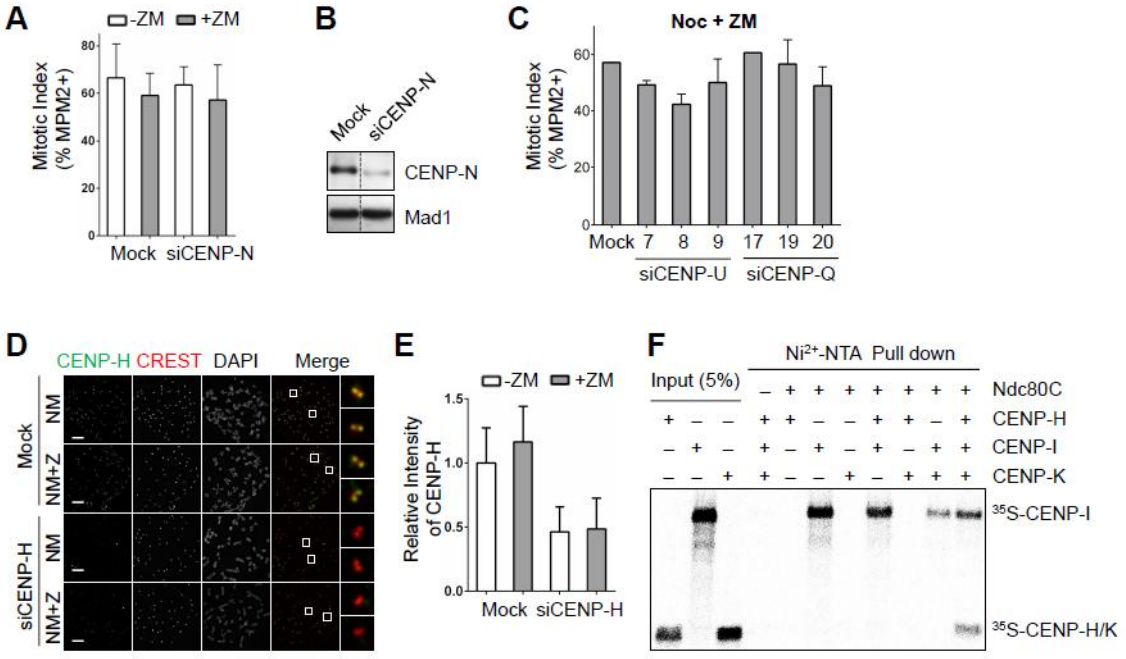

Figure 4-16. CENP-I physically interacts with Ndc80C. (**A**) HeLa Tet-On cells were mock transfected or transfected with siCENP-N, treated with thymidine for 14 hr, released into nocodazole-containing medium for 12 hr, and treated with or without ZM for 2 hr. Their mitotic index was determined by flow cytometry. Means and SDs of three experiments are shown. (**B**) Lysates of cells in **A** were blotted with the indicated antibodies. (**C**) HeLa Tet-On cells were mock transfected or transfected with the indicated siRNAs, treated with thymidine for 14 hr, released into nocodazole-containing medium for 12 hr, and treated with ZM for 2 hr. Their mitotic index was determined by flow cytometry. Means and SDs of three experiments are shown. (**D**) HeLa Tet-On cells were mock transfected or transfected with siCENP-H and arrested in mitosis by nocodazole. Cells were further incubated with MG132 (MG) for 2 hr (NM) or with both MG and ZM for 2 hr (NM+Z), and stained with the indicated antibodies and DAPI. The boxed regions of the merged images with the indicated channels were magnified and shown in the rightmost column. Scale bars, 5 μm. (**E**) Quantification of the relative intensities of the indicated proteins stained in **D**. The intensities of 40 kinetochores per cell in 10 cells per condition were measured, with means and SDs shown. (**F**) Recombinant Ndc80C was immobilized on Ni^{2+}-NTA beads and incubated with ^{35}S-methionine labeled CENP-H, -I, or -K. The 5% input and bound proteins were separated by SDS-PAGE and analyzed with a phosphorimager. Note that the untagged CENP-H

and -K co-migrated in this experiment, while Myc-CENP-K migrated more slowly than HA-CENP-H did in Figure. 4-11A.

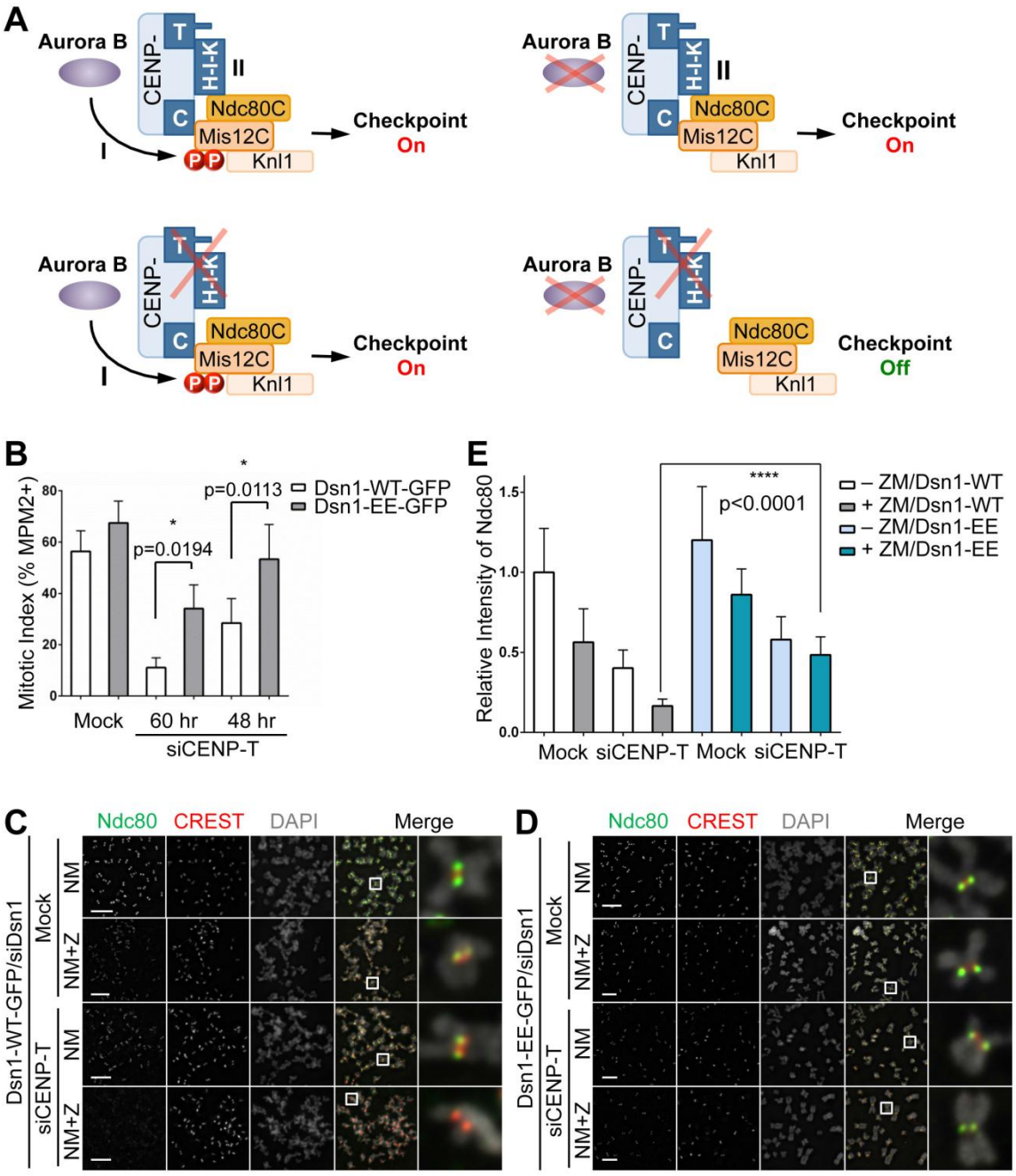

Figure 4-17. Two parallel pathways attach KMN to mitotic kinetochores. (**A**) Two proposed pathways of KMN assembly at kinetochores. In cells with depolymerized microtubules, inactivation of both is required to reduce the KMN level at kinetochores below that needed for checkpoint signaling. (**B**) HeLa Tet-On cells stably expressing Dsn1-WT-GFP or Dsn1-EE-GFP were transfected with siCENP-T for 48 or 60 hr. Cells

were treated with thymidine for 14 hr, released into nocodazole-containing medium for 12 hr, and treated with ZM for 2 hr. Their mitotic index was determined by FACS. Means and SDs of three experiments are shown. (**C,D**) HeLa Tet-On cells stably expressing Dsn1-WT-GFP or Dsn1-EE-GFP were transfected siDsn1 for 24 hr and then mock transfected or transfected with siCENP-T. Cells were arrested in mitosis by nocodazole and further incubated with MG132 (MG) for 2 hr (NM) or with both MG and ZM for 2 hr (NM+Z). Mitotic cells were collected by shake-off and stained with DAPI (grey in merge), CREST (red), and the α-Ndc80 antibody (green). The boxed regions were magnified and shown in the rightmost column. Scale bars, 5 μm. (**E**) Quantification of the relative intensity of Ndc80 in **C,D**. The intensities of 40 kinetochores per cell in 10 cells per condition were measured, with means and SDs shown.

CHAPTER V: PERSPECTIVES

I have described three related stories in the thesis. First, I studied the structural and functional effects of Mad2 phosphorylation. Next, I investigated the kinetochore-targeting mechanism of Mad1 through structural and cellular analyses. Finally, I defined the mitosis-specific assembly pathways of the spindle checkpoint sensor KMN. These studies have provided key insights into the molecular mechanisms that regulate key checkpoint proteins Mad2 and Mad1 and into the assembly pathways of the checkpoint sensor at kinetochores. My research also raises many interesting unanswered questions.

In the first story, I showed that S195 phosphorylation of Mad2 hinders its O-C conformational transition, and the binding to its target Cdc20. My results provided the first evidence of posttranslational regulation for the conformational change of Mad2, which might be critical for the timely inactivation of the spindle checkpoint signal. The lack of a phospho-specific antibody for Mad2-pS195 impeded further investigation of the *in vivo* regulation of this Mad2 inhibitory phosphorylation. Furthermore, in addition to S195, Mad2 is phosphorylated at several other serine residues in its C-terminal region (Wassmann, Liberal et al. 2003; Zich, Sochaj et al. 2012). Paradoxically, the levels of overall phosphorylation of Mad2 increase during mitosis (Wassmann, Liberal et al. 2003) when Mad2 is supposed to be activated to produce spindle checkpoint signals. One intriguing possibility is that not all Mad2 phosphorylation events are inhibitory. Some of these phosphorylation events might activate Mad2. In the future, it will be interesting to

examine the effects of different phosphorylation events on the conformational transition of Mad2 and to identify the responsible kinases.

In the second story, I showed that the kinetochore targeting of Mad1 is mediated by an extensive binding surface, rather than a small, defined domain. Mad1-CTD contributes to its kinetochore targeting, possibly through an interaction with Bub1. In budding yeast, the kinetochore localization of Mad1 is solely dependent on Bub1. Mad1 and Bub1 form a stable complex when the checkpoint is on (Brady and Hardwick 2000; London and Biggins 2014). In human cells, however, Bub1 is not the only kinetochore receptor for Mad1, as Bub1 depletion only partially diminishes Mad1 kinetochore localization. A metazoan-specific protein complex containing RZZ and spindly has been suggested as another Mad1 receptor at kinetochores in higher organisms (Karess 2005; Yamamoto, Watanabe et al. 2008). How Bub1 and RZZ-spindly collaborate to target Mad1 to kinetochores is not understood. A recent study reported that the kinetochore localization of Mad1-Mad2 is indeed graded, depending on the microtubule attachment status of kinetochores (Collin, Nashchekina et al. 2013). It will be interesting to test whether there are multiple pools of Mad1 at kinetochores, with each pool binding different receptors and performing different functions. Artificially targeting Mad1 to attached kinetochores by tethering it to Mis12, a KMN component, is insufficient to maintain checkpoint signals, without the activities of upstream kinases such as Aurora B and Mps1. This result suggests that spindle checkpoint activation requires positive inputs from upstream regulators, in addition to the kinetochore targeting of Mad1-Mad2.

Understanding the nature of these upstream signals remains an important challenge for the future.

In the third story, I established the KMN network as a critical spindle checkpoint sensor at kinetochores. We propose that antagonistic KMN binding between the spindle checkpoint proteins and microtubules underlies the detection of unattached kinetochores. Mitosis-specific assembly of KMN at kinetochores requires two quasi-independent pathways: (1) Aurora B-dependent binding of Mis12C to CENP-C; and (2) CENP-T-dependent CCAN binding to Ndc80C. The relative contributions of these two pathways to KMN assembly at different spindle-damaging conditions remain to be established. It is also unclear why human cells use multiple, semi-redundant mechanisms to install KMN at kinetochores.

The mammalian kinetochore is a massive protein assembly with more than 100 components. In vitro reconstitution of a functional minimal kinetochore with purified or semi-purified components will greatly facilitate the molecular dissection of this complex protein machine, but remains a formidable challenge. Through affinity purification of the tagged KMN component Dsn1, I was able to isolate the core components of a human kinetochore, including KMN and CCAN. It will be interesting to test whether this system will form the foundation for the reconstitution of a functional human kinetochore *in vitro* that can activate the spindle checkpoint proteins. Missing components from this preparation can be supplemented by purified recombinant proteins. Purified recombinant spindle checkpoint proteins and regulatory factors, including Bub1-Bub3, BubR1-Bub3, Mps1, Mad1, Mad2, and Cdc20, will be added to this system to test whether the

reconstituted kinetochore is sufficient to catalyze the formation of MCC. Taxol-stabilized microtubules will be added to test whether microtubule attachment to the reconstituted kinetochores can silence checkpoint signaling. This approach will be instrumental in answering the unresolved questions of the spindle checkpoint.

BIBLIOGRAPHY

Abrieu, A., L. Magnaghi-Jaulin, et al. (2001). "Mps1 is a kinetochore-associated kinase essential for the vertebrate mitotic checkpoint." Cell **106**(1): 83-93.

Adams, P. D., P. V. Afonine, et al. (2010). "PHENIX: a comprehensive Python-based system for macromolecular structure solution." Acta Crystallogr. D Biol. Crystallogr. **66**(Pt 2): 213-221.

Akiyoshi, B., C. R. Nelson, et al. (2013). "The aurora B kinase promotes inner and outer kinetochore interactions in budding yeast." Genetics **194**(3): 785-789.

Barisic, M., B. Sohm, et al. (2010). "Spindly/CCDC99 is required for efficient chromosome congression and mitotic checkpoint regulation." Mol. Biol. Cell **21**(12): 1968-1981.

Bharadwaj, R., W. Qi, et al. (2004). "Identification of two novel components of the human NDC80 kinetochore complex." J. Biol. Chem. **279**(13): 13076-13085.

Bharadwaj, R. and H. Yu (2004). "The spindle checkpoint, aneuploidy, and cancer." Oncogene **23**: 2016-2027.

Black, B. E. and D. W. Cleveland (2011). "Epigenetic centromere propagation and the nature of CENP-a nucleosomes." Cell **144**(4): 471-479.

Bock, L. J., C. Pagliuca, et al. (2012). "Cnn1 inhibits the interactions between the KMN complexes of the yeast kinetochore." Nat. Cell Biol. **14**(6): 614-624.

Bolanos-Garcia, V. M., T. Lischetti, et al. (2011). "Structure of a Blinkin-BUBR1 complex reveals an interaction crucial for kinetochore-mitotic checkpoint regulation via an unanticipated binding Site." Structure **19**(11): 1691-1700.

Brady, D. M. and K. G. Hardwick (2000). "Complex formation between Mad1p, Bub1p and Bub3p is crucial for spindle checkpoint function." Curr. Biol. **10**(11): 675-678.

Burroughs, A. M., M. Jaffee, et al. (2008). "Anatomy of the E2 ligase fold: implications for enzymology and evolution of ubiquitin/Ub-like protein conjugation." J. Struct. Biol. **162**(2): 205-218.

Burton, J. L. and M. J. Solomon (2007). "Mad3p, a pseudosubstrate inhibitor of APCCdc20 in the spindle assembly checkpoint." Genes Dev. **21**(6): 655-667.

Buschhorn, B. A., G. Petzold, et al. (2011). "Substrate binding on the APC/C occurs between the coactivator Cdh1 and the processivity factor Doc1." Nat Struct Mol Biol **18**(1): 6-13.

Carroll, C. W., M. Enquist-Newman, et al. (2005). "The APC subunit Doc1 promotes recognition of the substrate destruction box." Curr. Biol. **15**(1): 11-18.

Carroll, C. W., K. J. Milks, et al. (2010). "Dual recognition of CENP-A nucleosomes is required for centromere assembly." J. Cell Biol. **189**(7): 1143-1155.

Carroll, C. W. and D. O. Morgan (2002). "The Doc1 subunit is a processivity factor for the anaphase-promoting complex." Nat. Cell Biol. **4**(11): 880-887.

Carroll, C. W., M. C. Silva, et al. (2009). "Centromere assembly requires the direct recognition of CENP-A nucleosomes by CENP-N." Nat. Cell Biol. **11**(7): 896-902.

Chan, Y. W., L. L. Fava, et al. (2009). "Mitotic control of kinetochore-associated dynein and spindle orientation by human Spindly." J. Cell Biol. **185**(5): 859-874.

Cheeseman, I. M., J. S. Chappie, et al. (2006). "The conserved KMN network constitutes the core microtubule-binding site of the kinetochore." Cell **127**(5): 983-997.

Cheeseman, I. M. and A. Desai (2008). "Molecular architecture of the kinetochore-microtubule interface." Nat. Rev. Mol. Cell Biol. **9**(1): 33-46.

Cheeseman, I. M., T. Hori, et al. (2008). "KNL1 and the CENP-H/I/K complex coordinately direct kinetochore assembly in vertebrates." Mol. Biol. Cell **19**(2): 587-594.

Chen, R. H. (2004). "Phosphorylation and activation of Bub1 on unattached chromosomes facilitate the spindle checkpoint." EMBO J. **23**(15): 3113-3121.

Chen, V. B., W. B. Arendall, 3rd, et al. (2010). "MolProbity: all-atom structure validation for macromolecular crystallography." Acta Crystallogr. D Biol. Crystallogr. **66**(Pt 1): 12-21.

Chi, Y. H., K. Haller, et al. (2008). "Requirements for protein phosphorylation and the kinase activity of polo-like kinase 1 (Plk1) for the kinetochore function of mitotic arrest deficiency protein 1 (Mad1)." J. Biol. Chem. **283**(51): 35834-35844.

Choi, E., H. Choe, et al. (2009). "BubR1 acetylation at prometaphase is required for modulating APC/C activity and timing of mitosis." EMBO J. **28**(14): 2077-2089.

Chung, E. and R. H. Chen (2002). "Spindle checkpoint requires Mad1-bound and Mad1-free Mad2." Mol. Biol. Cell **13**(5): 1501-1511.

Chung, E. and R. H. Chen (2003). "Phosphorylation of Cdc20 is required for its inhibition by the spindle checkpoint." Nat. Cell Biol. **5**(8): 748-753.

Ciferri, C., S. Pasqualato, et al. (2008). "Implications for kinetochore-microtubule attachment from the structure of an engineered Ndc80 complex." Cell **133**(3): 427-439.

Cleveland, D. W., Y. Mao, et al. (2003). "Centromeres and kinetochores: from epigenetics to mitotic checkpoint signaling." Cell **112**(4): 407-421.

Collin, P., O. Nashchekina, et al. (2013). "The spindle assembly checkpoint works like a rheostat rather than a toggle switch." Nat. Cell Biol. **15**(11): 1378-1385.

Corbett, K. D., C. K. Yip, et al. (2010). "The monopolin complex crosslinks kinetochore components to regulate chromosome-microtubule attachments." Cell **142**(4): 556-567.

Cui, Y., X. Cheng, et al. (2010). "Degradation of the human mitotic checkpoint kinase Mps1 is cell cycle-regulated by APC-cCdc20 and APC-cCdh1 ubiquitin ligases." J. Biol. Chem. **285**(43): 32988-32998.

D'Angiolella, V., C. Mari, et al. (2003). "The spindle checkpoint requires cyclin-dependent kinase activity." Genes Dev. **17**(20): 2520-2525.

D'Arcy, S., O. R. Davies, et al. (2010). "Defining the molecular basis of BubR1 kinetochore interactions and APC/C-CDC20 inhibition." J. Biol. Chem. **285**(19): 14764-14776.

da Fonseca, P. C., E. H. Kong, et al. (2011). "Structures of APC/C(Cdh1) with substrates identify Cdh1 and Apc10 as the D-box co-receptor." Nature **470**(7333): 274-278.
Davenport, J., L. D. Harris, et al. (2006). "Spindle checkpoint function requires Mad2-dependent Cdc20 binding to the Mad3 homology domain of BubR1." Exp. Cell Res. **312**(10): 1831-1842.
De Antoni, A., C. G. Pearson, et al. (2005). "The Mad1/Mad2 complex as a template for Mad2 activation in the spindle assembly checkpoint." Curr. Biol. **15**(3): 214-225.
Dick, A. E. and D. W. Gerlich (2013). "Kinetic framework of spindle assembly checkpoint signalling." Nat. Cell Biol. **15**(11): 1370-1377.
Elowe, S., K. Dulla, et al. (2010). "Uncoupling of the spindle-checkpoint and chromosome-congression functions of BubR1." J. Cell Sci. **123**(Pt 1): 84-94.
Emsley, P. and K. Cowtan (2004). "Coot: model-building tools for molecular graphics." Acta Crystallogr. D Biol. Crystallogr. **60**(Pt 12 Pt 1): 2126-2132.
Fang, G. (2002). "Checkpoint protein BubR1 acts synergistically with Mad2 to inhibit anaphase-promoting complex." Mol. Biol. Cell **13**(3): 755-766.
Fang, G., H. Yu, et al. (1998). "The checkpoint protein MAD2 and the mitotic regulator CDC20 form a ternary complex with the anaphase-promoting complex to control anaphase initiation." Genes Dev. **12**(12): 1871-1883.
Foley, E. A. and T. M. Kapoor (2013). "Microtubule attachment and spindle assembly checkpoint signalling at the kinetochore." Nat. Rev. Mol. Cell Biol. **14**(1): 25-37.
Foltz, D. R., L. E. Jansen, et al. (2006). "The human CENP-A centromeric nucleosome-associated complex." Nat. Cell Biol. **8**(5): 458-469.
Gascoigne, K. E. and I. M. Cheeseman (2013). "CDK-dependent phosphorylation and nuclear exclusion coordinately control kinetochore assembly state." J. Cell Biol. **201**(1): 23-32.
Gascoigne, K. E., K. Takeuchi, et al. (2011). "Induced ectopic kinetochore assembly bypasses the requirement for CENP-A nucleosomes." Cell **145**(3): 410-422.
Gassmann, R., A. J. Holland, et al. (2010). "Removal of Spindly from microtubule-attached kinetochores controls spindle checkpoint silencing in human cells." Genes Dev. **24**(9): 957-971.
Griffis, E. R., N. Stuurman, et al. (2007). "Spindly, a novel protein essential for silencing the spindle assembly checkpoint, recruits dynein to the kinetochore." J. Cell Biol. **177**(6): 1005-1015.
Guse, A., C. W. Carroll, et al. (2011). "In vitro centromere and kinetochore assembly on defined chromatin templates." Nature **477**(7364): 354-358.
Habu, T., S. H. Kim, et al. (2002). "Identification of a MAD2-binding protein, CMT2, and its role in mitosis." EMBO J. **21**(23): 6419-6428.
Hauf, S., R. W. Cole, et al. (2003). "The small molecule Hesperadin reveals a role for Aurora B in correcting kinetochore-microtubule attachment and in maintaining the spindle assembly checkpoint." J. Cell Biol. **161**(2): 281-294.
Heinrich, S., E. M. Geissen, et al. (2013). "Determinants of robustness in spindle assembly checkpoint signalling." Nat. Cell Biol. **15**(11): 1328-1339.
Hellwig, D., S. Emmerth, et al. (2011). "Dynamics of CENP-N kinetochore binding during the cell cycle." J. Cell Sci. **124**(Pt 22): 3871-3883.

Herzog, F., I. Primorac, et al. (2009). "Structure of the anaphase-promoting complex/cyclosome interacting with a mitotic checkpoint complex." Science **323**(5920): 1477-1481.

Hewitt, L., A. Tighe, et al. (2010). "Sustained Mps1 activity is required in mitosis to recruit O-Mad2 to the Mad1-C-Mad2 core complex." J. Cell Biol. **190**(1): 25-34.

Hori, T., M. Amano, et al. (2008). "CCAN makes multiple contacts with centromeric DNA to provide distinct pathways to the outer kinetochore." Cell **135**(6): 1039-1052.

Howell, B. J., B. F. McEwen, et al. (2001). "Cytoplasmic dynein/dynactin drives kinetochore protein transport to the spindle poles and has a role in mitotic spindle checkpoint inactivation." J. Cell Biol. **155**(7): 1159-1172.

Jelluma, N., A. B. Brenkman, et al. (2008). "Mps1 phosphorylates Borealin to control Aurora B activity and chromosome alignment." Cell **132**(2): 233-246.

Jelluma, N., T. B. Dansen, et al. (2010). "Release of Mps1 from kinetochores is crucial for timely anaphase onset." J. Cell Biol. **191**(2): 281-290.

Jia, L., S. Kim, et al. (2013). "Tracking spindle checkpoint signals from kinetochores to APC/C." Trends Biochem. Sci. **38**(6): 302-311.

Kang, J., Y. Chen, et al. (2007). "Autophosphorylation-dependent activation of human Mps1 is required for the spindle checkpoint." Proc. Natl. Acad. Sci. U. S. A. **104**(51): 20232-20237.

Kang, J., M. Yang, et al. (2008). "Structure and substrate recruitment of the human spindle checkpoint kinase Bub1." Mol. Cell **32**(3): 394-405.

Kang, Y. H., J. E. Park, et al. (2006). "Self-regulated Plk1 recruitment to kinetochores by the Plk1-PBIP1 interaction is critical for proper chromosome segregation." Mol. Cell **24**(3): 409-422.

Karess, R. (2005). "Rod-Zw10-Zwilch: a key player in the spindle checkpoint." Trends Cell Biol. **15**(7): 386-392.

Kastenmayer, J. P., M. S. Lee, et al. (2005). "The C-terminal half of Saccharomyces cerevisiae Mad1p mediates spindle checkpoint function, chromosome transmission fidelity and CEN association." Genetics **170**(2): 509-517.

Kawashima, S. A., Y. Yamagishi, et al. (2010). "Phosphorylation of H2A by Bub1 prevents chromosomal instability through localizing shugoshin." Science **327**(5962): 172-177.

Kelly, A. E., C. Ghenoiu, et al. (2010). "Survivin reads phosphorylated histone H3 threonine 3 to activate the mitotic kinase Aurora B." Science **330**(6001): 235-239.

Kelly, A. E., S. C. Sampath, et al. (2007). "Chromosomal enrichment and activation of the Aurora B pathway are coupled to spatially regulate spindle assembly." Dev. Cell **12**(1): 31-43.

Kim, S., H. Sun, et al. (2010). "Phosphorylation of the spindle checkpoint protein Mad2 regulates its conformational transition." Proc. Natl. Acad. Sci. U. S. A. **107**(46): 19772-19777.

Kim, S., H. Sun, et al. (2012). "Structure of human Mad1 C-terminal domain reveals its involvement in kinetochore targeting." Proc. Natl. Acad. Sci. U. S. A. **109**(17): 6549-6554.

King, E. M., S. J. van der Sar, et al. (2007). "Mad3 KEN boxes mediate both Cdc20 and Mad3 turnover, and are critical for the spindle checkpoint." PLoS ONE **2**(4): e342.

Kiyomitsu, T., H. Murakami, et al. (2011). "Protein interaction domain mapping of human kinetochore protein Blinkin reveals a consensus motif for binding of spindle assembly checkpoint proteins Bub1 and BubR1." Mol. Cell Biol. **31**(5): 998-1011.

Kiyomitsu, T., C. Obuse, et al. (2007). "Human Blinkin/AF15q14 is required for chromosome alignment and the mitotic checkpoint through direct interaction with Bub1 and BubR1." Dev. Cell **13**(5): 663-676.

Klebig, C., D. Korinth, et al. (2009). "Bub1 regulates chromosome segregation in a kinetochore-independent manner." J. Cell Biol. **185**(5): 841-858.

Kline, S. L., I. M. Cheeseman, et al. (2006). "The human Mis12 complex is required for kinetochore assembly and proper chromosome segregation." J. Cell Biol. **173**(1): 9-17.

Kraft, C., H. C. Vodermaier, et al. (2005). "The WD40 propeller domain of Cdh1 functions as a destruction box receptor for APC/C substrates." Mol. Cell **18**(5): 543-553.

Krenn, V., K. Overlack, et al. (2014). "KI Motifs of Human Knl1 Enhance Assembly of Comprehensive Spindle Checkpoint Complexes around MELT Repeats." Curr. Biol. **24**(1): 29-39.

Krenn, V., A. Wehenkel, et al. (2012). "Structural analysis reveals features of the spindle checkpoint kinase Bub1-kinetochore subunit Knl1 interaction." J. Cell Biol. **196**(4): 451-467.

Kulukian, A., J. S. Han, et al. (2009). "Unattached kinetochores catalyze production of an anaphase inhibitor that requires a Mad2 template to prime Cdc20 for BubR1 binding." Dev. Cell **16**(1): 105-117.

Kwiatkowski, N., N. Jelluma, et al. (2010). "Small-molecule kinase inhibitors provide insight into Mps1 cell cycle function." Nat. Chem. Biol. **6**(5): 359-368.

Lad, L., S. Lichtsteiner, et al. (2009). "Kinetic analysis of Mad2-Cdc20 formation: conformational changes in Mad2 are catalyzed by a C-Mad2-ligand complex." Biochemistry **48**(40): 9503-9515.

Lampson, M. A. and I. M. Cheeseman (2011). "Sensing centromere tension: Aurora B and the regulation of kinetochore function." Trends Cell Biol. **21**(3): 133-140.

Lara-Gonzalez, P., F. G. Westhorpe, et al. (2012). "The spindle assembly checkpoint." Curr. Biol. **22**(22): R966-980.

Li, M., X. Fang, et al. (2009). "Loss of spindle assembly checkpoint-mediated inhibition of Cdc20 promotes tumorigenesis in mice." J. Cell Biol. **185**(6): 983-994.

Liu, D., G. Vader, et al. (2009). "Sensing chromosome bi-orientation by spatial separation of Aurora B kinase from kinetochore substrates." Science **323**(5919): 1350-1353.

Liu, S. T., J. B. Rattner, et al. (2006). "Mapping the assembly pathways that specify formation of the trilaminar kinetochore plates in human cells." J. Cell Biol. **175**(1): 41-53.

London, N. and S. Biggins (2014). "Mad1 kinetochore recruitment by Mps1-mediated phosphorylation of Bub1 signals the spindle checkpoint." Genes Dev **28**(2): 140-152.

London, N., S. Ceto, et al. (2012). "Phosphoregulation of Spc105 by Mps1 and PP1 regulates Bub1 localization to kinetochores." Curr. Biol. **22**(10): 900-906.

Luo, X., G. Fang, et al. (2000). "Structure of the Mad2 spindle assembly checkpoint protein and its interaction with Cdc20." Nat. Struct. Biol. **7**(3): 224-229.

Luo, X., Z. Tang, et al. (2002). "The Mad2 spindle checkpoint protein undergoes similar major conformational changes upon binding to either Mad1 or Cdc20." Mol. Cell **9**(1): 59-71.

Luo, X., Z. Tang, et al. (2004). "The Mad2 spindle checkpoint protein has two distinct natively folded states." Nat. Struct. Mol. Biol. **11**(4): 338-345.

Luo, X. and H. Yu (2008). "Protein metamorphosis: the two-state behavior of Mad2." Structure **16**(11): 1616-1625.

Maciejowski, J., K. A. George, et al. (2010). "Mps1 directs the assembly of Cdc20 inhibitory complexes during interphase and mitosis to control M phase timing and spindle checkpoint signaling." J. Cell Biol. **190**(1): 89-100.

Maldonado, M. and T. M. Kapoor (2011). "Constitutive Mad1 targeting to kinetochores uncouples checkpoint signalling from chromosome biorientation." Nat. Cell Biol. **13**(4): 475-482.

Mali, P., K. M. Esvelt, et al. (2013). "Cas9 as a versatile tool for engineering biology." Nat. Methods **10**(10): 957-963.

Malureanu, L. A., K. B. Jeganathan, et al. (2009). "BubR1 N terminus acts as a soluble inhibitor of cyclin B degradation by APC/C(Cdc20) in interphase." Dev. Cell **16**(1): 118-131.

Malvezzi, F., G. Litos, et al. (2013). "A structural basis for kinetochore recruitment of the Ndc80 complex via two distinct centromere receptors." EMBO J. **32**(3): 409-423.

Mapelli, M., F. V. Filipp, et al. (2006). "Determinants of conformational dimerization of Mad2 and its inhibition by p31comet." EMBO J. **25**(6): 1273-1284.

Mapelli, M., L. Massimiliano, et al. (2007). "The Mad2 conformational dimer: structure and implications for the spindle assembly checkpoint." Cell **131**(4): 730-743.

Mapelli, M. and A. Musacchio (2007). "MAD contortions: conformational dimerization boosts spindle checkpoint signaling." Curr. Opin. Struct. Biol. **17**(6): 716-725.

Martin-Lluesma, S., V. M. Stucke, et al. (2002). "Role of Hec1 in spindle checkpoint signaling and kinetochore recruitment of Mad1/Mad2." Science **297**(5590): 2267-2270.

Matson, D. R., P. B. Demirel, et al. (2012). "A conserved role for COMA/CENP-H/I/N kinetochore proteins in the spindle checkpoint." Genes Dev. **26**(6): 542-547.

McCleland, M. L., R. D. Gardner, et al. (2003). "The highly conserved Ndc80 complex is required for kinetochore assembly, chromosome congression, and spindle checkpoint activity." Genes Dev. **17**(1): 101-114.

Meraldi, P., V. M. Draviam, et al. (2004). "Timing and checkpoints in the regulation of mitotic progression." Dev. Cell **7**(1): 45-60.

Mikami, Y., T. Hori, et al. (2005). "The functional region of CENP-H interacts with the Nuf2 complex that localizes to centromere during mitosis." Mol. Cell Biol. **25**(5): 1958-1970.

Muralidharan, V. and T. W. Muir (2006). "Protein ligation: an enabling technology for the biophysical analysis of proteins." Nat. Methods **3**(6): 429-438.

Musacchio, A. and E. D. Salmon (2007). "The spindle-assembly checkpoint in space and time." Nat. Rev. Mol. Cell Biol. **8**(5): 379-393.

Musacchio, A. and E. D. Salmon (2007). "The spindle-assembly checkpoint in space and time." Nat Rev Mol Cell Biol **8**(5): 379-393.

Nameki, N., M. Yoneyama, et al. (2004). "Solution structure of the RWD domain of the mouse GCN2 protein." Protein Sci. **13**(8): 2089-2100.

Nijenhuis, W., E. von Castelmur, et al. (2013). "A TPR domain-containing N-terminal module of MPS1 is required for its kinetochore localization by Aurora B." J. Cell Biol. **201**(2): 217-231.

Nilsson, J., M. Yekezare, et al. (2008). "The APC/C maintains the spindle assembly checkpoint by targeting Cdc20 for destruction." Nat. Cell Biol. **10**(12): 1411-1420.

Nishino, T., F. Rago, et al. (2013). "CENP-T provides a structural platform for outer kinetochore assembly." EMBO J.

Nishino, T., K. Takeuchi, et al. (2012). "CENP-T-W-S-X forms a unique centromeric chromatin structure with a histone-like fold." Cell **148**(3): 487-501.

Okada, M., I. M. Cheeseman, et al. (2006). "The CENP-H-I complex is required for the efficient incorporation of newly synthesized CENP-A into centromeres." Nat. Cell Biol. **8**(5): 446-457.

Otwinowski, Z. and W. Minor (1997). "Processing X-ray diffraction data collected in oscillation mode." Methods Enzymol. **276**: 307-326.

Palframan, W. J., J. B. Meehl, et al. (2006). "Anaphase inactivation of the spindle checkpoint." Science **313**(5787): 680-684.

Pan, J. and R. H. Chen (2004). "Spindle checkpoint regulates Cdc20p stability in Saccharomyces cerevisiae." Genes Dev. **18**(12): 1439-1451.

Peters, J. M. (2006). "The anaphase promoting complex/cyclosome: a machine designed to destroy." Nat. Rev. Mol. Cell Biol. **7**(9): 644-656.

Petrovic, A., S. Mosalaganti, et al. (2014). "Modular Assembly of RWD Domains on the Mis12 Complex Underlies Outer Kinetochore Organization." Mol. Cell **53**(4): 591-605.

Petrovic, A., S. Pasqualato, et al. (2010). "The MIS12 complex is a protein interaction hub for outer kinetochore assembly." J. Cell Biol. **190**(5): 835-852.

Pinsky, B. A., C. Kung, et al. (2006). "The Ipl1-Aurora protein kinase activates the spindle checkpoint by creating unattached kinetochores." Nat. Cell Biol. **8**(1): 78-83.

Prendergast, L., C. van Vuuren, et al. (2011). "Premitotic assembly of human CENPs -T and -W switches centromeric chromatin to a mitotic state." PLoS Biol. **9**(6): e1001082.

Primorac, I., J. R. Weir, et al. (2013). "Bub3 reads phosphorylated MELT repeats to promote spindle assembly checkpoint signaling." eLife **2**: e01030.

Qi, W. and H. Yu (2006). "The spindle checkpoint and chromosomal stability." Genome Dyn. **1**: 116-130.

Qi, W. and H. Yu (2007). "KEN-box-dependent degradation of the Bub1 spindle checkpoint kinase by the anaphase-promoting complex/cyclosome." J. Biol. Chem. **282**(6): 3672-3679.

Rahmani, Z., M. E. Gagou, et al. (2009). "Separating the spindle, checkpoint, and timer functions of BubR1." J. Cell Biol. **187**(5): 597-605.

Reddy, S. K., M. Rape, et al. (2007). "Ubiquitination by the anaphase-promoting complex drives spindle checkpoint inactivation." Nature **446**(7138): 921-925.

Rieder, C. L., R. W. Cole, et al. (1995). "The checkpoint delaying anaphase in response to chromosome monoorientation is mediated by an inhibitory signal produced by unattached kinetochores." J. Cell Biol. **130**(4): 941-948.

Rischitor, P. E., K. M. May, et al. (2007). "Bub1 is a fission yeast kinetochore scaffold protein, and is sufficient to recruit other spindle checkpoint proteins to ectopic sites on chromosomes." PLoS ONE **2**(12): e1342.

Ruchaud, S., M. Carmena, et al. (2007). "Chromosomal passengers: conducting cell division." Nat. Rev. Mol. Cell Biol. **8**(10): 798-812.

Santaguida, S., A. Tighe, et al. (2010). "Dissecting the role of MPS1 in chromosome biorientation and the spindle checkpoint through the small molecule inhibitor reversine." J. Cell Biol. **190**(1): 73-87.

Santaguida, S., C. Vernieri, et al. (2011). "Evidence that Aurora B is implicated in spindle checkpoint signalling independently of error correction." EMBO J. **30**(8): 1508-1519.

Saurin, A. T., M. S. van der Waal, et al. (2011). "Aurora B potentiates Mps1 activation to ensure rapid checkpoint establishment at the onset of mitosis." Nat. Commun. **2**: 316.

Schleiffer, A., M. Maier, et al. (2012). "CENP-T proteins are conserved centromere receptors of the Ndc80 complex." Nat. Cell Biol. **14**(6): 604-613.

Schreiber, A., F. Stengel, et al. (2011). "Structural basis for the subunit assembly of the anaphase-promoting complex." Nature **470**(7333): 227-232.

Screpanti, E., A. De Antoni, et al. (2011). "Direct Binding of Cenp-C to the Mis12 Complex Joins the Inner and Outer Kinetochore." Curr. Biol. **21**: 391-398.

Sczaniecka, M., A. Feoktistova, et al. (2008). "The spindle checkpoint functions of Mad3 and Mad2 depend on a Mad3 KEN box-mediated interaction with Cdc20-anaphase-promoting complex (APC/C)." J. Biol. Chem. **283**(34): 23039-23047.

Seeley, T. W., L. Wang, et al. (1999). "Phosphorylation of human MAD1 by the BUB1 kinase in vitro." Biochem. Biophys. Res. Commun. **257**(2): 589-595.

Shah, J. V., E. Botvinick, et al. (2004). "Dynamics of centromere and kinetochore proteins; implications for checkpoint signaling and silencing." Curr. Biol. **14**(11): 942-952.

Shepperd, L. A., J. C. Meadows, et al. (2012). "Phosphodependent recruitment of Bub1 and Bub3 to Spc7/KNL1 by Mph1 kinase maintains the spindle checkpoint." Curr. Biol. **22**(10): 891-899.

Simonetta, M., R. Manzoni, et al. (2009). "The influence of catalysis on mad2 activation dynamics." PLoS Biol. **7**(1): e10.

Sironi, L., M. Mapelli, et al. (2002). "Crystal structure of the tetrameric Mad1-Mad2 core complex: implications of a 'safety belt' binding mechanism for the spindle checkpoint." EMBO J. **21**(10): 2496-2506.

Sironi, L., M. Mapelli, et al. (2002). "Crystal structure of the tetrameric Mad1-Mad2 core complex: implications of a 'safety belt' binding mechanism for the spindle checkpoint." EMBO. J. **21**(10): 2496-2506.

Stegmeier, F., M. Rape, et al. (2007). "Anaphase initiation is regulated by antagonistic ubiquitination and deubiquitination activities." Nature **446**(7138): 876-881.

Stucke, V. M., C. Baumann, et al. (2004). "Kinetochore localization and microtubule interaction of the human spindle checkpoint kinase Mps1." Chromosoma **113**(1): 1-15.

Subramanian, R. and T. M. Kapoor (2013). "Slipping past the spindle assembly checkpoint." Nat. Cell Biol. **15**(11): 1261-1263.

Sudakin, V., G. K. Chan, et al. (2001). "Checkpoint inhibition of the APC/C in HeLa cells is mediated by a complex of BUBR1, BUB3, CDC20, and MAD2." J. Cell Biol. **154**(5): 925-936.

Takeuchi, K. and T. Fukagawa (2012). "Molecular architecture of vertebrate kinetochores." Exp. Cell Res. **318**(12): 1367-1374.

Takeuchi, K., T. Nishino, et al. (2014). "The centromeric nucleosome-like CENP-T-W-S-X complex induces positive supercoils into DNA." Nucleic Acids Res. **42**(3): 1644-1655.

Tanaka, T. U., N. Rachidi, et al. (2002). "Evidence that the Ipl1-Sli15 (Aurora kinase-INCENP) complex promotes chromosome bi-orientation by altering kinetochore-spindle pole connections." Cell **108**(3): 317-329.

Tang, Z., R. Bharadwaj, et al. (2001). "Mad2-Independent inhibition of APCCdc20 by the mitotic checkpoint protein BubR1." Dev. Cell **1**(2): 227-237.

Tang, Z., B. Li, et al. (2001). "APC2 Cullin protein and APC11 RING protein comprise the minimal ubiquitin ligase module of the anaphase-promoting complex." Mol. Biol. Cell **12**(12): 3839-3851.

Tang, Z., H. Shu, et al. (2004). "Phosphorylation of Cdc20 by Bub1 provides a catalytic mechanism for APC/C inhibition by the spindle checkpoint." Mol. Cell **16**(3): 387-397.

Taylor, S. S. and F. McKeon (1997). "Kinetochore localization of murine Bub1 is required for normal mitotic timing and checkpoint response to spindle damage." Cell **89**(5): 727-735.

Thornton, B. R. and D. P. Toczyski (2006). "Precise destruction: an emerging picture of the APC." Genes Dev **20**(22): 3069-3078.

Tighe, A., O. Staples, et al. (2008). "Mps1 kinase activity restrains anaphase during an unperturbed mitosis and targets Mad2 to kinetochores." J. Cell Biol. **181**(6): 893-901.

Tsukahara, T., Y. Tanno, et al. (2010). "Phosphorylation of the CPC by Cdk1 promotes chromosome bi-orientation." Nature **467**(7316): 719-723.

Van Duyne, G. D., R. F. Standaert, et al. (1993). "Atomic structures of the human immunophilin FKBP-12 complexes with FK506 and rapamycin." J. Mol. Biol. **229**(1): 105-124.

Vleugel, M., E. Tromer, et al. (2013). "Arrayed BUB recruitment modules in the kinetochore scaffold KNL1 promote accurate chromosome segregation." J. Cell Biol. **203**(6): 943-955.

Wang, E., E. R. Ballister, et al. (2011). "Aurora B dynamics at centromeres create a diffusion-based phosphorylation gradient." J. Cell Biol. **194**(4): 539-549.

Wang, F., J. Dai, et al. (2010). "Histone H3 Thr-3 phosphorylation by Haspin positions Aurora B at centromeres in mitosis." Science **330**(6001): 231-235.

Wassmann, K., V. Liberal, et al. (2003). "Mad2 phosphorylation regulates its association with Mad1 and the APC/C." EMBO J. **22**(4): 797-806.

Wassmann, K., V. Liberal, et al. (2003). "Mad2 phosphorylation regulates its association with Mad1 and the APC/C." EMBO J **22**(4): 797-806.

Wei, R. R., J. R. Schnell, et al. (2006). "Structure of a central component of the yeast kinetochore: the Spc24p/Spc25p globular domain." Structure **14**(6): 1003-1009.

Welburn, J. P., M. Vleugel, et al. (2010). "Aurora B phosphorylates spatially distinct targets to differentially regulate the kinetochore-microtubule interface." Mol. Cell **38**(3): 383-392.

Xia, G., X. Luo, et al. (2004). "Conformation-specific binding of p31(comet) antagonizes the function of Mad2 in the spindle checkpoint." EMBO J. **23**(15): 3133-3143.

Yamagishi, Y., T. Honda, et al. (2010). "Two histone marks establish the inner centromere and chromosome bi-orientation." Science **330**(6001): 239-243.

Yamagishi, Y., C. H. Yang, et al. (2012). "MPS1/Mph1 phosphorylates the kinetochore protein KNL1/Spc7 to recruit SAC components." Nat. Cell Biol. **14**(7): 746-752.

Yamamoto, T. G., S. Watanabe, et al. (2008). "SPDL-1 functions as a kinetochore receptor for MDF-1 in Caenorhabditis elegans." J. Cell Biol. **183**(2): 187-194.

Yang, M., B. Li, et al. (2008). "Insights into mad2 regulation in the spindle checkpoint revealed by the crystal structure of the symmetric mad2 dimer." PLoS Biol. **6**(3): e50.

Yang, M., B. Li, et al. (2007). "p31comet blocks Mad2 activation through structural mimicry." Cell **131**(4): 744-755.

Yang, Y., F. Wu, et al. (2008). "Phosphorylation of HsMis13 by Aurora B kinase is essential for assembly of functional kinetochore." J. Biol. Chem. **283**(39): 26726-26736.

Yu, H. (2002). "Regulation of APC-Cdc20 by the spindle checkpoint." Curr. Opin. Cell Biol. **14**(6): 706-714.

Yu, H. (2006). "Structural activation of Mad2 in the mitotic spindle checkpoint: the two-state Mad2 model versus the Mad2 template model." J. Cell Biol. **173**(2): 153-157.

Yu, H. (2007). "Cdc20: a WD40 activator for a cell cycle degradation machine." Mol. Cell **27**(1): 3-16.

Zeng, X., F. Sigoillot, et al. (2010). "Pharmacologic inhibition of the anaphase-promoting complex induces a spindle checkpoint-dependent mitotic arrest in the absence of spindle damage." Cancer Cell **18**(4): 382-395.

Zich, J., A. M. Sochaj, et al. (2012). "Kinase activity of fission yeast Mph1 is required for Mad2 and Mad3 to stably bind the anaphase promoting complex." Curr Biol **22**(4): 296-301.